European Commission

JRC TECHNICAL REPORTS

Numerical Simulations in Support of the Blast Actuator Development

Administrative Arrangement N° JRC 32253-2011 with DG-HOME
Activity A5 - Blast Simulation Technology Development

Georgios Valsamos
Martin Larcher
George Solomos
Armelle Anthoine

2013

Report EUR 26430 EN

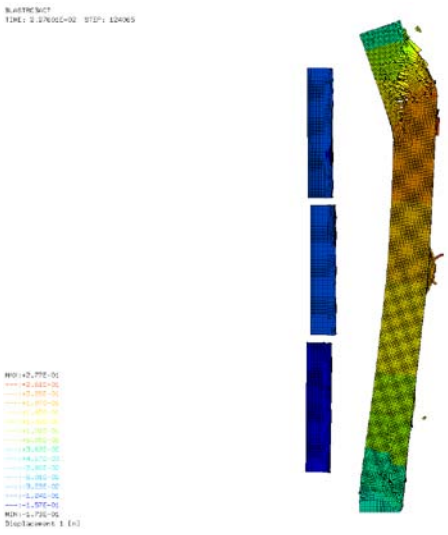

European Commission
Joint Research Centre
Institute for the Protection and Security of the Citizen

Contact information
Georgios Valsamos
Address: Joint Research Centre, Via Enrico Fermi 2749, TP 480, 21027 Ispra (VA), Italy
E-mail: georgios.valsamos@jrc.ec.europa.eu
Tel.: +39 0332 78 9004
Fax: +39 0332 78 9049

http://ipsc.jrc.ec.europa.eu/
http://www.jrc.ec.europa.eu/

Legal Notice
Neither the European Commission nor any person acting on behalf of the Commission
is responsible for the use which might be made of this publication.

Europe Direct is a service to help you find answers to your questions about the European Union
Freephone number (*): 00 800 6 7 8 9 10 11
(*) Certain mobile telephone operators do not allow access to 00 800 numbers or these calls may be billed.

A great deal of additional information on the European Union is available on the Internet.
It can be accessed through the Europa server http://europa.eu/.

JRC86464

EUR 26430 EN

ISBN 978-92-79-35069-6 (PDF)
ISBN 978-92-79-35070-2 (print)

ISSN 1018-5593 (print)
ISSN 1831-9424 (online)

doi:10.2788/53372

Luxembourg: Publications Office of the European Union, 2013

© European Union, 2013

Printed in Italy

CONTENTS

1 Introduction

The objective of this report is to present the numerical simulation investigation with the EUROPLEXUS code, which took place to support the preparation of the blast actuator. The blast actuator project [1] targets to develop an apparatus that can simulate an explosive loading at a lower cost and in a safer way (higher degree of control) than real explosives. EUROPLEXUS [2] is a computer code for fast explicit transient dynamic analysis of fluid-structure systems jointly developed by the French Commissariat à l'Energie Atomique (CEA Saclay) and by the Joint Research Centre of the European Commission (JRC Ispra).

The report is divided into 3 chapters. The first one presents the numerical model constructed for the evaluation of the several parameters. The finite element model is considered with the appropriate boundary conditions and the definition of the contact-impact model. Then a reference to the materials used for the simulation is made. The basic materials, such as the metallic and the concrete parts, are briefly presented while a more detailed enumeration has been done for several types of hyperelastic materials, which have been tested for the contact interlayer between the impacting mass and the specimen.

The second chapter discusses the results from the calculations. A comparison between several tests with different hyperelastic materials is taking place. The behaviour of each different material type is presented and the one that fits best to the desired load is selected. Two more parameters have been checked for their influence to the produced load, the impact velocity and the thickness of the interlayer material. For both parameters several tests gives valuable information on how the user of the blast actuator should prepare the experimental apparatus. Finally, a numerical validation of the impact model with a direct implementation on the column for an ideal explosive is presented.

The last chapter concludes the report and emphasizes the main achievements and results from the numerical study. The reader can find in the appendix all input files used for the numerical calculations.

2 Numerical model

The construction of the blast actuator for simulation of a blast loading is a complex and laborious work, where several parameters must be taken into account. The target of the simulations is to support the preparation and optimize the design of such a device by testing several parameters, for example the type and the size of the desired materials to be employed for the construction of the impactor. This will lead to a much smaller number of required experiments in order to calibrate the apparatus and finally to the minimization of the total cost of the project.

2.1 Experimental Model

The description of the experimental details is beyond the scope of this report but a quick reference to the idea of the blast actuator is necessary. Figure 1 presents the initial concept of the experimental device composed of two fast actuators. The actuators shafts accelerate the impacting masses, which afterwards punch the specimen generating pressures similar to those of an explosion. The numerical model will try to capture the phenomenon after the detachment (and the achievement of the final velocity) of the impacting mass from the actuator shafts.

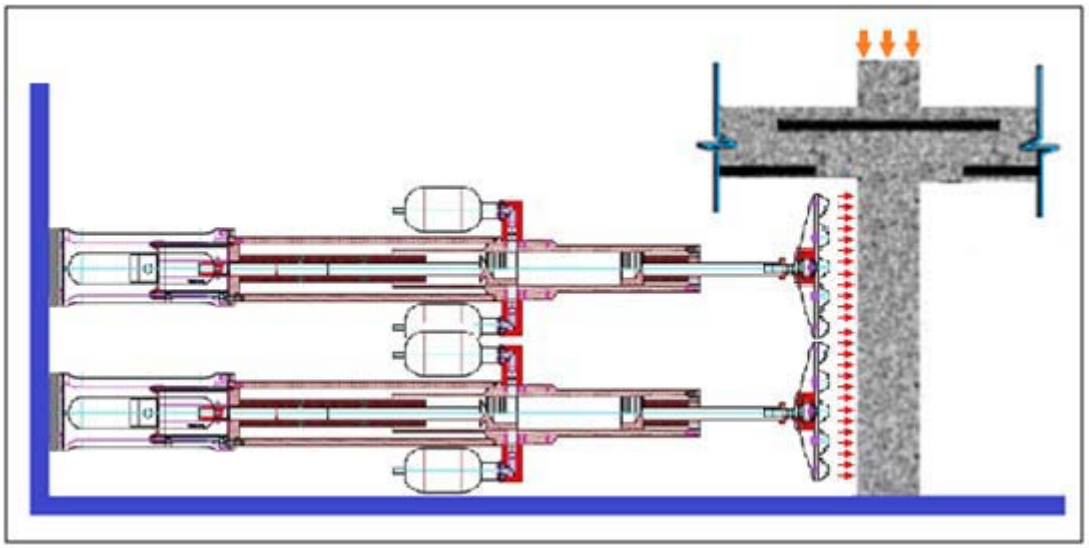

Figure 1: Principle of concept of the JRC Blast Simulator.

2.2 Finite element model

The geometrical model of the facility under consideration contains two main parts, the impacting mass (impactor) and the specimen as depicted in Figure 2. The impacting mass is the object that is

accelerated by the fast actuator and impacts the specimen in such a way that the loading that it produces is similar to the loading that it would have been caused by an explosion. The impactor needs to have a mass of about 40 kg so it should be composed by a (relatively) heavy and stiff material like aluminium or steel (magenta colour in Figure 2) and a weaker hyperelastic material (blue colour in Figure 2) that should be placed in the contact interface with the specimen. The layer of the hyperelastic material is used not only to protect from damage the metallic part of the impactor but also to make the time of the contact between the two parts longer and the loading smoother.

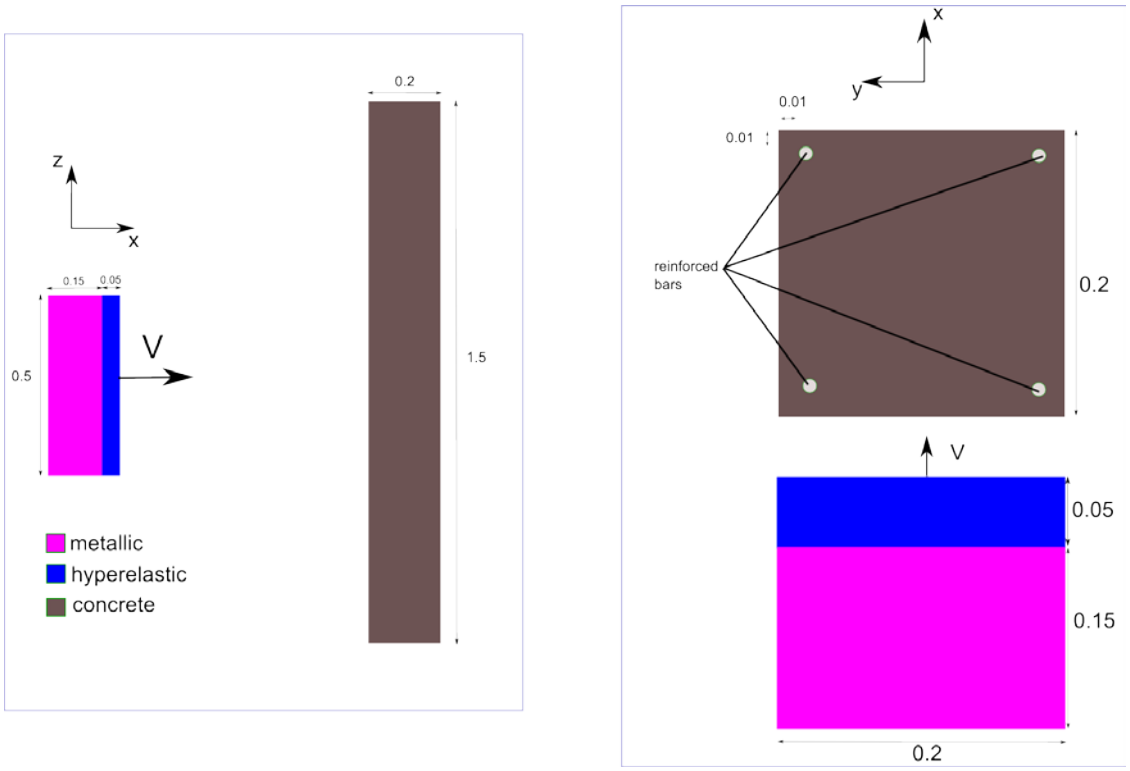

Figure 2: Basic sketch of blast actuator and tested reinforced concrete column

The dimensions of the specimen for that first approach are relatively small in order to have fast enough solution of the calculations. The column has a square cross section of 0.2m edge size and height of 1.5m. In the concrete columns there are 4 reinforcement bars with circular cross-section of diameter 10mm. The cover depth of the reinforcement is 10 mm. Table 1 summarizes the data concerning the size of the reinforced concrete column specimen.

The impacting mass is a parallelepiped shaped box of 0.2m width (x-direction), 0.2m depth (y-direction) and 0.5m height (z-direction). The thickness of the metallic part is 0.15m while the thickness of the interlayer part is 0.05m. The configuration of the impacting mass is presented in Table 2. The thickness of the metallic part is the same in all calculations, while for the thickness of the contact interlayer there are some variations in order to identify the effect of its size in the final result. The impacting mass is moving with a constant velocity towards the column (in the x-direction Figure 2).

Table 1: Configuration of the reinforced concrete column specimen

Width [m]	Depth [m]	Height [m]	Longitudinal reinforcement [mm]	Cover depth [mm]
0.2	0.2	1.5	4Ø10	10

Table 2: Configuration of the impacting mass

Width [m]	Depth [m]	Height [m]	Aluminium mass [kg]
0.2	0.2 (0.15 aluminium and 0.05 of hyperelastic layer)	0.5	40.5

For the construction of the volume mesh for the EUROPLEXUS simulations the cubic solid element *CUBE* has been used. This type of solid finite element has 8 nodes and is using one integration point. The concrete reinforcement is constructed with *BR3D* bar elements. Two different meshes are tested for the current model. For the construction of both meshes CAST3M code [3] has been used. The first one is a coarse mesh, where the size of the edge of the cubic elements is 0.025m; the same size is used also for the bar elements. The coarse model contains 4992 cubic elements and 240 bar elements while the total number of nodes is 6724. The coarse model is used for a quick rough solution in order to identify possible errors before launching the calculation of the fine mesh where the execution time is much longer. The size of the elements in the fine mesh is 0.01m and this results to a model of 80000 cubic elements, 600 bar elements and 89686 nodes in total. The fine mesh model has been used to produce more accurate results.

Table 3 presents the data concerning the size and the number of elements for each model. The last column of that table contains a ratio that shows the difference between the times needed for each calculation. The computational time for the calculation of the finer mesh is almost 40 times larger than the one needed for the coarse mesh. This is because the number of the elements in the fine model is 16 times larger so each time step will take 16 times more to be calculated. Also the time step size in the case of the fine model is about 2.5 times smaller, so the number of the steps needed to reach the final time will be 2.5 times larger. Thus, in total the ratio is 16x2.5 = 40. This means that if the calculation for the coarse model is taking (e.g.) 10 min then for the fine mesh it will take approximately 400 min (6.6 hours).

Table 3: Information about the size of the mesh for each model

Model	Element size [m]	Number of cubic elements	Number of bar elements	Total number of nodes	Time ratio
Coarse	0.025	4992	240	6724	1
Fine	0.01	80000	600	89686	40

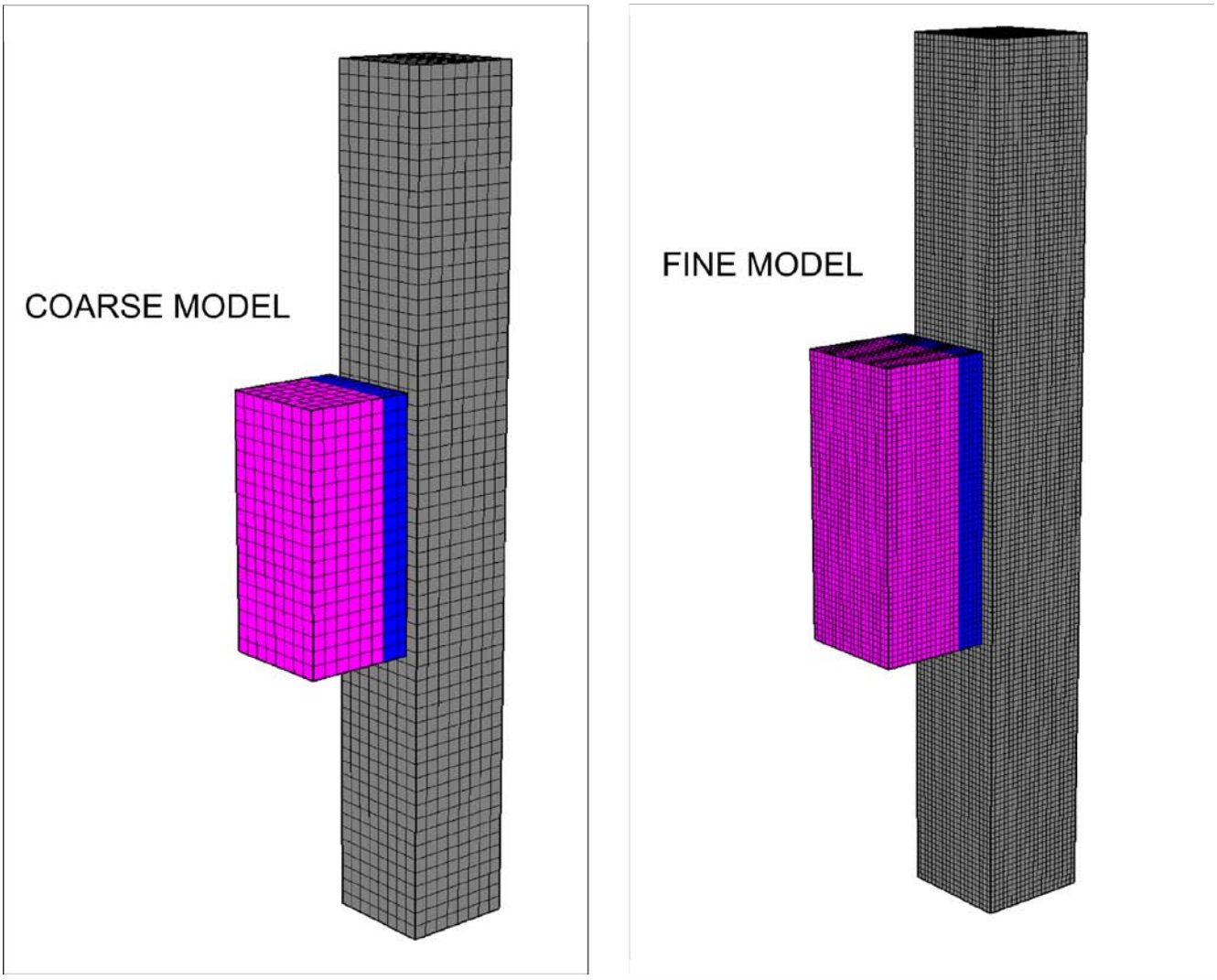

Figure 3: Coarse and fine mesh of the model.

2.3 Boundary conditions

Boundary conditions are applied on the reinforced concrete column at the bottom and the top surface, as presented in Figure 4. The bottom surface is fixed (x, y, z – directions are blocked) while in the top surface the horizontal x,y-directions are blocked and the vertical z-direction is free to move.

On the metallic part of the impactor boundary conditions are applied on the four edges as shown in Figure 4. These nodes are free only in the direction where the mass is been accelerated by the fast actuator (x-direction). These boundary conditions are imposed in order to simulate the actual experiment, where the impactor is guided before (and after) the contact. The metallic impacting mass in the experiment is guided by two bars in order to assure that the trajectory of the mass will be normal to the specimen surface.

This constraint of the impacting mass is useful also (for the period) after the impact. The impacting mass after the impact on the specimen rebounds so its velocity changes direction. Since the boundary conditions at the top and at the bottom of the column are not the same, the loading on the impacting mass is not symmetric during the contact. This will result to a rotation of the impactor in the phase of the rebound if the mass is not guided by the appropriate boundary conditions. Figure 5 shows the rotation of the impacting mass in the case that it is not guided. It is a figure from the very first calculations where the impacting mass was not guided. This behaviour renders necessary the imposition of the boundary conditions on the impacting mass especially for the final configuration where more than one fast actuators will be used and this rotation of the impacting masses might lead to a collision between them.

The blockages are introduced in the simulation though the *COUP BLOQ* directive of EUROPLEXUS. This directive imposes zero displacement to the selected degrees of freedom.

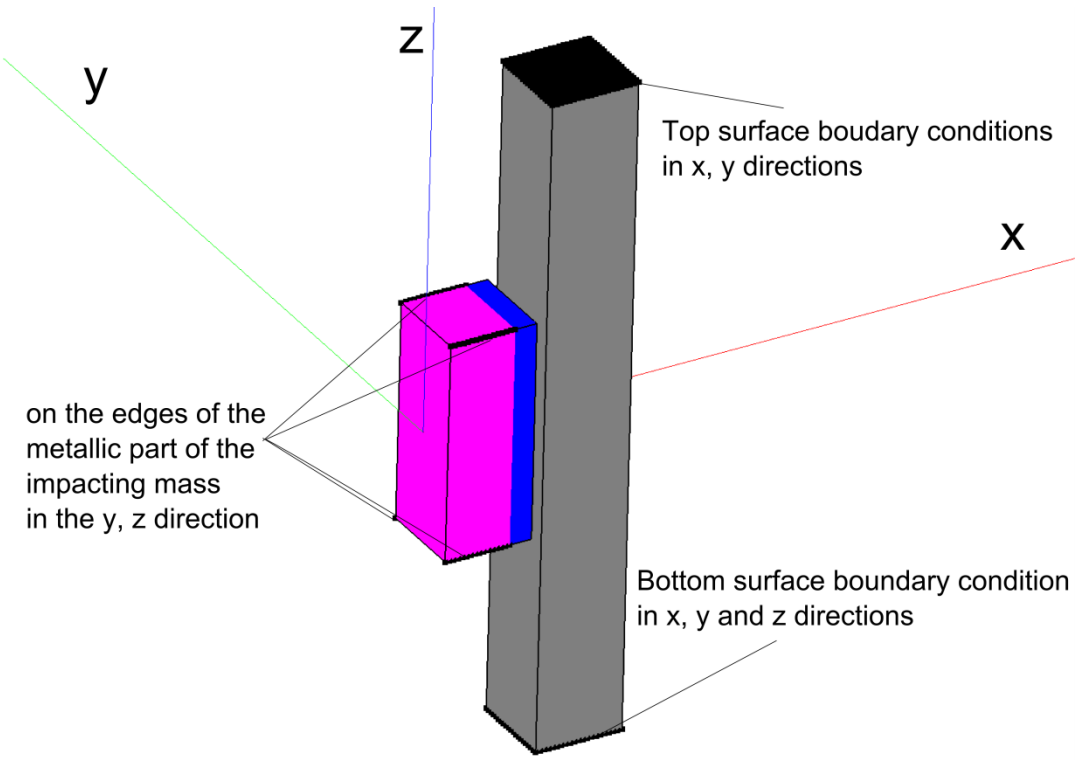

Figure 4: Boundary conditions

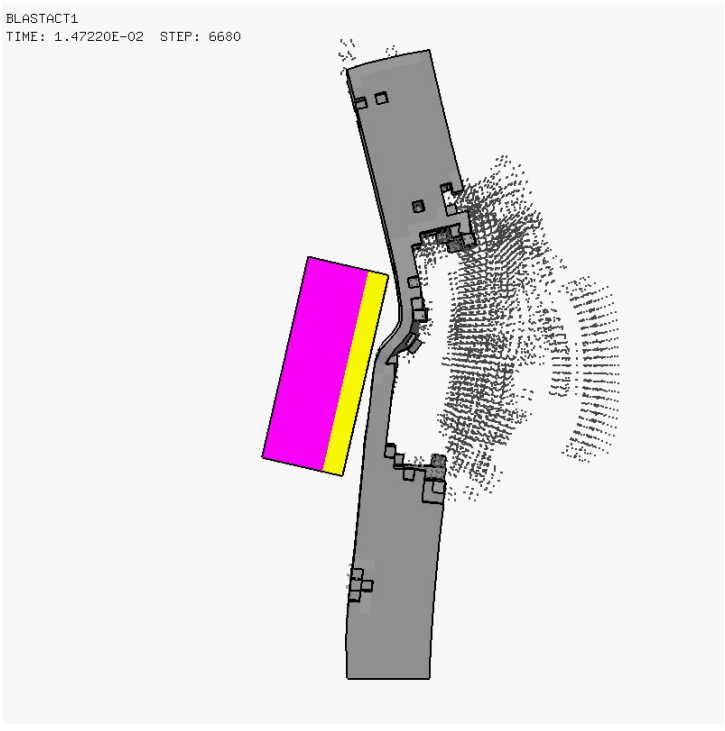

Figure 5: Rotation of the impacting mass at the rebound phase.

2.4 Contact model

For the simulation of the contact between the impacting mass and the specimen, the pinball method has been used [4], [5]. For the implementation of the pinball method *PINB* at least two bodies should

be defined that are possible to interact with each other. In the current model the two objects that participate in the contact are the impacting mass and the column specimen. The pinball method associates spheres (pinballs) to the participated elements, so in every step of the calculation it is checked if the area defined by the spheres of each body penetrates the area that is defined from the spheres of another body. When there is penetration between two bodies then appropriate normal force is applied by the method of Lagrange multipliers.

Since only a certain part of the two concerned objects is participating in the impact, it is prudent to select this area as a contact body and not the whole mesh. For the impacting mass the layer of the interlayer material and the first layers of the metallic part are selected as the candidate area for putting pinballs since this is the area that actually will be in contact with the specimen. For the column, the area that is selected to contain pinball's is a box that it is composed by the projection of the surface of the interlayer material that hits the column (and a slightly wider) and the first layers of elements of the concrete, as shown in Figure 6.

As already mentioned the imposition of the contact forces begins at the time step that the pinball's of the two different bodies penetrates each other. It is clear that the time step where the contact begins depends on the radius of the pinball (spheres) connected to each element. It is preferable that there is no penetration between the pinballs of each body at time step zero of the calculation, so the initial distance between the two bodies is selected to be sufficient for the impacting mass to move with the constant velocity for some steps before the impact.

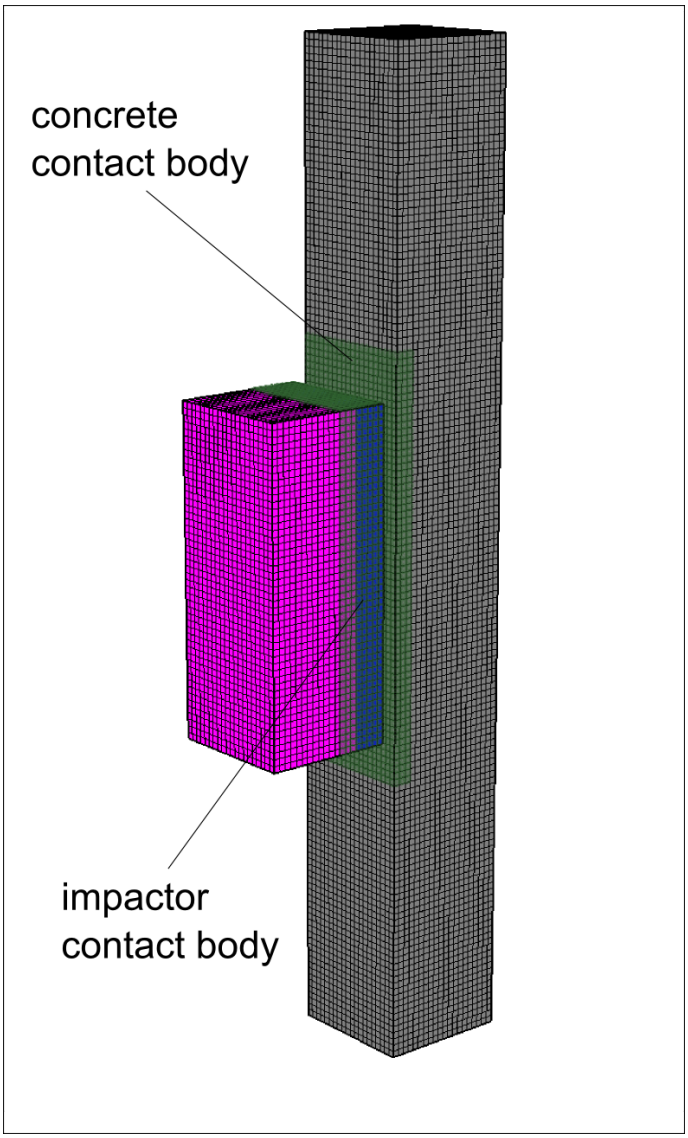

Figure 6: Definition of contact bodies.

2.5 Material definition

This chapter targets to define the properties of the materials used for the simulation. Typical material properties are selected for the concrete, the steel (for the reinforcement) and the aluminium (for the impacting mass) while for the interlayer part, three different materials have been checked in order to reach the best solution.

EUROPLEXUS includes a large variety of material models. This gives the opportunity to the user to choose the most suitable material formulation for each case. From the other point of view the big variety of the material models might be confusing to the user. The full presentation of the material formulation is beyond the scope of this report but a study has been conducted concerning the behaviour of several types of material models for the current simulation [7].

2.5.1 Concrete

The concrete is a brittle material where its behaviour [6] can be described by the curves of Figure 7. In both tension and compression stress–strain curves a softening effect is evident after a certain point. The material properties of the concrete used for the present simulation are shown in Table 4. The material model "*DPDC*" from EUROPLEXUS has been selected for the simulation after a study presented in [7]. This material formulation is a dynamic plastic damage concrete model that can represent the softening effect really well but without including any strain-rate effects.

Table 4: Concrete properties

Density [kg/m^3]	Young's modulus [N/m^2]	Poisson's ratio	Unconfined compressive strength [N/m^2]	Maximum aggregate size [mm]
2400	34.0E+09	0.21	42.0E+06	9.525

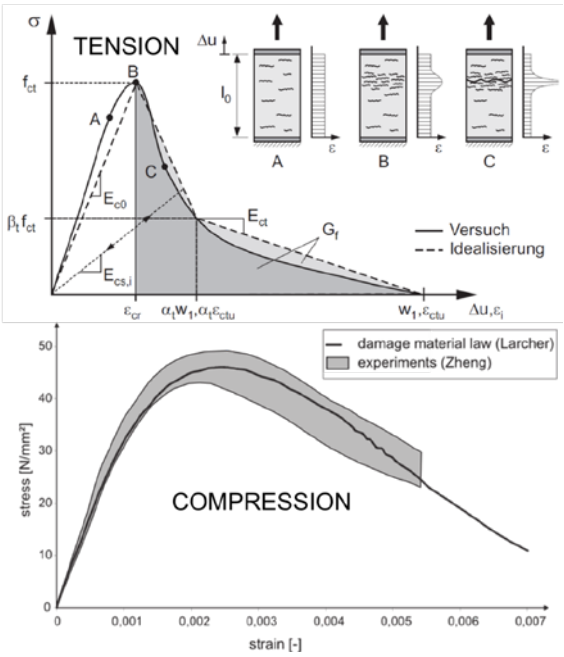

Figure 7: Behaviour of concrete under both tension and compression

2.5.2 Steel reinforcement

The material properties used for steel reinforcement bars are depicted in Table 5. The material model *VMIS ISOT* of EUROPLEXUS has been used for the description of the steel material in the calculation. This material formulation has an elasto-plastic isotropic behaviour that can include hardening effects. The erosion criterion is based upon plastic strains. It should be mentioned that the

ARMAT keyword has been used to link the displacements of the nodes belonging to the elements made of concrete with those of bar-like elements made of steel.

Table 5: Steel mechanical properties

Density [kg/m^3]	Young's modulus [N/m^2]	Poisson's ratio	Yield stress [N/m^2]	Ultimate strength [N/m^2]	Fracture strain
7800	2E+11	0.3	450E+06	510E+06	0.18

2.5.3 Aluminium

For the metallic part of the impacting mass there are two main choices the steel and the aluminium. The aluminium has been finally selected in order to achieve the target mass (40 kg) with a volume that is not too small, which would be the case if steel had been used. The properties of aluminium are presented in Table 6 . Since there is no significant hardening effect in the aluminium mechanical properties the *VMIS PARF* model of material library in EUROPLEXUS is used in the calculation. This formulation represents a perfectly plastic Von-Mises material behaviour.

Table 6: Aluminium mechanical properties

Density [kg/m^3]	Young's modulus [N/m^2]	Poisson's ratio	Yield stress [N/m^2]
2700	70E+09	0.35	120E+06

2.5.4 Hyperelastic material

For the hyperelastic material the stress-strain curve is nonlinear and the Young's modulus is increased with increasing strain. Material of this type can undergo large strains but the hysteresis loop is not significant. In the following sub-chapters the materials with such behaviour that were found in the ELSA laboratory are presented. These materials are tested in the laboratory in order to obtain their stress-strain curves.

Before presenting several hyperelastic materials used in the current study, it is preferable to make a reference to the material laws used in the calculations. The first choice for the representation of such materials through EUROPLEXUS is to use the formulation under the *HYPE* directive. This material formulation describes the hyperelastic law by using specific formulation for the strain energy density [8]. There are several expressions for the description of the strain energy density and this is discussed in [7]. For the present study the type 1 (Mooney-Rivlin) and type 4 (new Ogden) have been used [9].

An alternative way to represent the material properties of a hyperelastic material in EUROPLEXUS is to use the *FOAM* directive. This special material has been developed to simulate the aluminium foam. The "*FOAM*" material follows the Deshpande-Fleck model for metallic foams [10]. The model is basically an extension of the Von-Mises criterion where the hydrostatic stresses are incorporated in the equivalent stress. The EUROPLEXUS aluminium foam model is a 3D implementation without failure.

In order to implement the above material formulation it is necessary to define from the stress-strain curves the appropriate coefficients, as described in the EUROEPLEXUS user's manual. For the definition of the desired coefficients a best-fit procedure has been implemented, as indicated in [7]. This best-fit procedure scans for all possible values of the coefficients in a certain area and finds the combination which represents best the input stress-strain curve.

2.5.4.1 Rubber

The first material that has been tested is a rubber material as shown in Figure 8. The results of the one-dimensional unconfined compression test are presented in Figure 9. From the results obtained in the laboratory it came out that there is not a big strain-rate effect, possibly because the difference between the three chosen loading rates was minor. There is no significant hysteresis curve and the behaviour of the material can be characterized as hyperelastic since the stiffness is increased as the strains are increased.

After the implementation of the best-fit procedure the desired coefficients that describe the stress-strain curve are obtained. The *HYPE* material formulation has been used for type 1 [11] (Mooney-Rivlin), the input values for the properties are presented in Table 7. Figure 9 presents also the comparison between the data from the laboratory and the curve that is calculated after the best-fit procedure and used in the simulation.

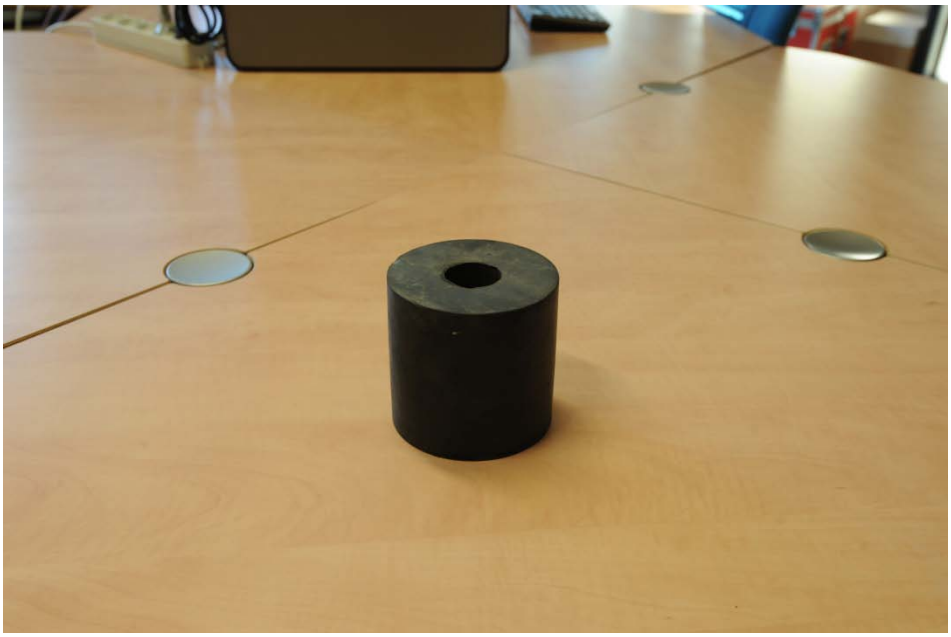

Figure 8: Rubber material from ELSA laboratory

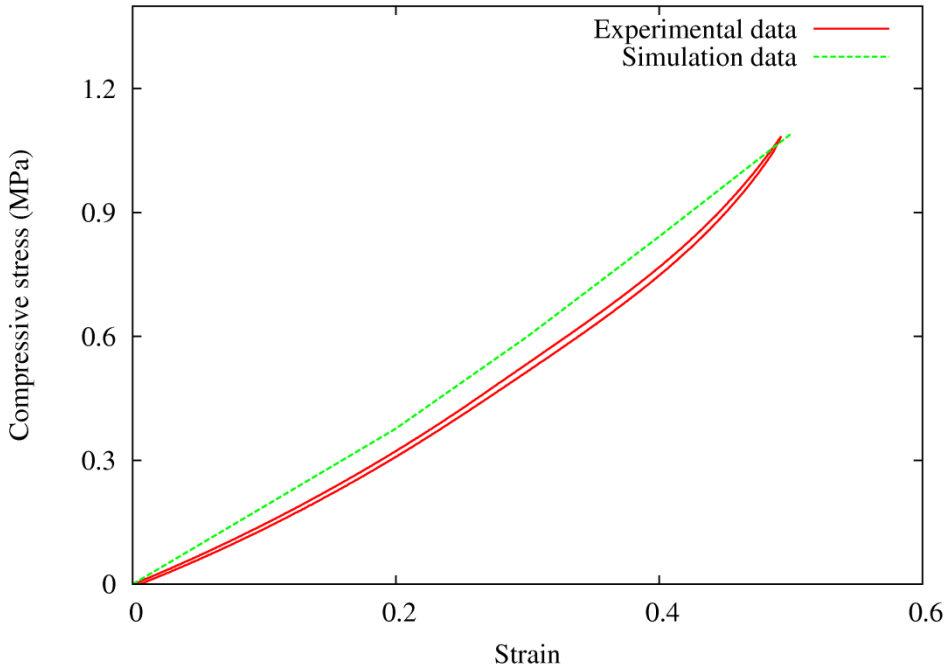

Figure 9: One dimensional compression test for the rubber like material

Table 7: Property parameters for type 1 *HYPE* material for the simulation of the rubber material

Type	Density (Kg/m^3)	Bulk modulus [N/m^2]	C01	C02	C03	C05	C06	C07
1	617	2e9	2.818e4	3.845e5	-	-	-	-

2.5.4.2 Elastic foam

Elastic polymeric foam is a material that can undergo large strains and its stiffness is increased rapidly under high strains. Initially the material undergoes a stress less (plateau) compression and this is due to the pores that are closing during this phase. Its plastic or damage limit is very high. Two types of elastic foam material Figure 10 were found and used in the ELSA repository. The stress-strain curves for both types of elastic foam material are similar so the one with the bigger density has been selected for the simulations (the black one is the denser). The stress strain curve for the elastic foam material obtained in the laboratory after the one-dimensional compression tests is shown in Figure 11.

As in the case of the rubber material, the experimental tests for the foam material revealed that strain rate effect is not significant so it is not taken into account in the calculation. For the simulation of the elastic foam material *HYPE* of type 4 (Ogden) has been tested. The coefficients calculated from the best-fit procedure are shown in Table 8. The curve that results from the calculated coefficients is presented together with the experimental data.

Figure 10: Elastic foam materials from ELSA laboratory

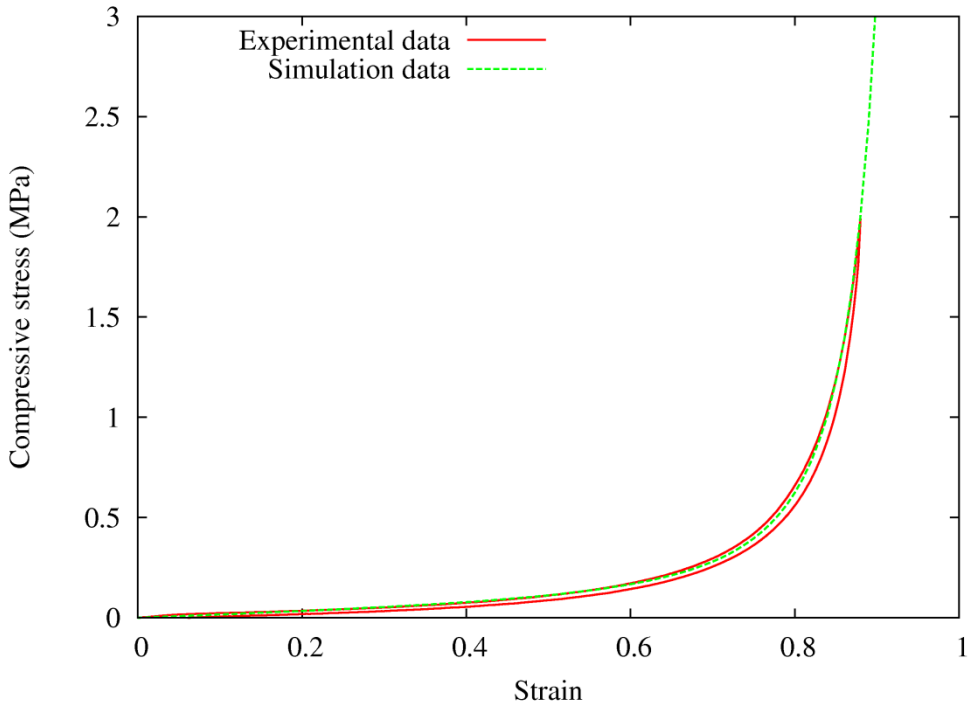

Figure 11: Stress-strain curves for the elastic foam material

Table 8: Property parameters for type 4 *HYPE* material for the simulation of the elastic foam material

Type	Density (Kg/m^3)	Bulk modulus [N/m^2]	C01	C02	C03	C05	C06	C07
4	134	7.44e6	-0.0049	11	11.3	5.119e5	4.36e3	1e4

2.5.4.3 Aluminium Foam

Aluminium foam is used often as energy absorber during impact loading due to its good energy absorbing capabilities. A typical stress-strain curve for aluminium foam material is presented in Figure 13. Several types of aluminium foam were found in the ELSA repository as Figure 12 depicts which have been checked for their performance in the current project although it cannot be characterized as hyperelastic material. The *FOAM* material model of EUROPLEXUS has been used in the calculation.

Three different type of aluminium foam have been tested each one of them with different Young's modulus. The simulations with the aluminium foam are a good example to investigate the influence of the stiffness of the material in the profile of the load applied on the concrete column. The parameters that describe the properties of the materials are shown in Table 9.

Figure 12: Aluminium foam from ELSA laboratory

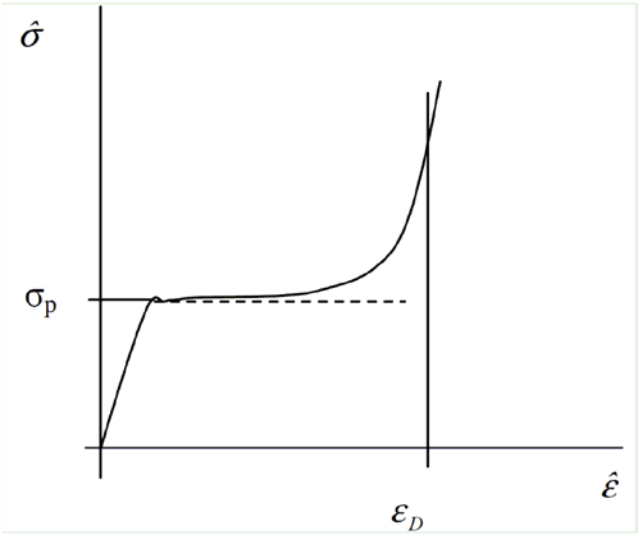

Figure 13: Typical stress-strain curve for aluminium foam material

Table 9: Material properties for Aluminium foam

TYPE	ρ_f [kg/m^3]	E [MPa]	v	σ_P [MPa]	ρ [kg/m^3]	α [MPa]	γ [MPa]	α_2 [MPa]	β
Type A	170	377E+06	0.2	1.15E+06	2700	2.12	1.87E+06	93.5E+06	5.79
Type B	340	1516E+06	0.2	5.76E+06	2700	2.12	3.92E+06	60.2E+06	4.39
Type C	510	5562E+06	0.2	14.82E+06	2700	2.12	5.37E+06	69.9E+06	2.99

3 Numerical results

This chapter presents the results obtained after several numerical simulations. The majority of the results refer to the fine mesh model which is considered as the most accurate one, but in some cases also the coarse mesh results are discussed. First the determination of all the output points and the output quantities is taking place. Then a study for different type of materials for the contact interface of the impactor is performed. In the simulations for the material selection the impacting mass approaches the specimen with a constant velocity of 20 m/s. Then a study of the influence of the velocity of the impacor in the produced load has been made. Next an investigation is taking place on how the thickness of the hyperelastic material affects the results while the velocity of the impacting mass is constant and equal to 20 m/s. A comparison of the various results and a general conclusion is provided. Also an effort has been made to validate some preliminary tests that took place in the laboratory for the blast actuator with an aluminium cylindrical specimen. Finally, a few more calculations have been made for a bigger column that is closer to the ones used in a real structure; such a column is similar to the ones that will be tested in the final configuration.

3.1 Definition of outputs

Before presenting the results it is preferable to define the type and the location of the outputs. Since the basic objective of the blast actuator is to apply to the specimen an impact load that can represent a real explosive load, the first output should be the pressure field applied from the impacting mass on the column. This can be achieved after the summation of all the contact force time histories on the surface of the column that interacts (see Figure 14) with the impacting mass. Then this quantity is divided by the area of the selected surface and the pressure profile is calculated. The integration of the pressure history can give the impulse history of the contact forces which is also a very important output.

The pressure profile and the impulse of the load produced from the impact of the blast actuator apparatus are compared with the ones derived from an ideal blast load with the same characteristics. From each simulation a pressure profile is produced, from this profile two important data are exported the peak pressure and the impulse. From these two quantities the loading curve for a blast load can be calculated according to [12], [13], [14]formulation.

The calculation of the equivalent blast load is performed with the association of a fortran routine called *AIRB* (see[15], [16]). This routine can be used independently to calculate the loading data of an explosion but it is also integrated in EUROPLEXUS in order to be used in the simulation of blast events. For every simulation apart from the curve of an ideal blast load also a table is provided with some parameters that are easier for the reader to understand. This table contains the scaled distance Z, a quantity which is characteristic for every detonating event and the standoff distance of a 1000 kg

TNT. The standoff distance is the location where a certain amount of TNT should be placed in order to produce a desired load.

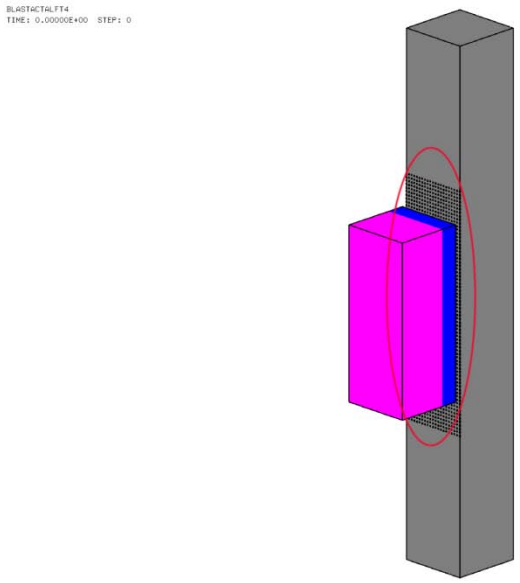

Figure 14: Definition of the area on the column that interacts with the impacting mass

Apart from the pressure profile and the impulse, outputs like displacements, velocities, stresses, strains etc. can give valuable information about the mechanics of the phenomenon. It is important to define the locations of the outputs that are presented later on. The main output points are the ones that are defined by the intersection of the x-axis of the model with the surfaces of the several parts of the structure. Practically, these points are located on the barycentre of each surface of the structure that is vertical to the axis of the movement of the impacting mass. Figure 15 depicts the location and Table 10 presents an overview of the output points.

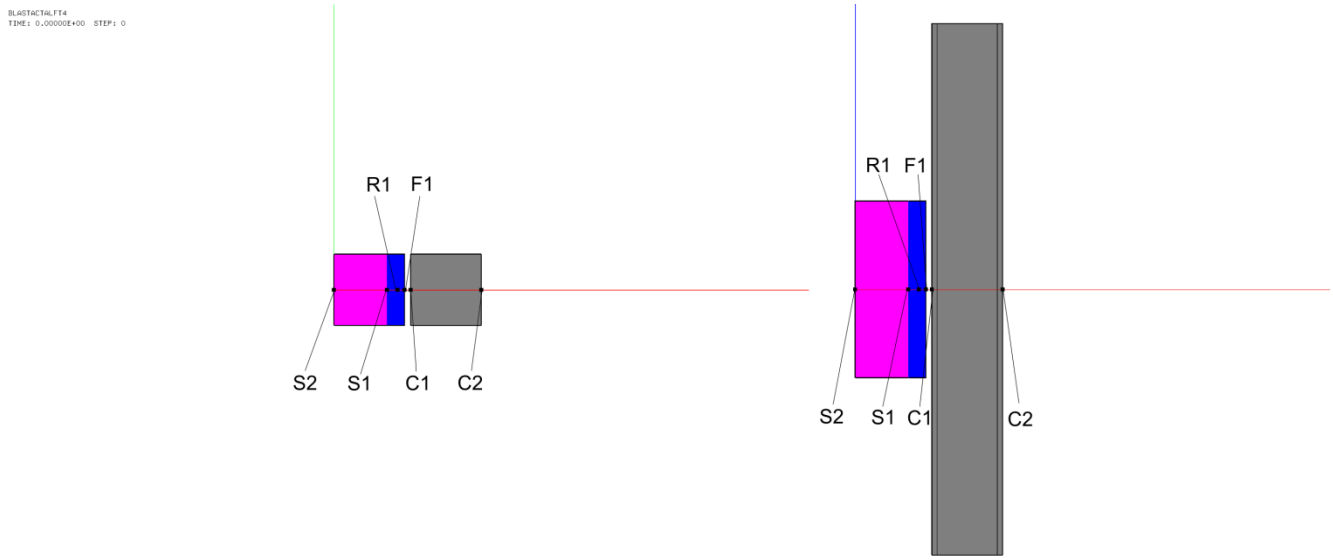

Figure 15: Definition of the output points

Table 10: Description of the location of the output points

Name	Object	Material	Location
C1	column	concrete	barycentre of the frontal surface (contact interface)
C2	column	concrete	barycentre of the rear surface
F1	impactor	hyperelastic	barycentre of the surface that interacts with the column
R1	impactor	hyperelastic	barycentre of the surface in the middle layer of the hyperelastic material, a surface that is parallel to the previous one
S1	impactor	aluminium	barycentre of the interface between the aluminium and the hyperelastic material
S2	impactor	aluminium	barycentre of frontal surface

In most of the calculations the displacements and the velocities in the x-direction for all the output points are presented because these data are the most critical for the understanding of the phenomenon. The z-directions displacements of the two concrete points are presented in order to show the deformation of the specimen. Another important output for the current study is the x-direction stresses and strains of the hyperelastic material on the contact interface (F1). In some cases also the loss of the mass of the concrete column has been discussed as a damage indicator. The finite element graphical representation of the final state of the model is presented for all the cases in order to compare the several simulations and to identify the damage of the column.

3.2 Material study

3.2.1 Without hyperelastic layer

In the first set of results for the blast actuator model the impacting mass consists only of aluminium; the hyperelastic layer is not included. This kind of simulation took place in order to prove the necessity of a hyperelastic layer on the contact interface.

Figure 16 depicts the pressure and the impulse profile of the load produced from the direct impact of the aluminium mass to the specimen. The produced pressure load increases rapidly and then goes to zero again very fast. This load is similar to a blast load as it can be shown from the curve of ideal load, but it is very acute load with very small duration (around 0.3 ms). This type of impact loads refers to very small scaled distance blast as it can be shown in Table 11. This means that the standoff distance

for the explosion of 1000 kg of TNT is 2.65 m which is very close to the specimen. If someone wants to produce different type of blast loads, this is almost impossible without an additional material layer.

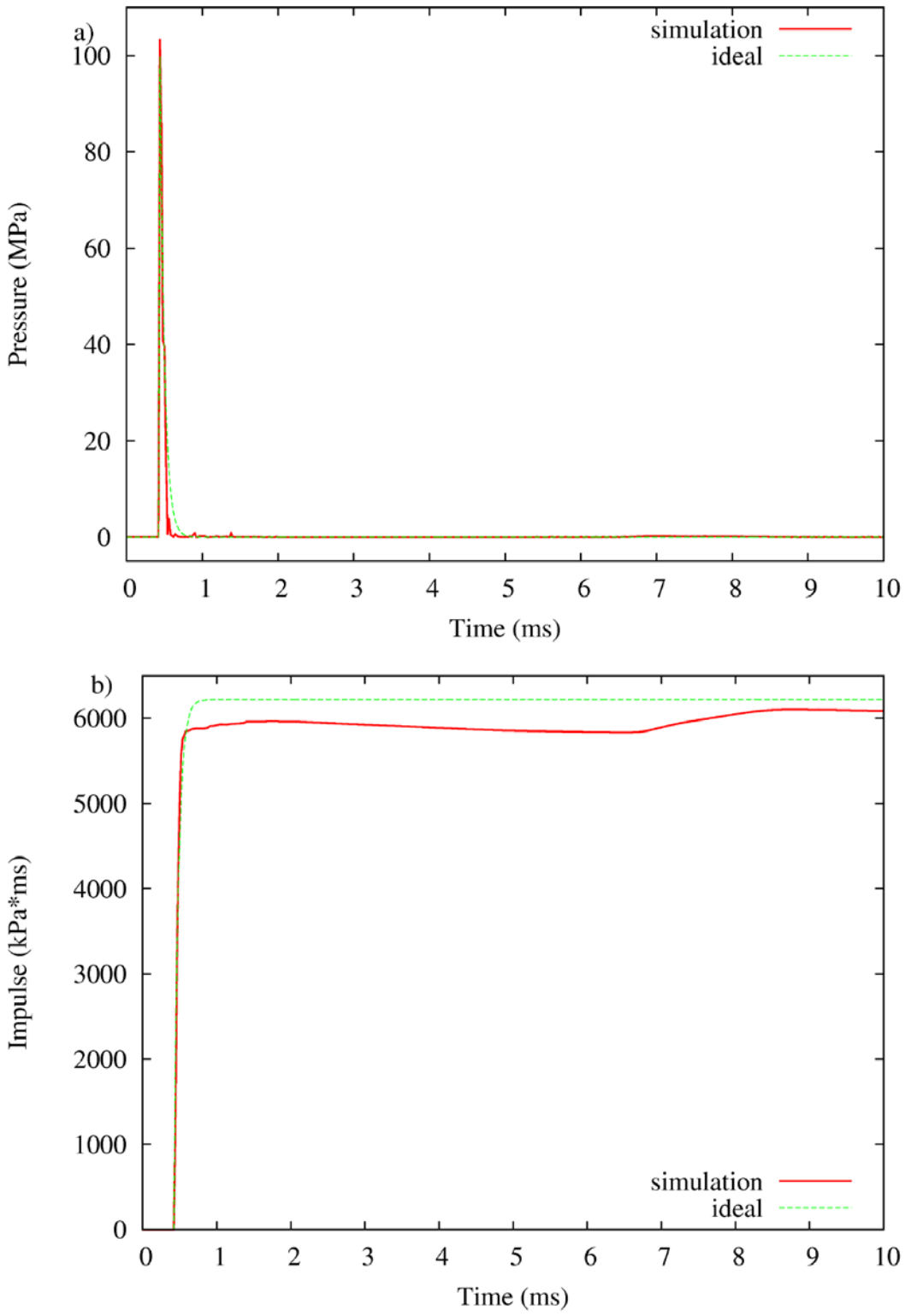

Figure 16: Pressure and Impulse profile for aluminium material

Table 11: Blast data for the impactor without any hyperelastic layer

Peak pressure [MPa]	Impulse [kPa*ms]	Z [m/kg$^{1/3}$]	Standoff [m]	Charge mass [kg]
103	6100	0.265	2.65	1000

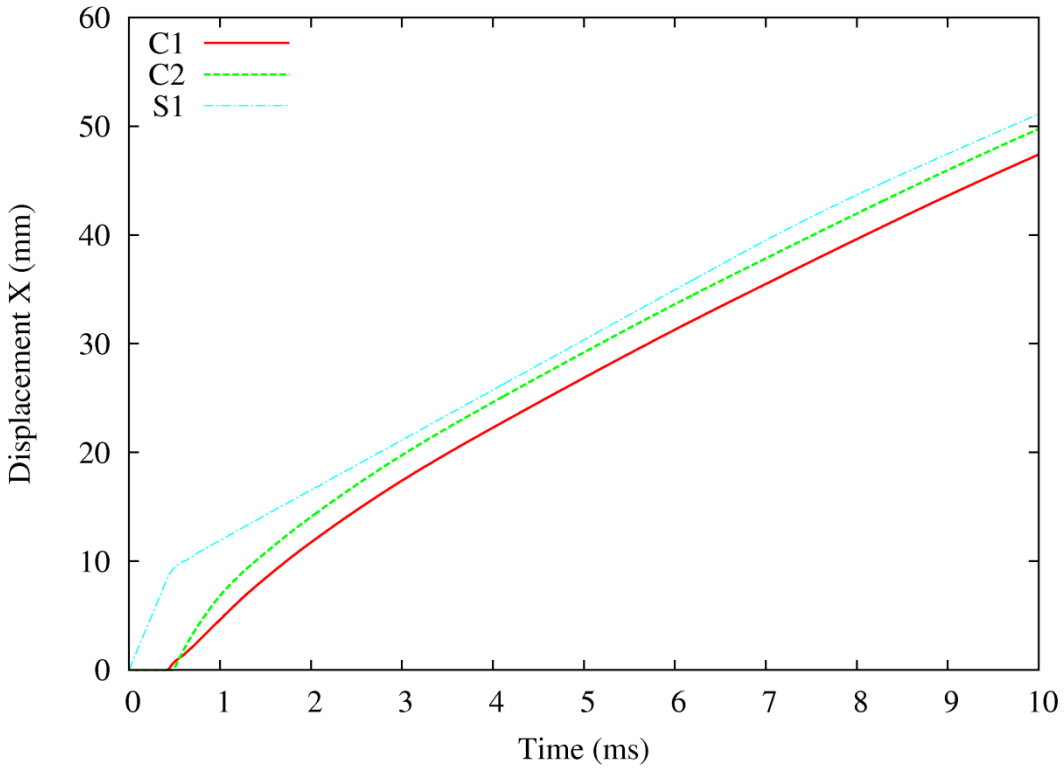

Figure 17: Displacement profile in the X-direction for several points of the model

From Figure 17 and Figure 19 it is obvious that the impactor hits the column and then travels in the same direction with almost the same velocity as the middle part of the specimen. The damage of the column is significant and the only way to reduce the load is to decrease the impact velocity. This restrains the performance of the blast actuator to a small range of explosive loads. Moreover, the direct impact of the aluminium onto the specimen might cause damage also to the impacting mass, which is not desired. The aluminium mass is weighted and calibrated for the experiment and it is preferable to be maintained sufficiently intact in order to be used for the several tests. Also for this reason it is required to be protected with a layer of a disposable and cheap material.

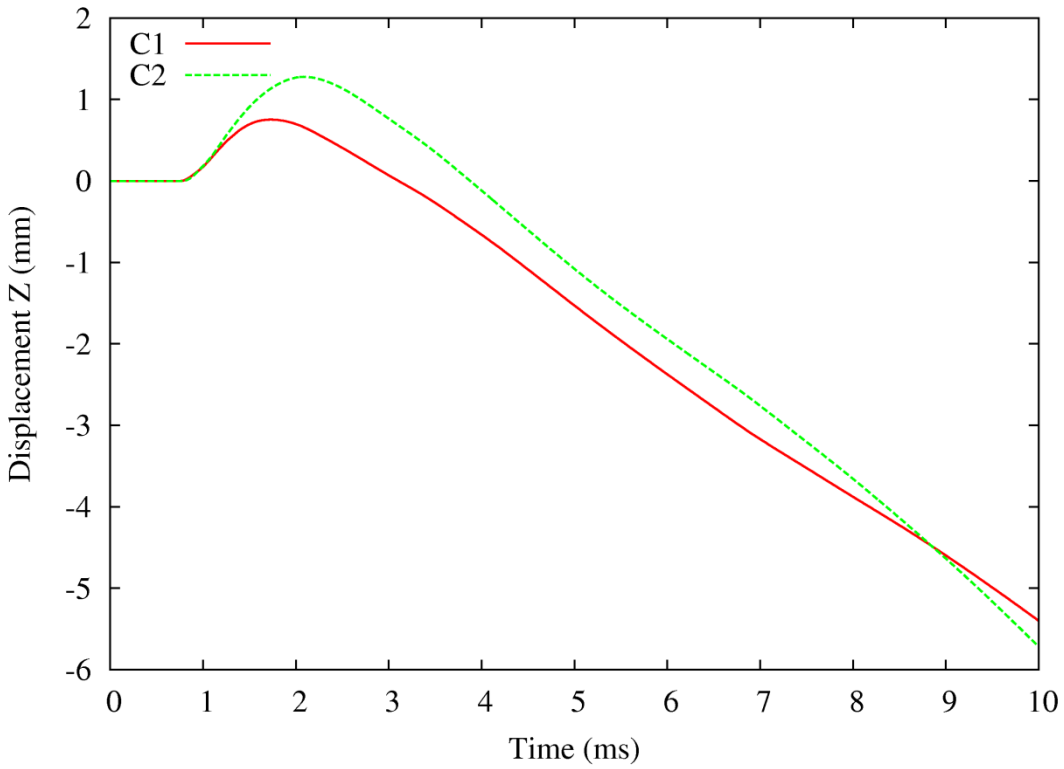

Figure 18: Displacement profile in the Z-direction for points on the spacemen

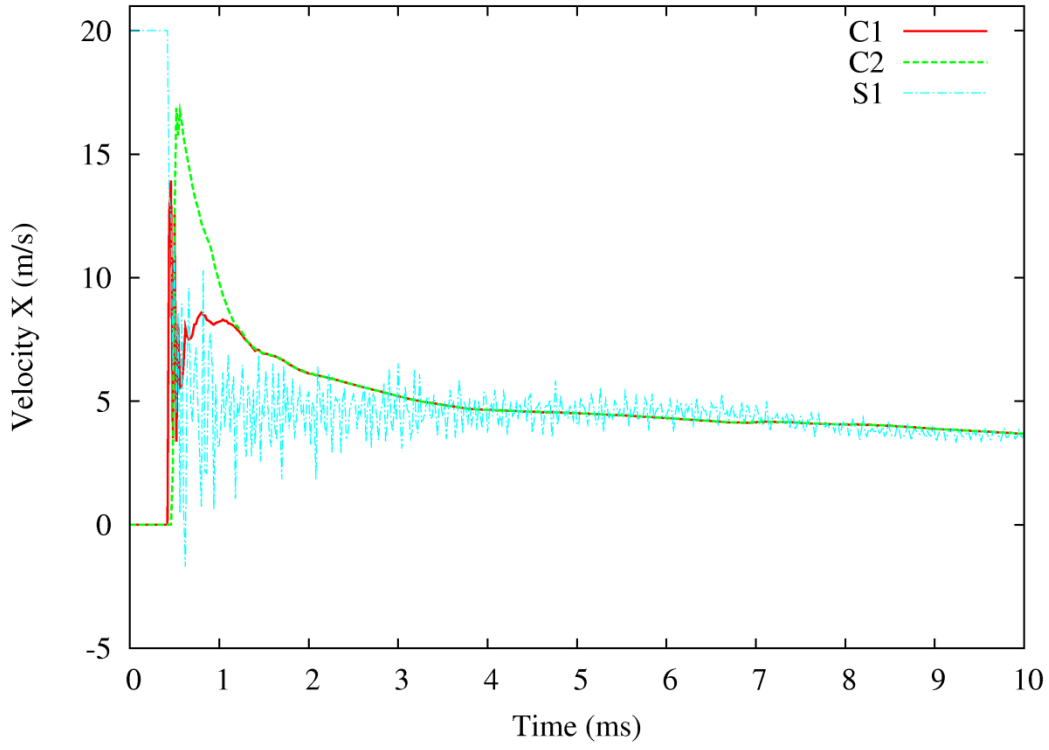

Figure 19: Velocity profile in the X-direction for several points on the model

3.2.2 Rubber material

The first material that is found and tested in the laboratory to serve as the interlayer between the metallic part of the impacting mass and the specimen is the rubber like material presented in 2.5.4.1. Figure 20 depicts the pressure profile of the impacting load on the column and its impulse. There is also a comparison with an ideal blast load with similar characteristics as shown in Table 12.

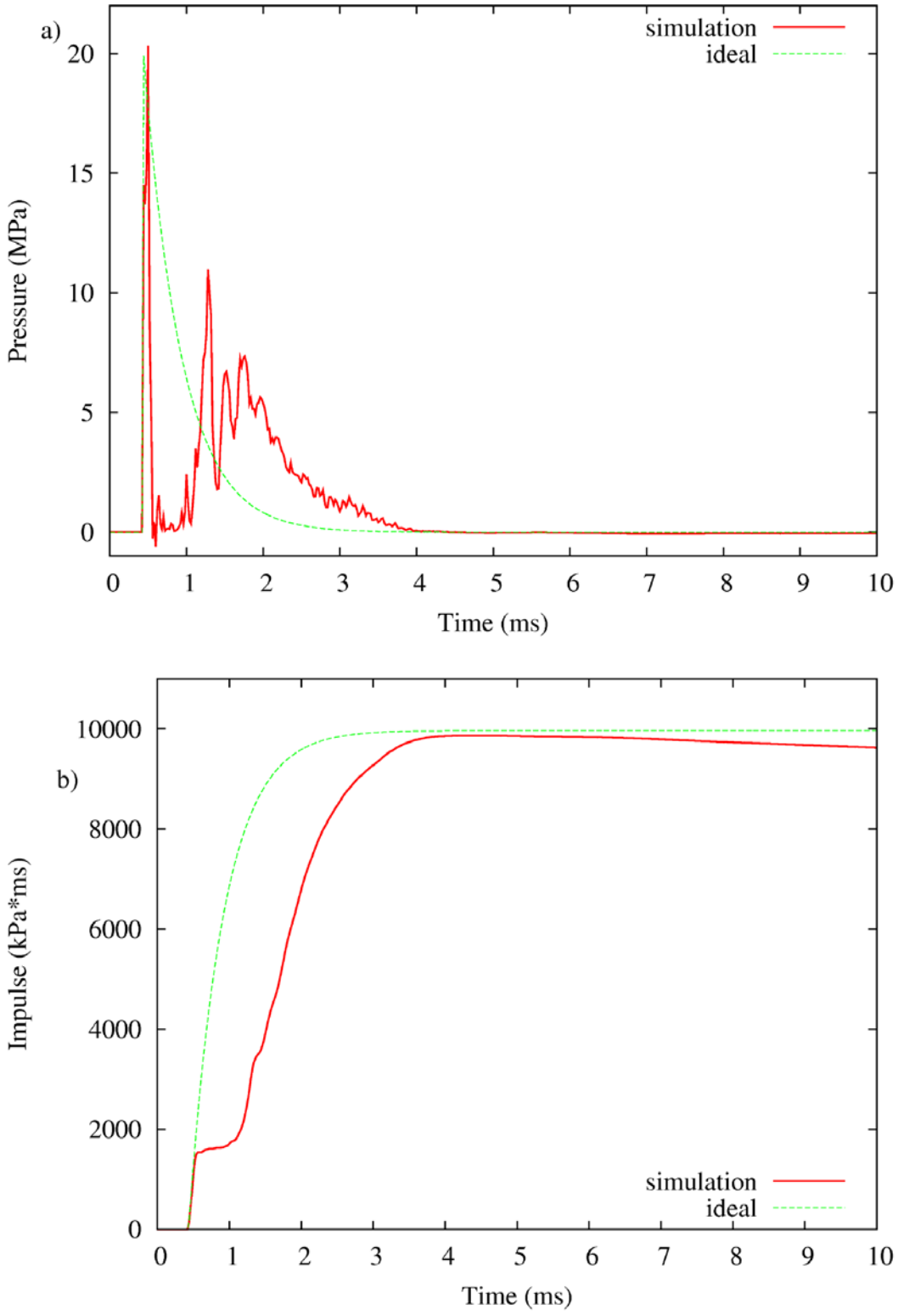

Figure 20: Pressure and Impulse profile for rubber material

Table 12: Blast data for rubber material interlayer

Peak pressure [MPa]	Impulse [kPa*ms]	Z [m/kg$^{1/3}$]	Standoff [m]	Charge mass [kg]
20.31	9869	0.592	5.92	1000

In this case the peak pressure is 20.31 MPa and the impulse 9869 kPa*ms data that refer to a blast load with Z=0.592. The load now is weaker than the previous one and also the duration is much bigger since it is around 3.5 ms. The duration of the load is bigger because of the rubber interlayer, that makes the impact between the two bodies softer. Also the final phase of the impact load fades out gradually without being very abrupt and this corresponds to a blast load with Z > 0.5.

On the other hand there is a remarkable difference between the actual impact load and the ideal blast load. This difference has to do with the profile of the load which after the first contact between the rubber interlayer and the concrete is decreased to zero and then increased again to around 10 MPa. This discrepancy is also evident in the impulse profile where in the case of the impacting load at the beginning rises and then it is constant for almost 0.8 ms.

This phenomenon is due to the oscillations of the rubber interlayer, as it can be observed also from Figure 21 and Figure 23. From the blue curve that refers to the point F1, which lies on rubber material on the centre of the contact interface, it is clear that after the first contact the rubber interface oscillates, moves back and is detached from the concrete surface. So until it comes to contact again with the specimen the contact force is nearly zero. When the rubber interlayer gets in contact with the concrete surface, it oscillates again but now the phenomenon is much smoother and the load from this point until the end is very close to the ideal one.

Figure 24 and Figure 25 show the strain and the stress respectively of the rubber material in the x-direction on the centre of the contact interface. The interruption of the contact load during the period that the rubber layer oscillates and detaches from the concrete surface can be observed on the stress time history. From the strain curve it can be pointed out that the rubber interlayer is compressed until a value of 0.6 and then it vibrates until it gets also positive values of stretch.

From the oscillating behaviour of the rubber interlayer it can be concluded that this type of material is not the most appropriate to be used in the blast actuator. The contact load that is produced diverges significantly from the ideal blast load especially because of the discontinuity of the pressure profile after the first contact between the two bodies.

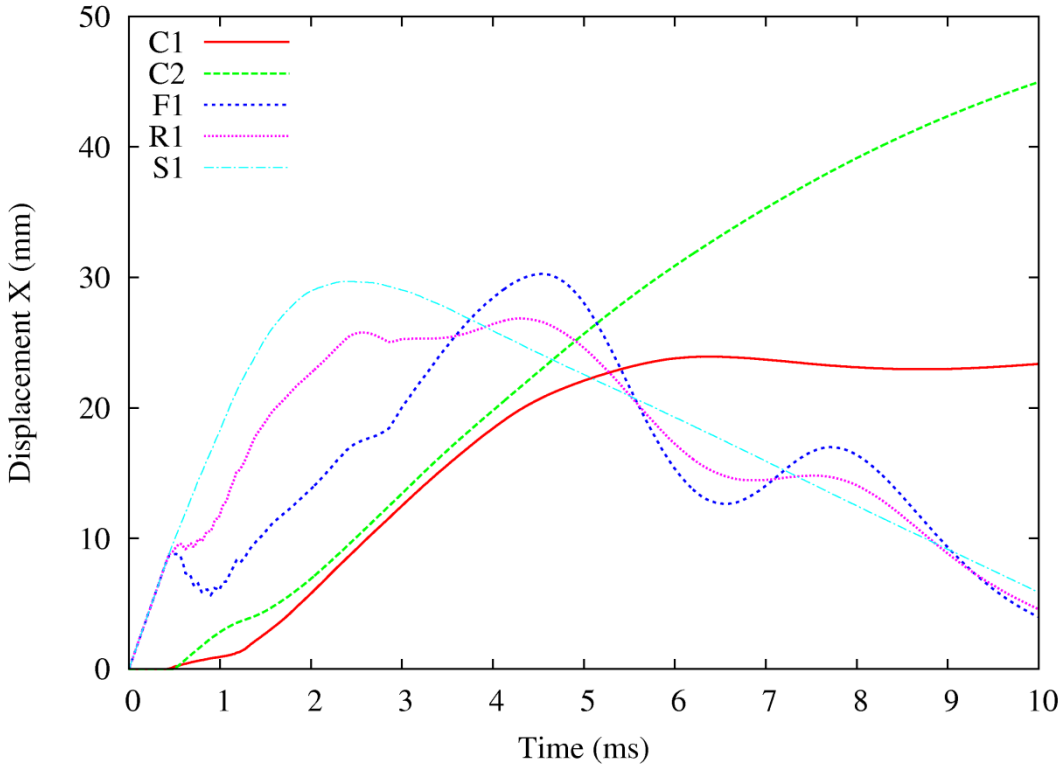

Figure 21: Displacement profile in the X-direction for several points (rubber material interlayer)

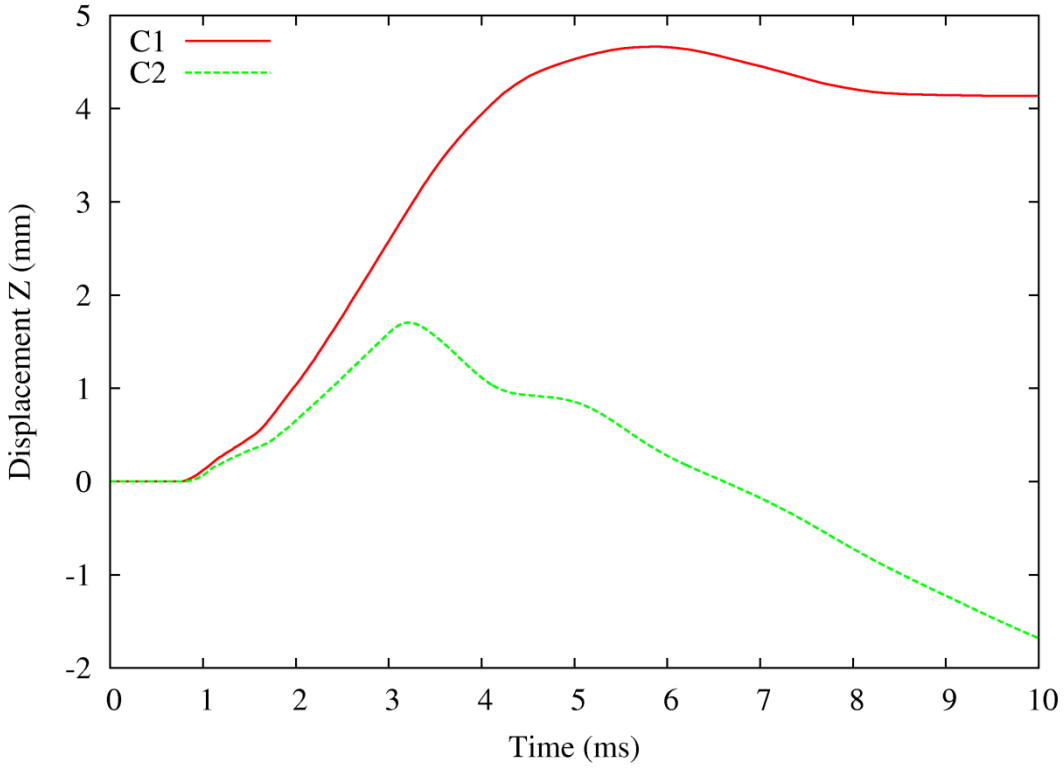

Figure 22: Displacement profile in the Z-direction for points on the specimen (rubber material interlayer)

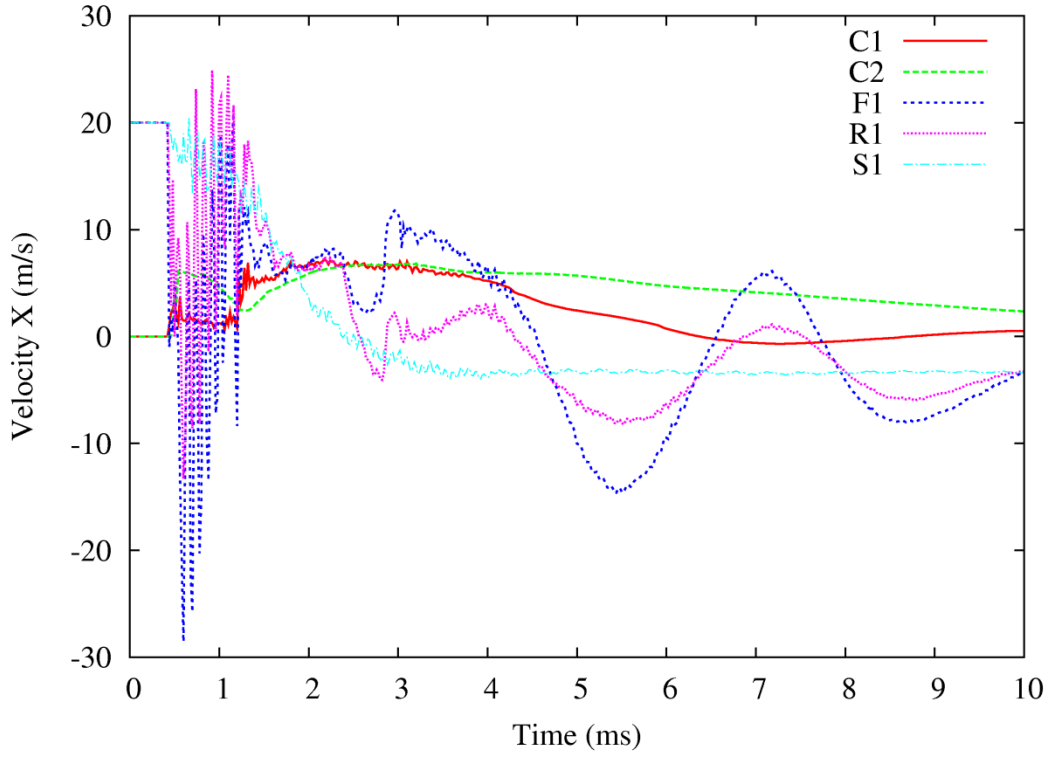

Figure 23: Velocity profile in the X-direction for several points (rubber material interlayer)

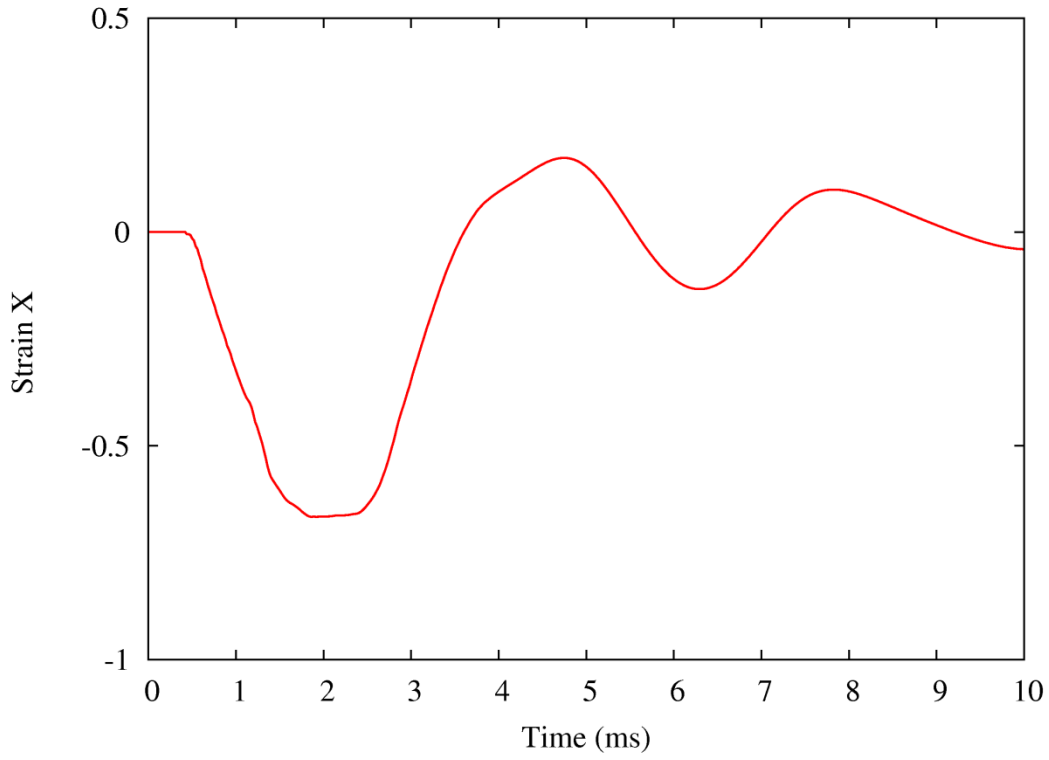

Figure 24: Strains in the X-direction for rubber material on the interface

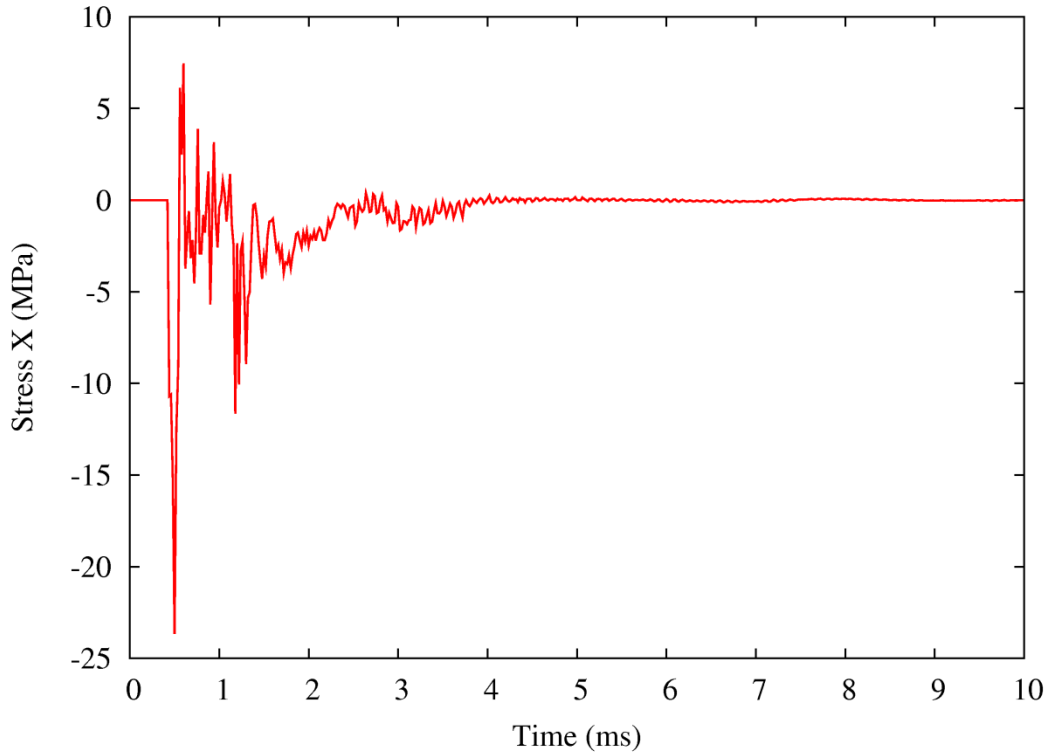

Figure 25: Stresses in the X-direction for rubber material on the interface

3.2.3 Elastic foam material

The second material that is under investigation for the hyperelastic interlayer of the impacting mass is the elastic foam material presented in 2.5.4.2. Figure 26 depicts the pressure and the impulse profile of the impact load produced from the collision of the impacting mass on the specimen. The peak pressure is of the order of 29 MPa and the impulse is 10373 kPa*ms. These data corresponds to an ideal blast load with Z=0.506, or to a standoff distance of 5.06 m for the detonation of 1000 kg of TNT.

The pressure time history produced from the contact of the impacting mass with the elastic foam interlayer on the specimen is very close to the ideal blast curve. The accordance is really good also in the case of the impulse profile. The impacting load increases very fast and reaches the maximum value. The rise of the load is not so abrupt as in the previous cases since the elastic foam layer makes the contact load smoother but as it can also be observed from the impulse profile the difference in that initial phase is not significant. The pressure after reaching its peak it fades out fast but on a smoother way than in the case where the impacting mass had no hyperelastic interlayer. The total duration of the load is almost 2 ms which is normal for the equivalent blast load.

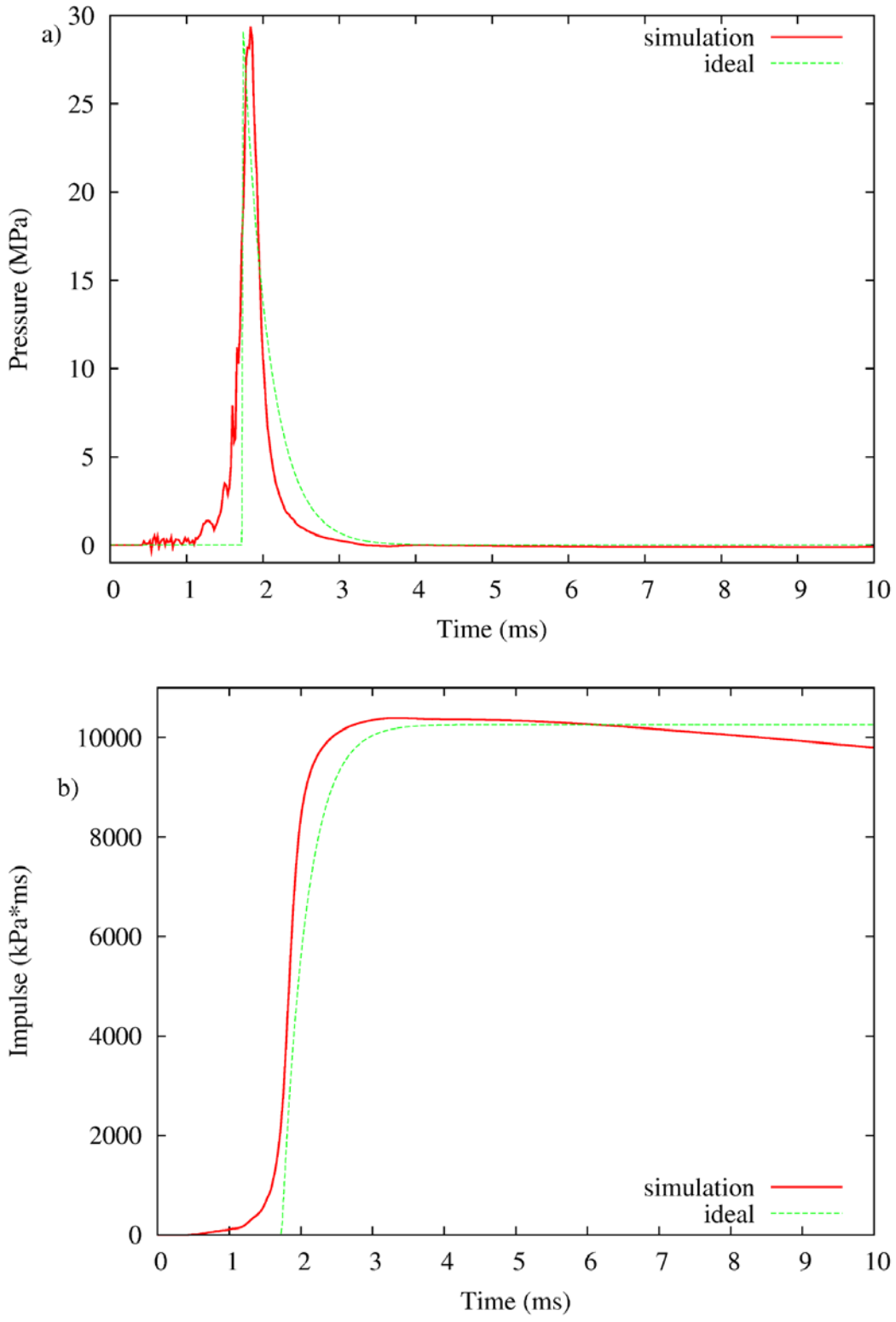

Figure 26: Pressure and Impulse profile for elastic foam material interlayer

Table 13: Blast data for elastic foam material interlayer

Peak pressure [MPa]	Impulse [kPa*ms]	Z [m/kg$^{1/3}$]	Standoff [m]	Charge mass [kg]
29.37	10373	0.506	5.06	1000

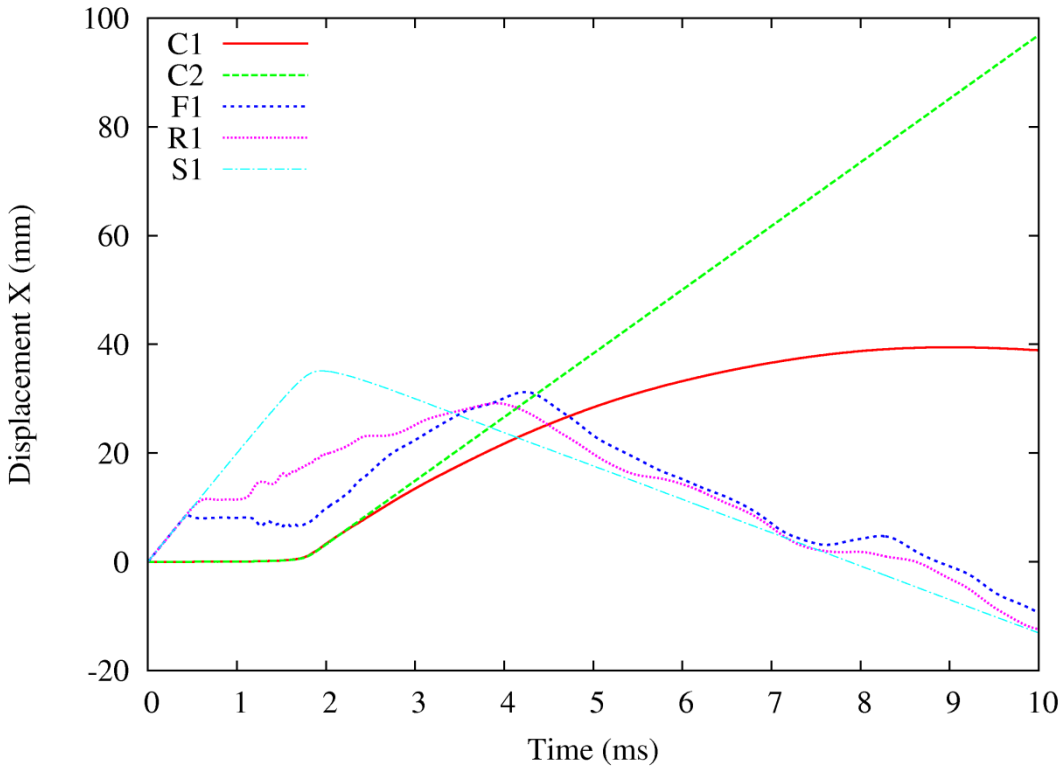

Figure 27: Displacement profile in the X-direction for several points (elastic foam material interlayer)

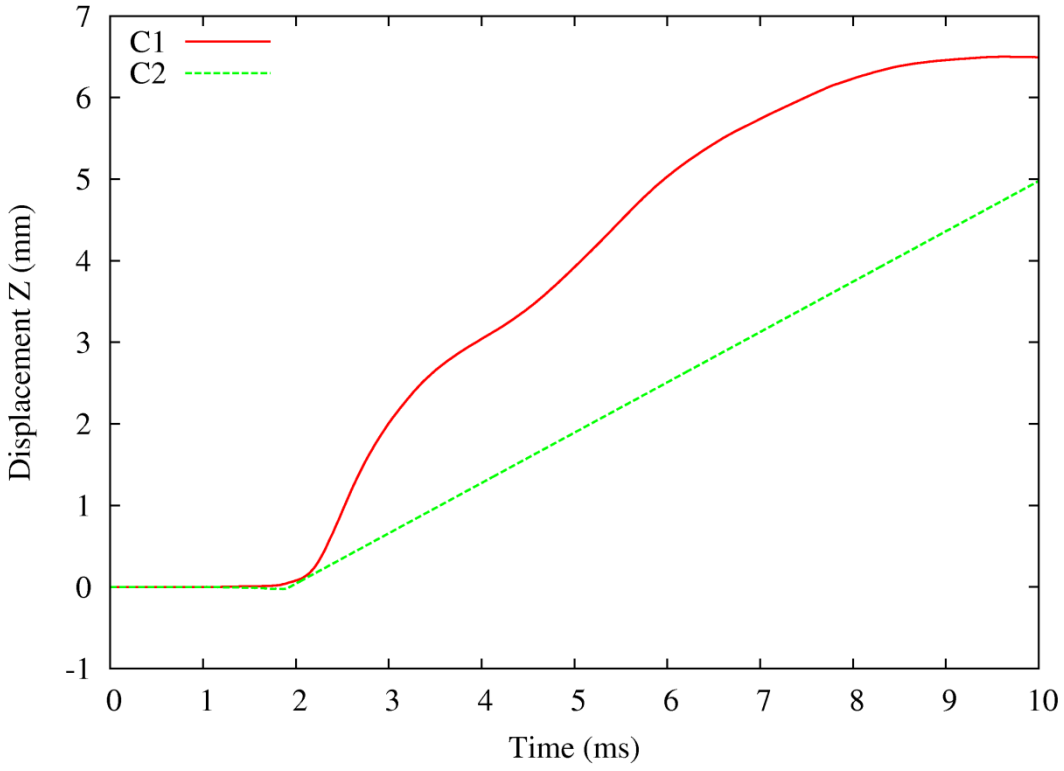

Figure 28: Displacement profile in the Z-direction for points on the specimen (elastic foam material interlayer)

Figure 27 presents the x-direction displacements on several points on the model under consideration. It can be pointed out that the elastic foam layer after the first contact starts to shrink until the maximum level where all the pores are closed. Then the aluminium mass starts pushing the concrete surface through the elastic foam interlayer and the contact force reaches its peak. Then the aluminium impacting mass rebounds while the foam interlayer starts to gain its original shape again. The displacement on the middle of the contact interface of the reinforced concrete column is reaching 40 mm. The displacement on the rear part, as shown the figure, is much bigger. However, this is misleading since that particular point is eroded and transformed into flying debris and it is travelling with a constant velocity, as it can be observed from Figure 29.

The most important characteristic of the elastic foam interlayer is that it does not oscillate during the contact phase and that is why the load is close to the desired one without discontinuities. The elastic foam material can undergo higher compressive strains than the rubber material and that is depicted in Figure 30. The strains in the x-direction of the foam material in the contact interface are going up to 0.8 for the face where the layer is being shrinked to the maximum level. Also from Figure 31 it is clear that stresses in the x-direction for the elastic foam layer are having a peak on the same time instant when the pressure time history is reaching its own peak and there are no significant oscillations on that quantity.

The behaviour of the elastic foam layer is really sufficient to associate the metallic part of the impacting mass in the representation of a blast load. In that point it is interesting to make a comparison of the results obtained from the two different meshes, the fine and the coarse one. Until now all the results refer to the fine mesh but Figure 32 presents the pressure time history calculations from both types of mesh. The two pressure profiles are very close, which means that even the coarse mesh can capture sufficiently the contact load. The drawback of the coarse mesh is that it is not able to represent accurately the response of the reinforced concrete column and this is depicted in Figure 33.

That figure shows a sideway view of the final state of the simulation for the two different models. In both models the impacting mass is in the rebound phase and the elastic foam layer has gained its original shape. The damage on the column is much higher in the case of the coarse mesh and this is not surprising since the modelling of the erosion of the elements needs a fine mesh.

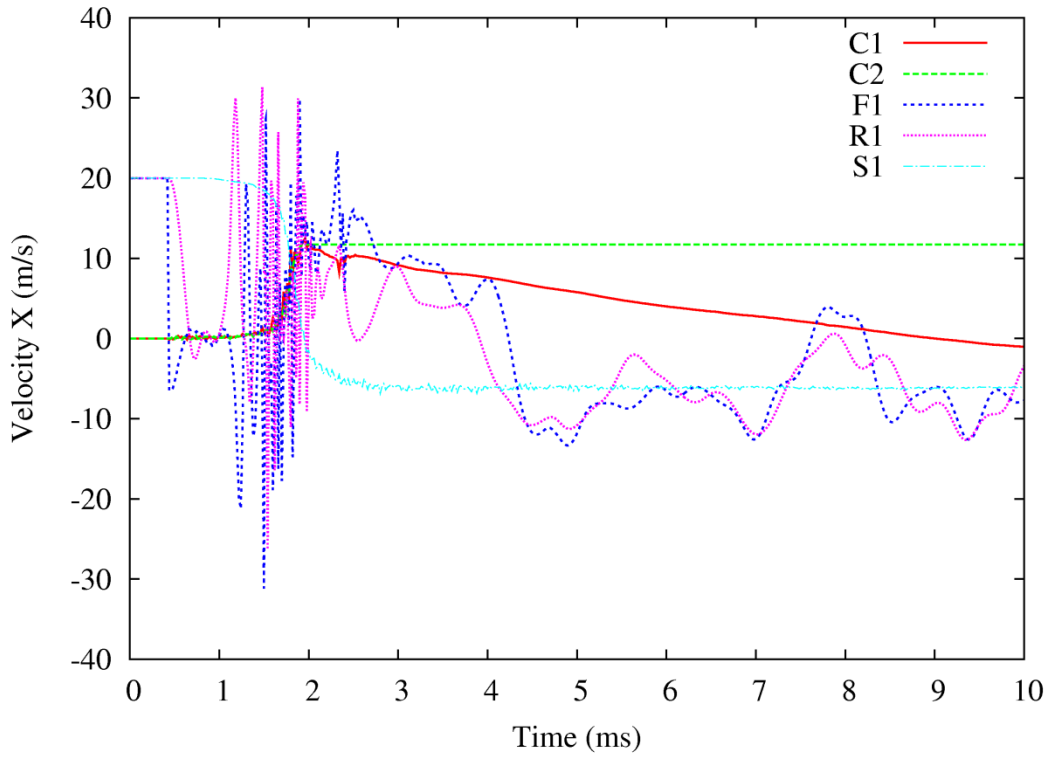

Figure 29: Velocity profile in the X-direction for several points (elastic foam material interlayer)

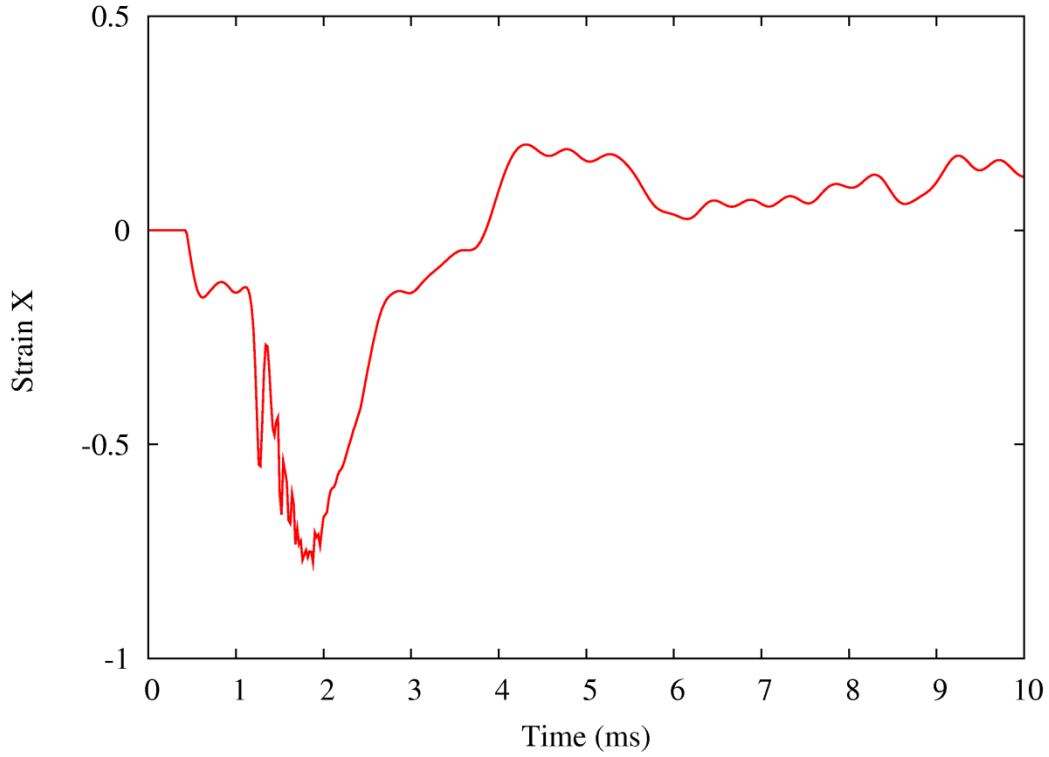

Figure 30: Strains in the X-direction for the elastic foam material on the interface

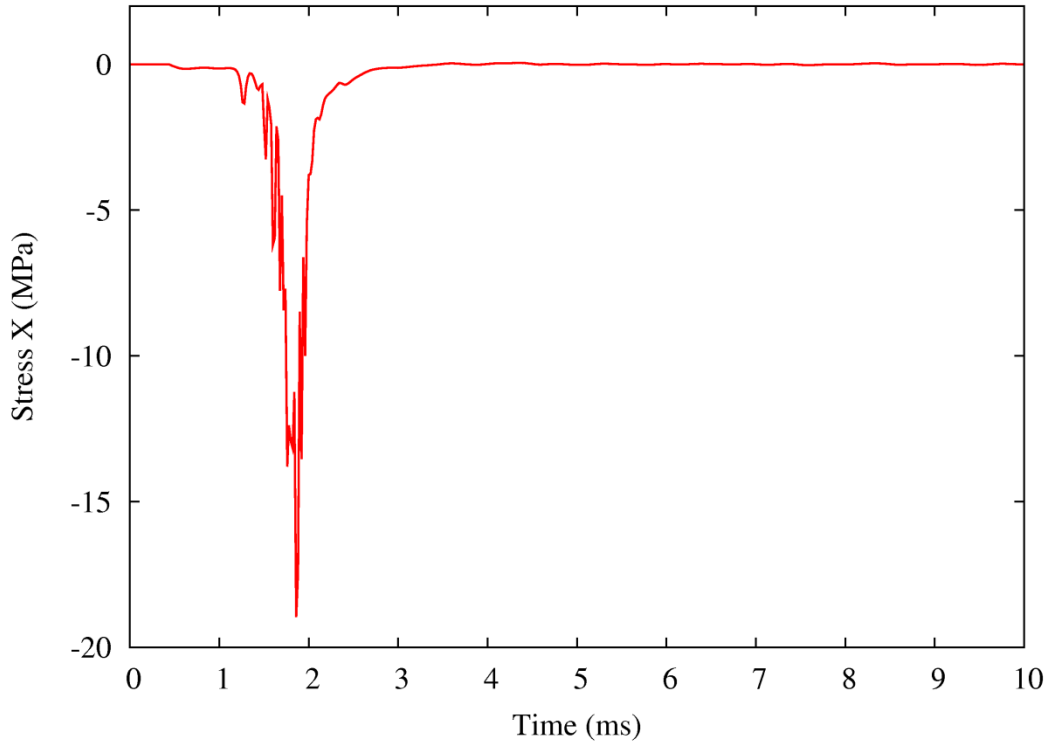

Figure 31: Stresses in the X-direction for the elastic foam material on the interface

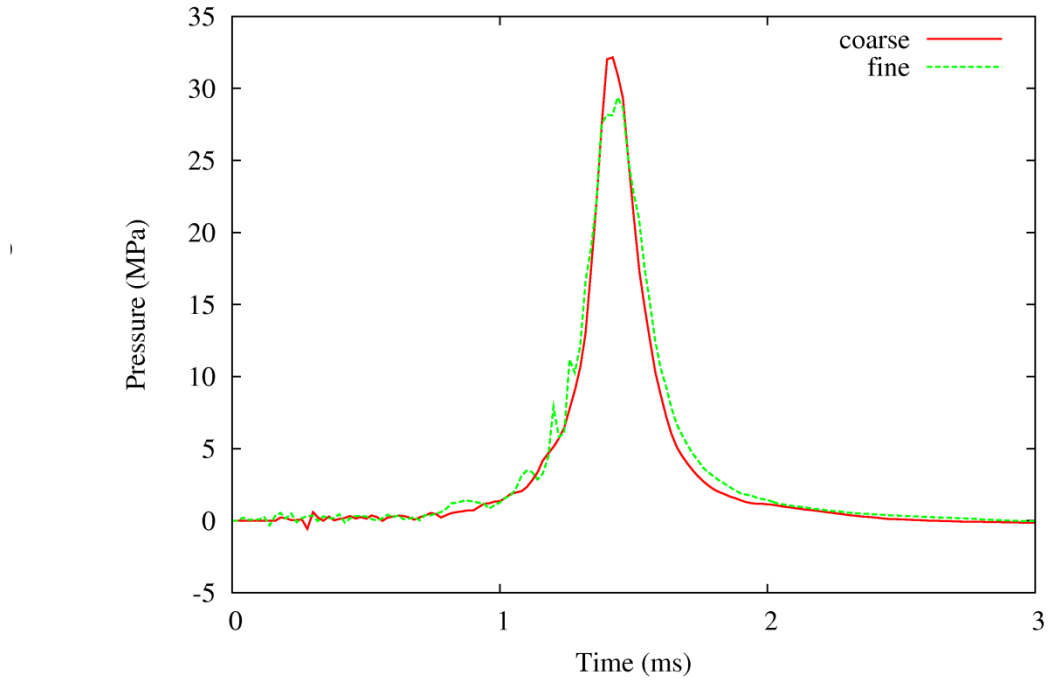

Figure 32: Comparison between the coarse and the fine mesh for the output pressure profiles

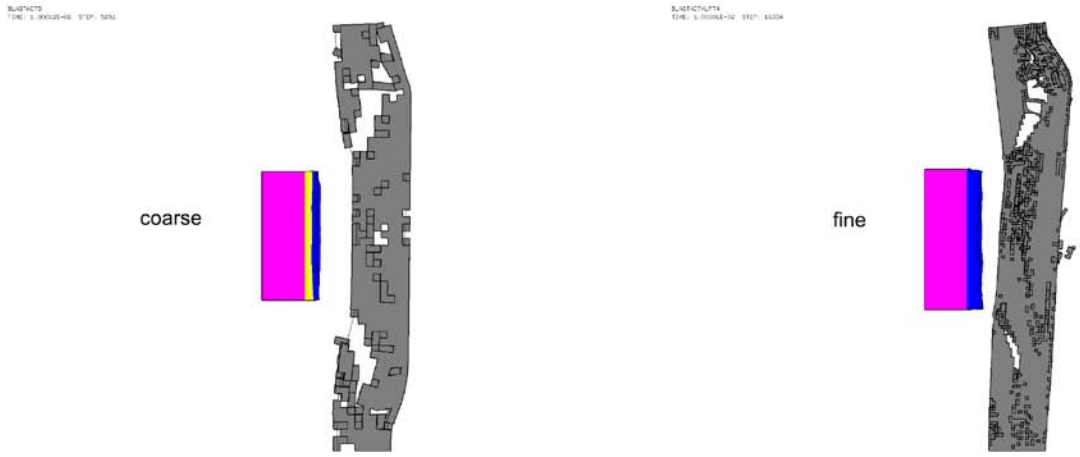

Figure 33: Comparison of the final state for the coarse fine meshes

3.2.4 Aluminium foam material

As already mentioned three different type of aluminium foam material have been tested. The main characteristics that change between the different types are the initial Young modulus. Figure 34 depicts the time history and the impulse of impact load on the surface of the specimen for the type A aluminium foam material. The duration of the load is around 6 ms and the peak pressure is 4.85 MPa while the impulse is 8370 kPa*ms. The comparison with the ideal blast load with the same characteristics shows that in the pressure profile there is a difference at the beginning of the excitation. The impact load rises abruptly to 0.8 MPa but then it reaches the peak pressure gradually after almost 3 ms. Then the impact load decreases very fast and after some small oscillations for 3 ms it fades out.

The profile of the impact pressure load can be explained from Figure 35 where the x-direction displacements of the objects participating in the simulations are presented. The first contact is taking place 0.44ms after the initiation of the calculation since this is the time that the impactor is travelling until it founds the target. At that time step the aluminium foam starts to shrink and pushes the concrete surface until the aluminium foam is taking its final state. Since the stiffness of that foam material is not that big its layer is diminished by 4 cm (squeezed). The duration of the squeeze affects the shape of the load profile and it makes it smoother in the initial part. This phenomenon leads to divergence from the ideal blast load since in that case the load should increase abruptly until it takes the peak pressure and then it attenuates gradually.

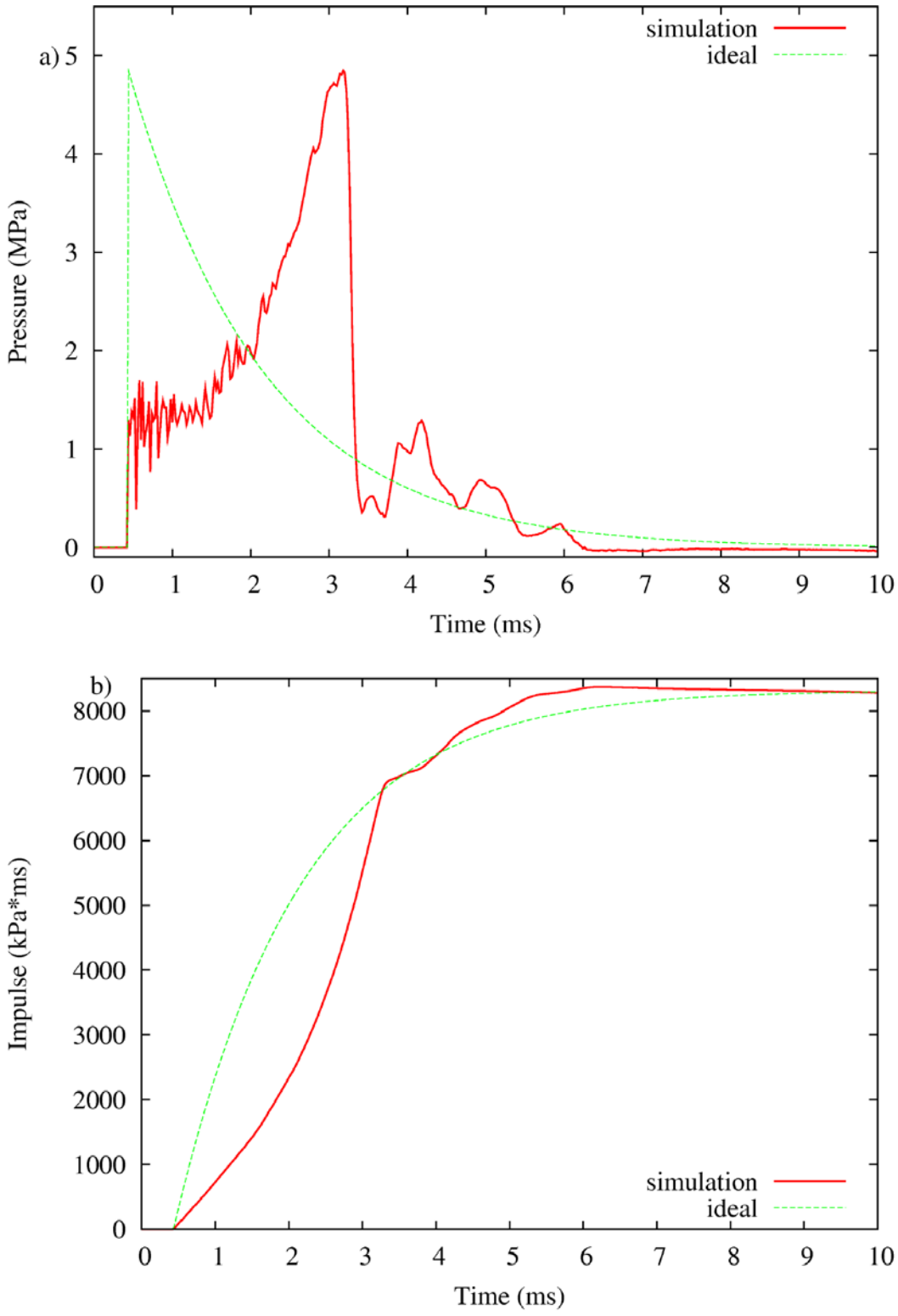

Figure 34: Pressure and Impulse profile for aluminium foam of type A

Table 14: Blast data for aluminium foam type A material interlayer

Peak pressure [MPa]	Impulse [kPa*ms]	Z [m/kg$^{1/3}$]	Standoff [m]	Charge mass [kg]
4.85	8370	1.011	10.11	1000

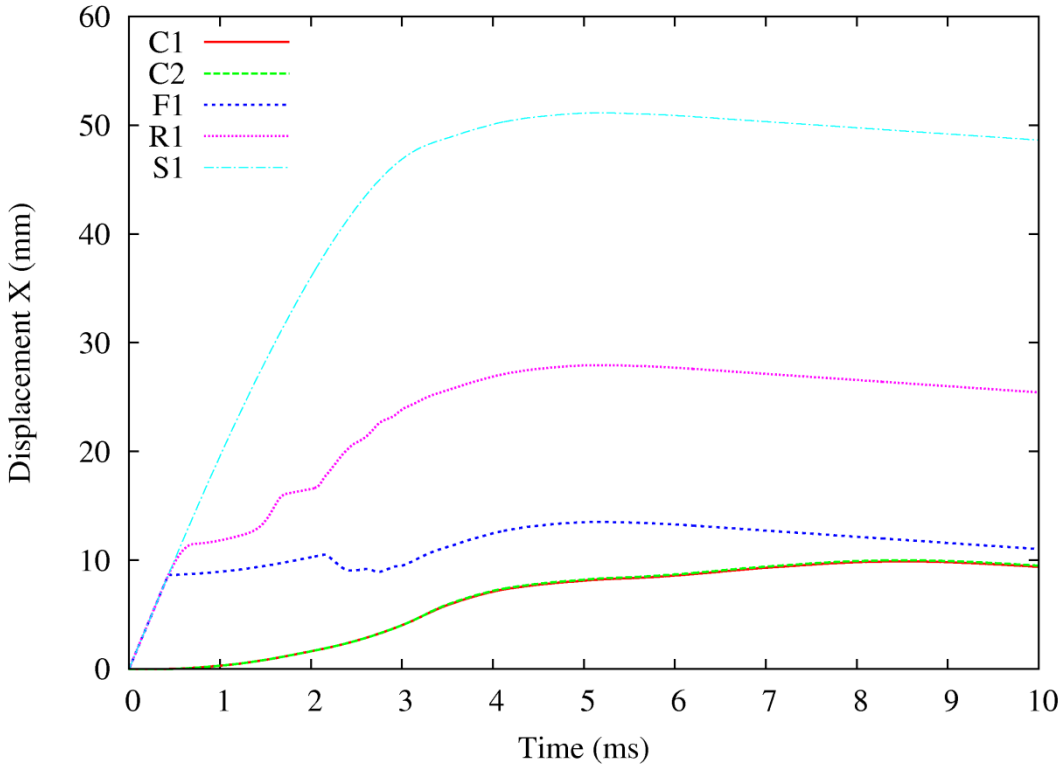

Figure 35: Displacement profile in the X-direction for several points (aluminium foam type A interlayer)

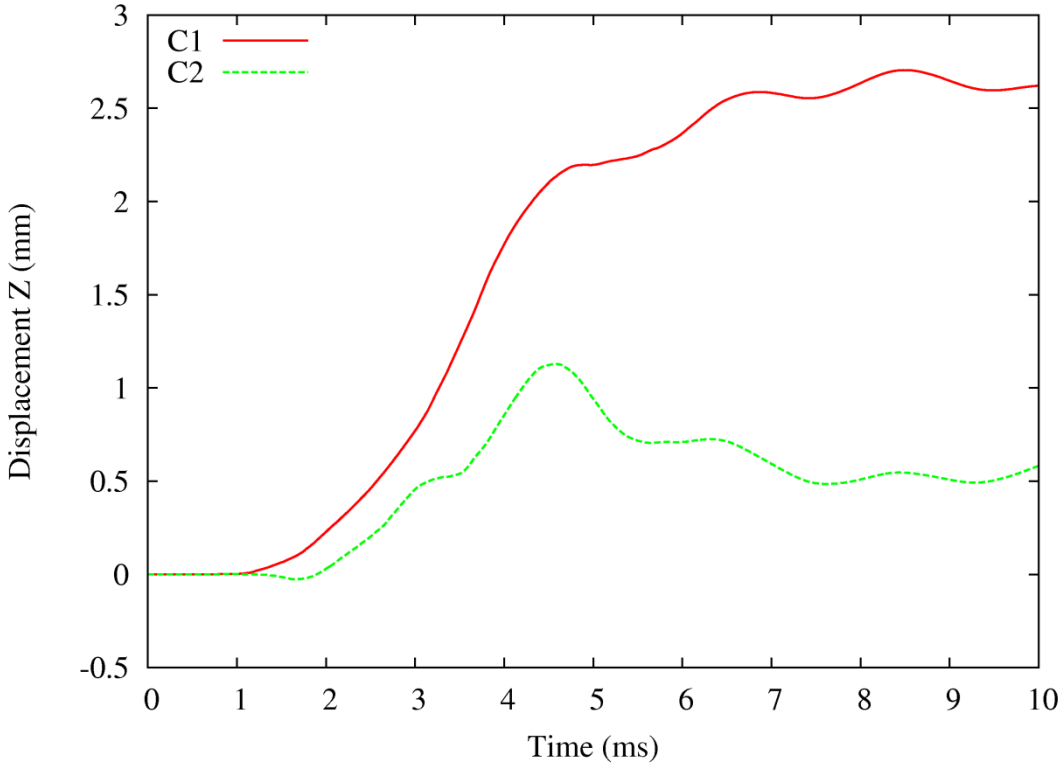

Figure 36: Displacement profile in the Z-direction for points on the specimen (aluminium foam type A interlayer)

From the displacement plot it can be observed that the final deflection of the column is around 9mmn and the final state of the column is depicted in Figure 48. In the specimen there is overall damage but not significant; Figure 47 depicts the mass loss of the concrete during the impact. The initial mass of the concrete was 144 kg and after the impact it goes to 127.45 kg, which corresponds to 11.45% of loss. The other figures present the x-direction velocity, the z-direction displacement.

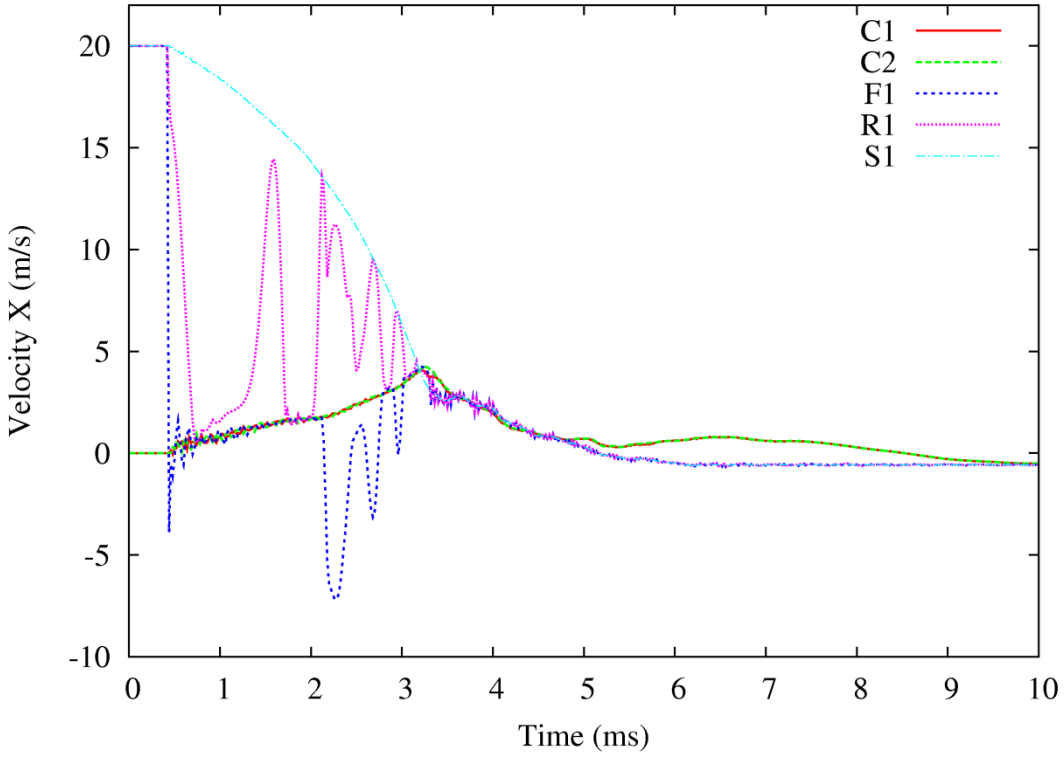

Figure 37: Velocity profile in the X-direction for several points (aluminium foam type A interlayer)

The type B aluminium foam material is stiffer than the previous one and this starts to modify the results of the impact. In that case the comparison between the impact pressure and the ideal one seems to give fewer differences. The impact load increases significantly at the beginning until it reaches the peak pressure. Then there is a small plateau for almost 1 ms where the pressure is nearly constant. At that phase the layer of the foam material decrease until it is taking its final state and then the pressure decreases rapidly and then oscillates a little until it goes to zero.

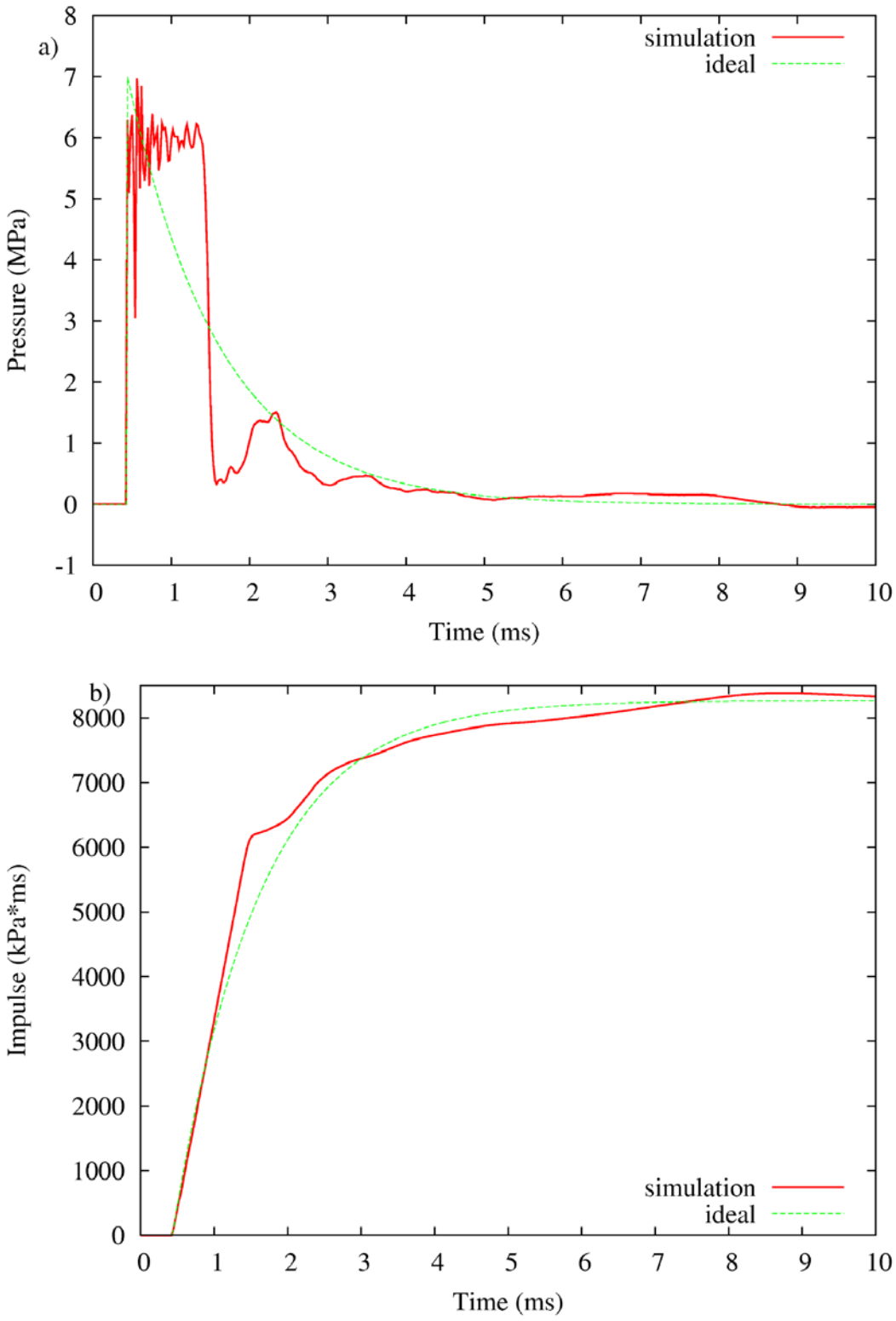

Figure 38: Pressure and Impulse profile for aluminium foam of type B interlayer

Table 15: Blast data for aluminium foam type B material interlayer

Peak pressure [MPa]	Impulse [kPa*ms]	Z [m/kg$^{1/3}$]	Standoff [m]	Charge mass [kg]
7	8370	0.889	8.89	1000

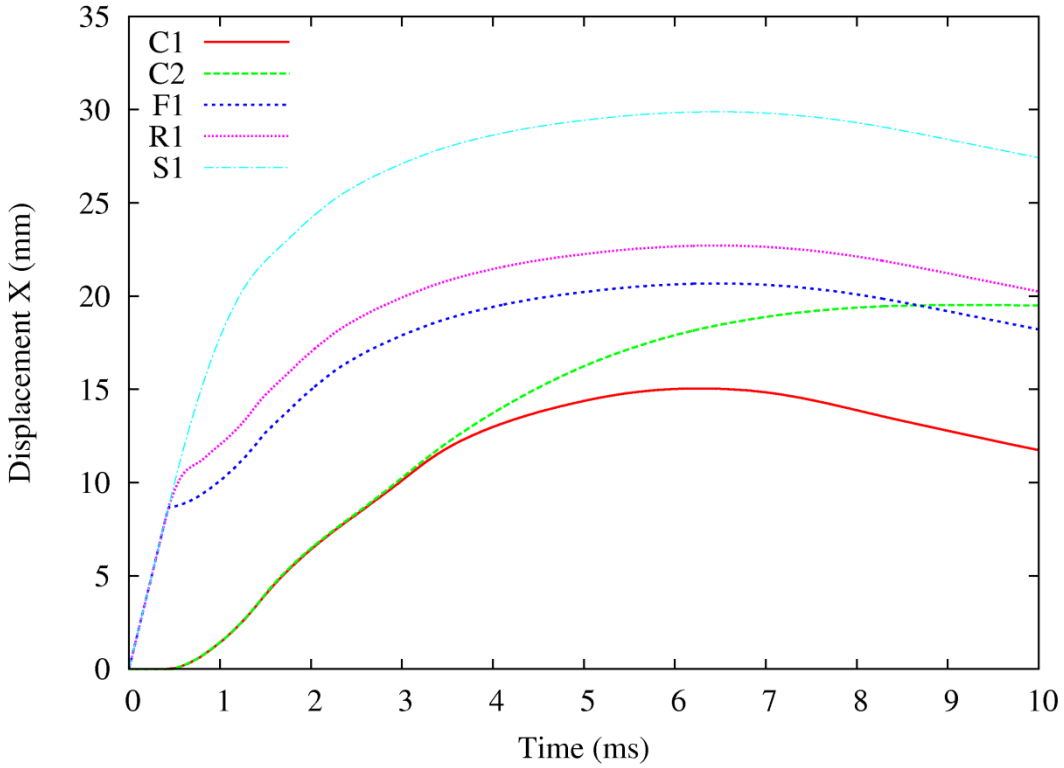

Figure 39: Displacement profile in the X-direction for several points (aluminium foam type B interlayer)

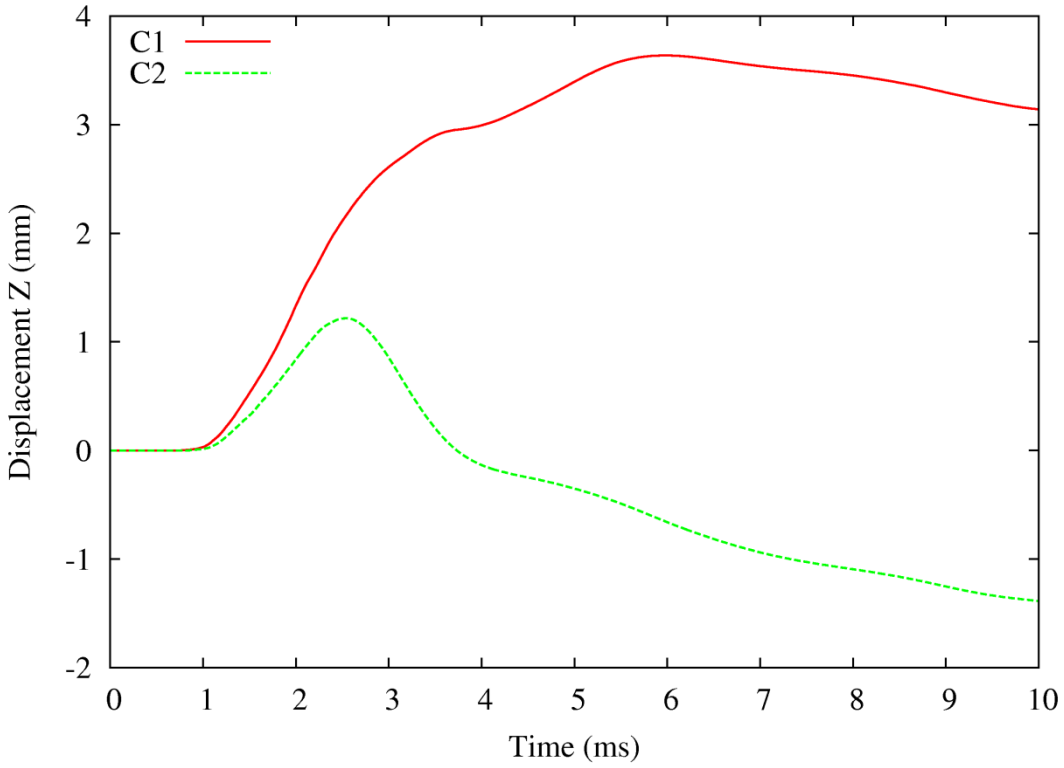

Figure 40: Displacement profile in the Z-direction for points on the specimen (aluminium foam type B interlayer)

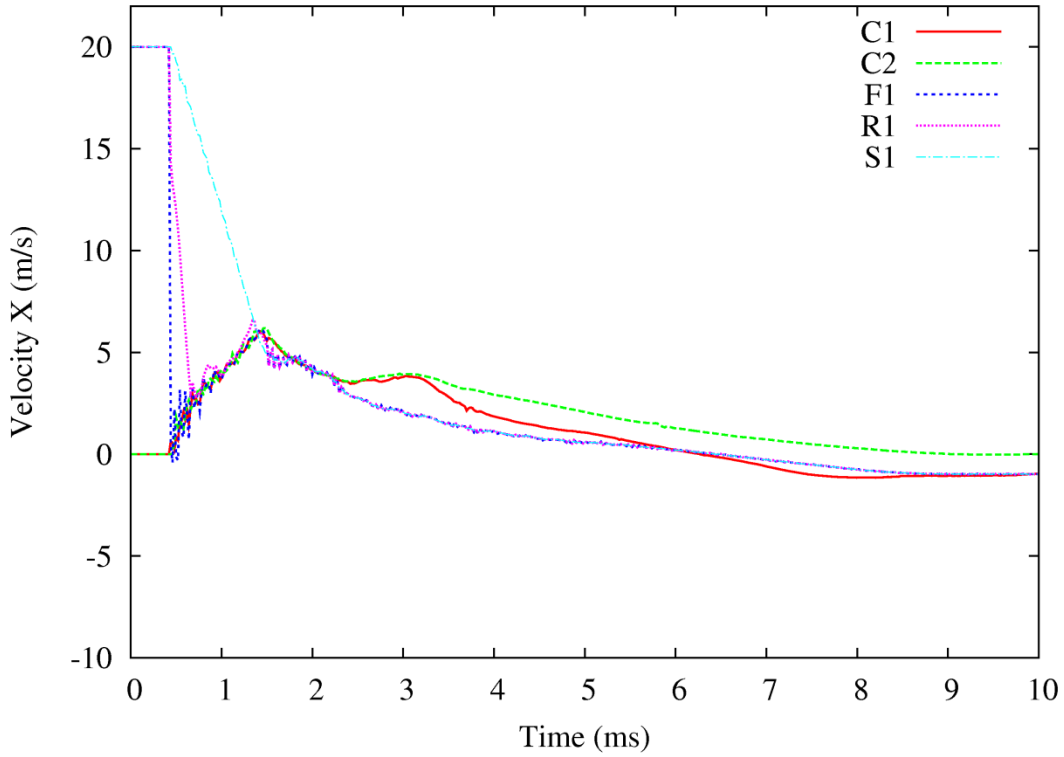

Figure 41: Velocity profile in the X-direction for several points (aluminium foam type B interlayer)

The total duration of the load is around 5 ms which is smaller than the previous material. The peak pressure is 7 MPa and the impulse 8370 kPa*ms. Compared to the previous material the peak pressure is bigger and the duration smaller, the profile of the load is much closer to the ideal one. In that case the final deflection of the front part of the column is 15mm and the damage is bigger than the previous simulation since the mass of the concrete has been decreased by 30%.

The type C aluminium foam material is the stiffer one. The pressure and the impulse profile of the impact are depicted in Figure 42. The load in that case is even closer to the ideal one while the plateau of the nearly constant pressure is been decreased in that case. The peak pressure is 18MPa and the impulse 8450 kPa*ms. The duration of the load is about 2.5 ms and is the shorter among the three tested types of aluminium foam. The shrinkage of the aluminium foam layer is small in that case and

the impactor functions almost as non-deformable body. The load in that case is harsher than the previous ones; as it can be observed from Figure 48 it causes significant damage to the specimen. The mass of the concrete column after the impact is 92.8 kg which corresponds to a 35.5% loss.

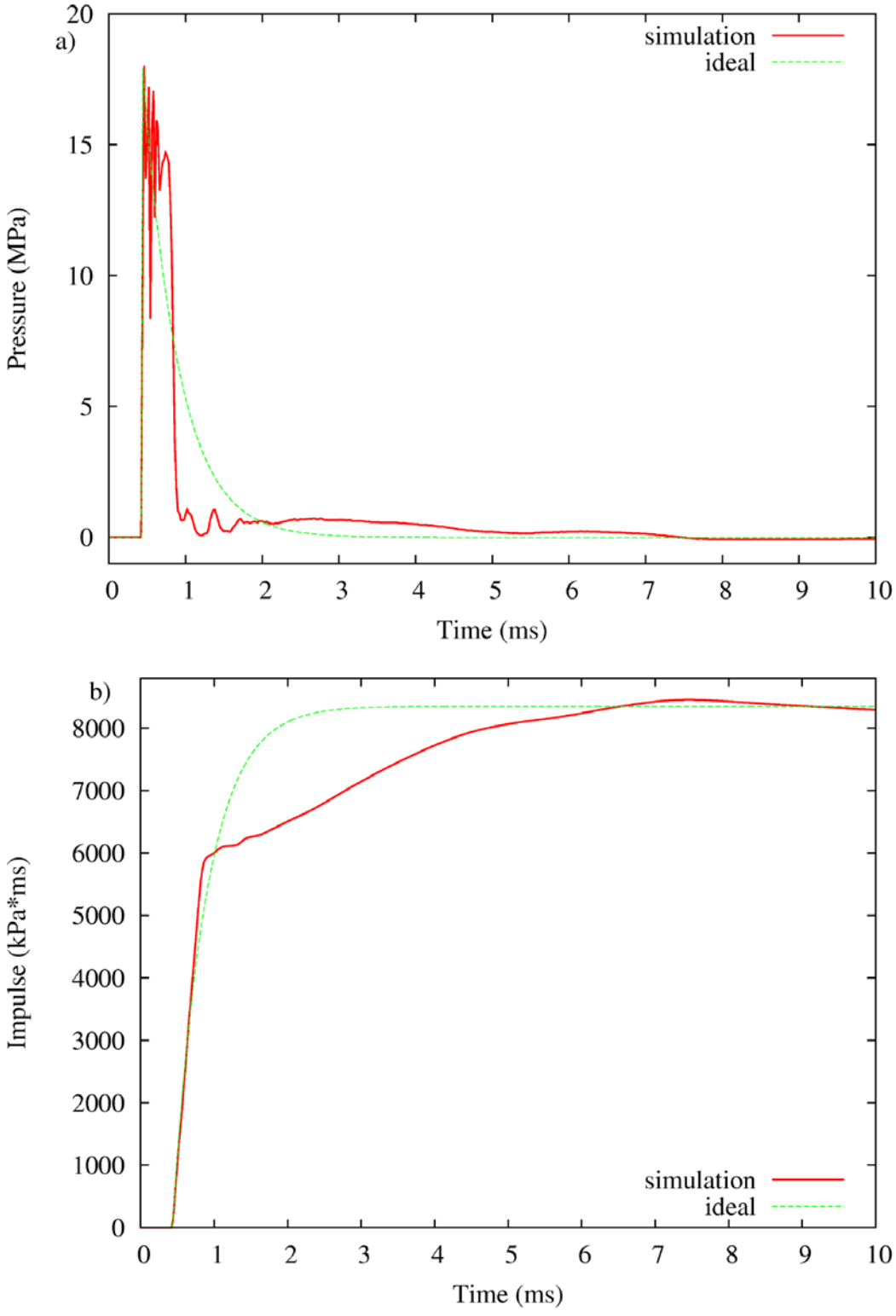

Figure 42: Pressure and Impulse profile for aluminium foam of type C

Table 16: Blast data for aluminium foam type C material

Peak pressure [MPa]	Impulse [kPa*ms]	Z [m/kg$^{1/3}$]	Standoff [m]	Charge mass [kg]
18	8450	0.624	6.24	1000

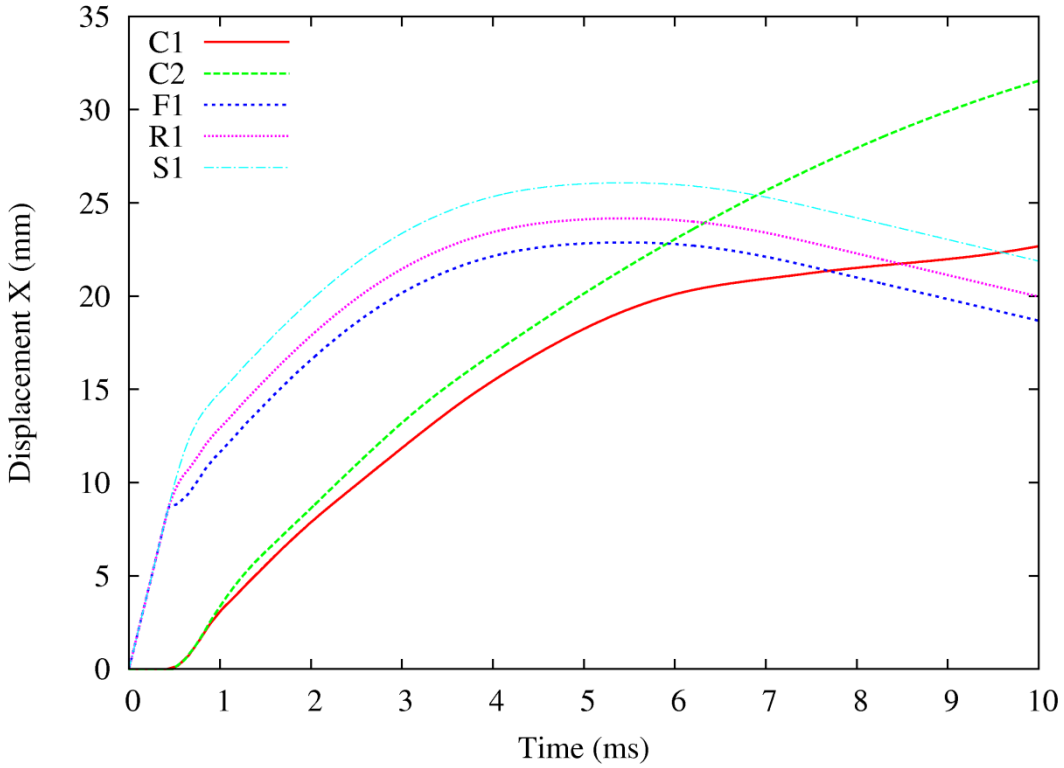

Figure 43: Displacement profile in the X-direction for several points for aluminium foam type C

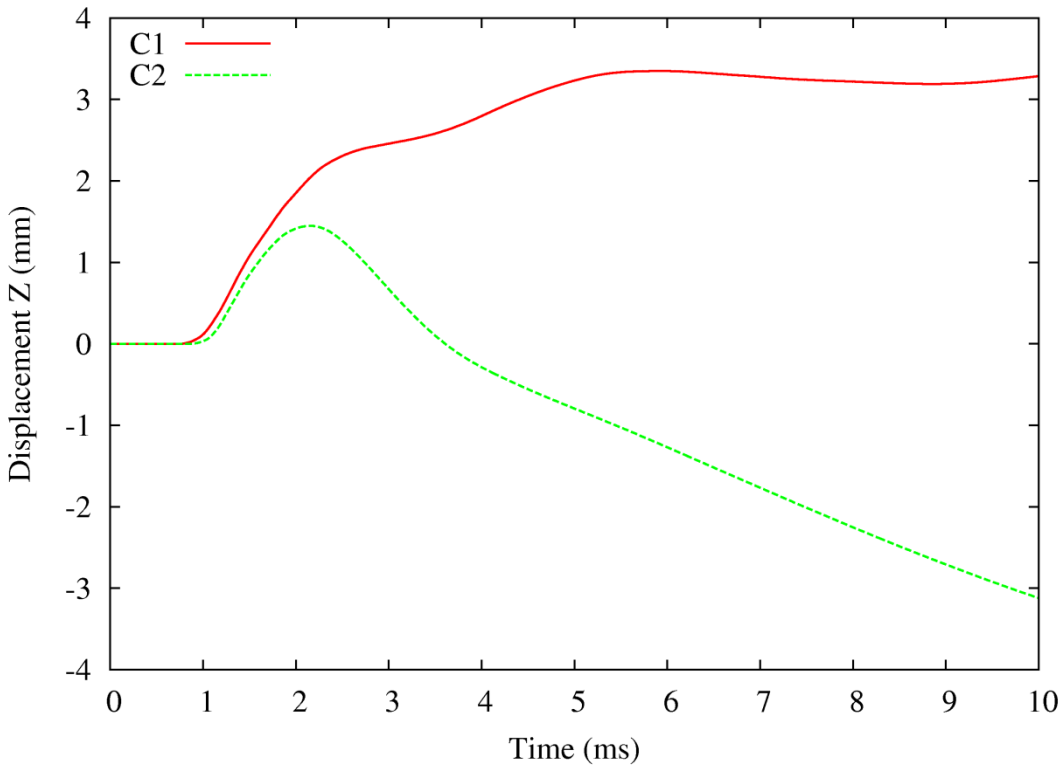

Figure 44: Displacement profile in the Z-direction for points on the specimen for aluminium foam type C

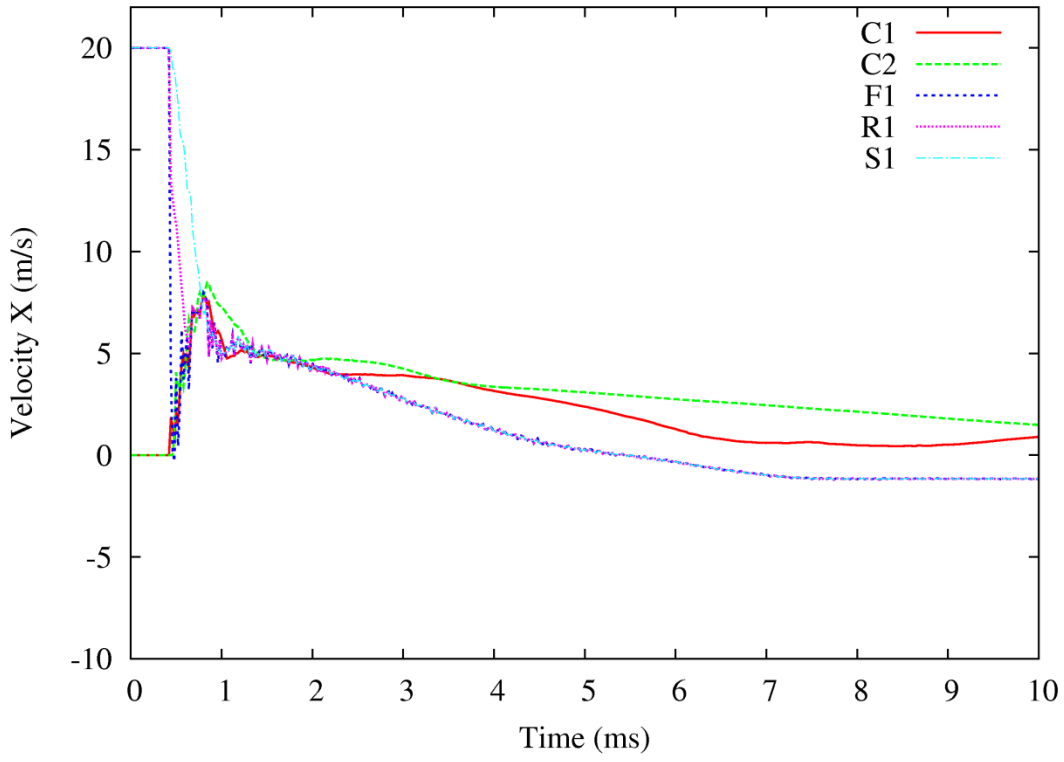

Figure 45: Velocity profile in the X-direction for several points on the specimen for aluminium foam type C

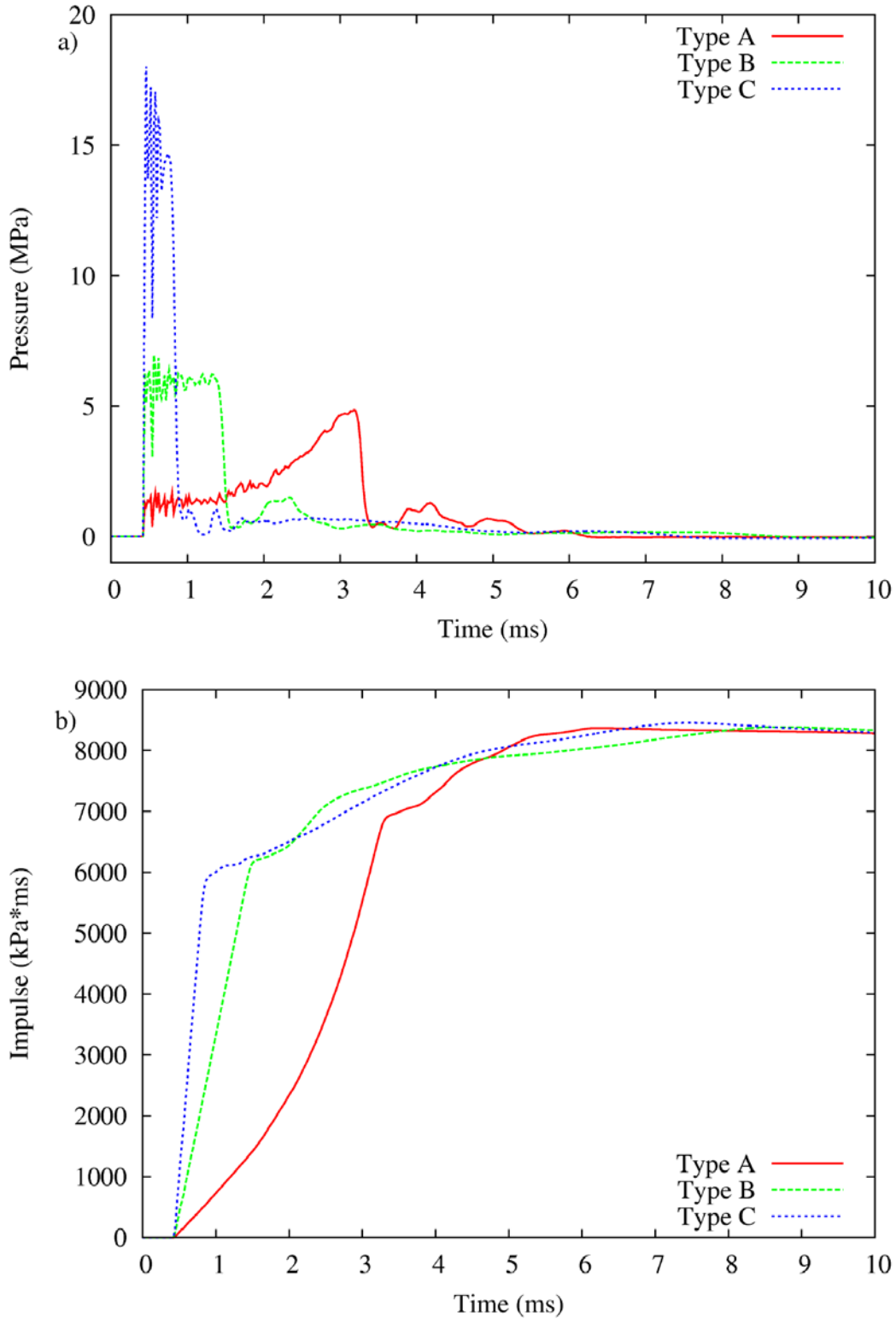

Figure 46: Comparison of pressure and Impulse profile for different aluminium foam materials

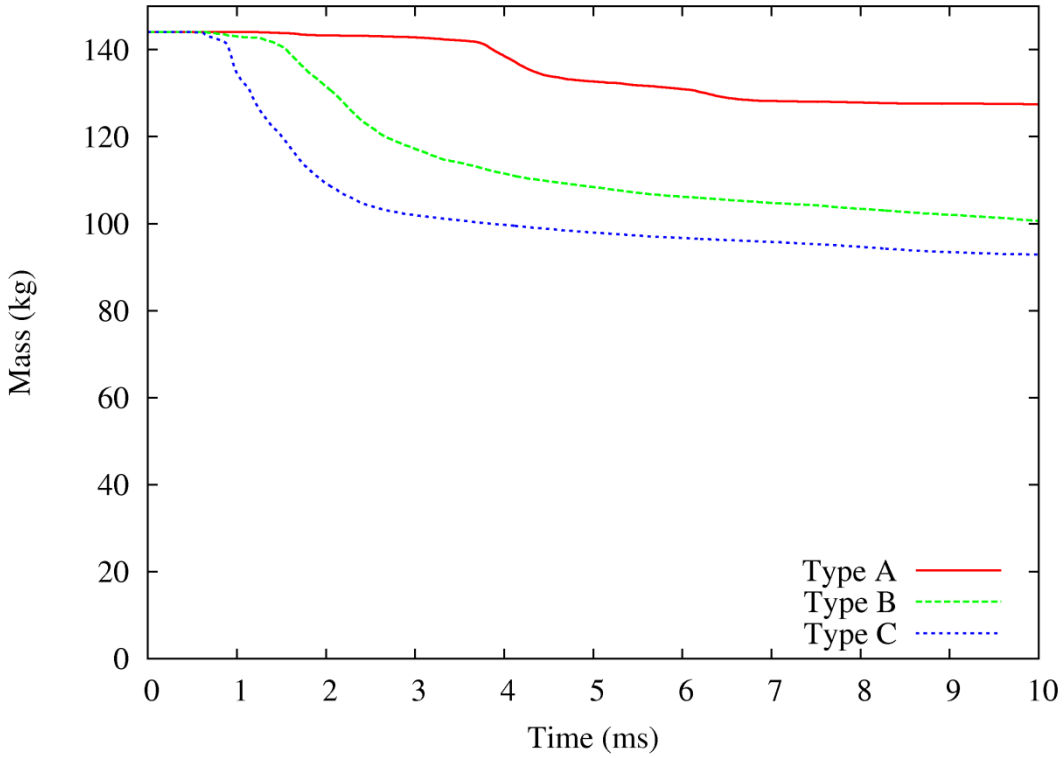

Figure 47: Mass profile for the concrete of the column for 3 different type of aluminium material

Figure 46 presents a comparison of pressure and the impulse profile for all the tested types of aluminium foam materials. It is obvious that the stiffer the material is the bigger the peak pressure becomes while the opposite is valid for the duration of the load. For the particular case of the aluminium foam material interlayer, the type C gives the results that are closer to the ideal load. This is because it is very stiff and it behaves as almost an undeformable body.

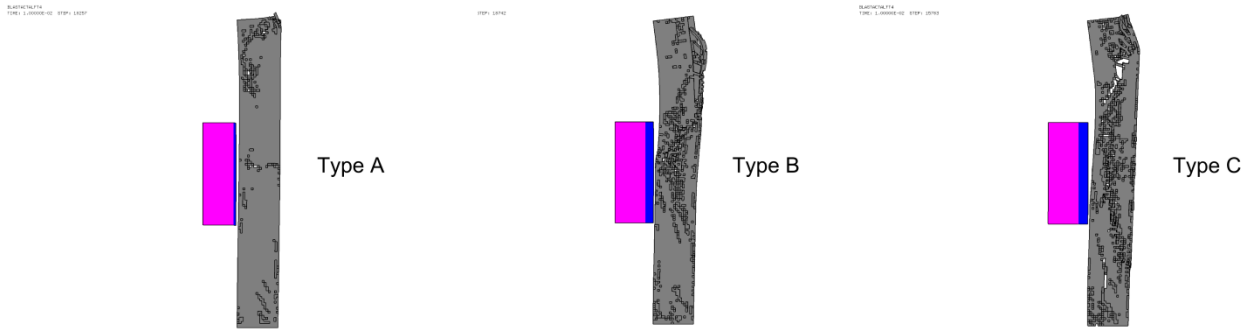

Figure 48: Final state of the simulation for several aluminium foam materials

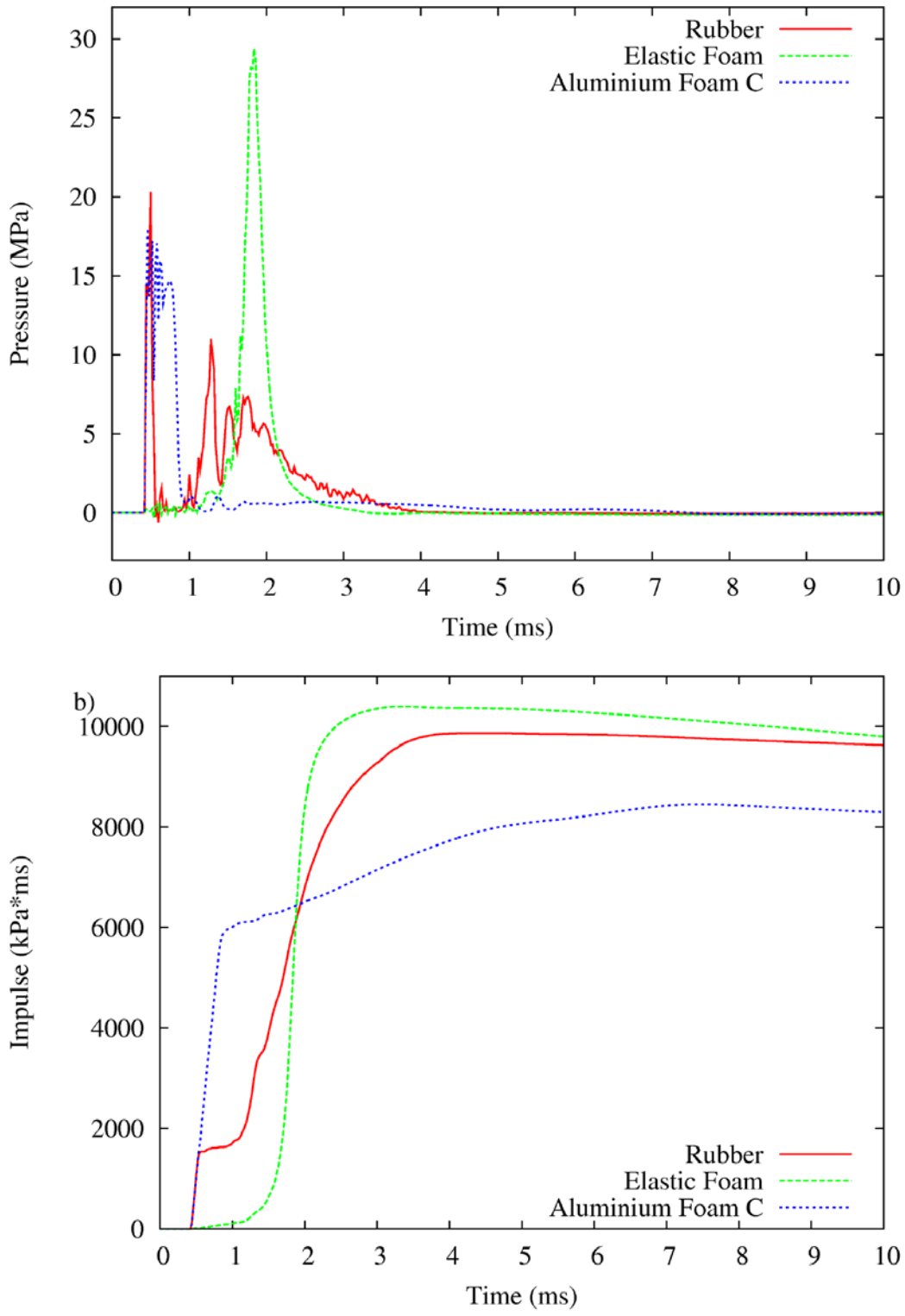

Figure 49: Comparison of pressure and Impulse profile for different materials

On that point it is important to present together all the pressure time histories obtained from the several material types in order to compare them. Figure 49 depicts the impacting load time histories for the rubber, the elastic foam and the aluminium foam of type C materials. The highest peak pressure appears in the elastic foam model while the longest duration appears in the rubber model. The total impulse for the rubber and the elastic foam models is very close while in the case of the aluminium foam it is much lower. The profile that matches better with an ideal blast load is the one produced from the elastic foam material interlayer and that is way it is selected for the farther investigations concerning other parameters that influence the results, like the impact velocity and the thickness of the interlayer.

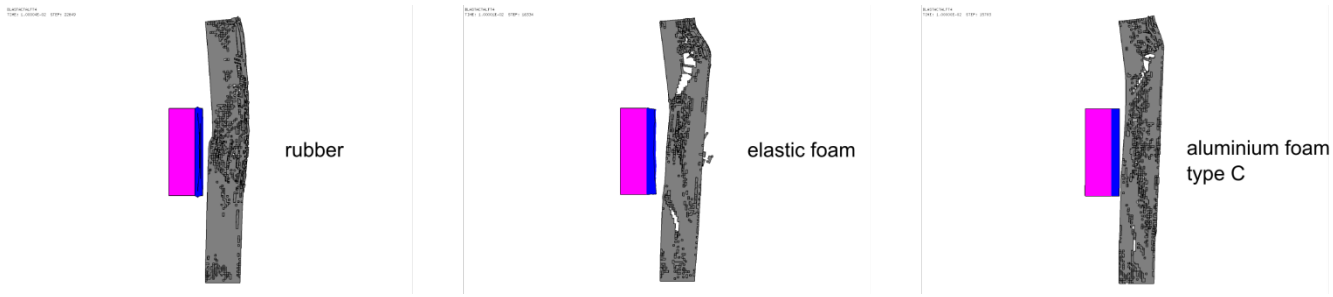

Figure 50: Final state of the simulation for several materials

Figure 50 presents the sideway view of the final state of the simulation for the different material layers that where investigated in the current section. The biggest damage on the reinforced concrete model is obtained in the case of the elastic foam interlayer. This is normal since in that case the Z parameter and the standoff distance are smaller and this refers to a stronger explosive load.

3.3 Velocity influance

A very important parameter to investigate for its influence to the produced load is the velocity of the impacting mass just before the contact with the specimen. For this investigation the model with the elastic foam interlayer is selected, since it has a better fit to the desired blast load. In the previous section the impacting mass hits the column with a velocity of 20 m/s, and in this section two more values (one higher and one lower) are tested. The lower impact velocity is selected at 10 m/s and the higher at 30 m/s.

Figure 51 depicts the comparison of the three pressure and impulse time histories for the different impact velocities. The loading in the case when the impact velocity is 10 m/s reaches a peak pressure of 4.18 MPa and an impulse of 6445 kPa*ms. These characteristics correspond to a Z=1.063 and a standoff distance of 10.63 m. The duration of the load is about 4 ms and the profile is similar to the one obtained in the previous section for the velocity of 20 m/s. The pressure rises fast but not abruptly until the peak pressure and then it goes to zero in more or less the same way.

On the other hand, in the case where the impact velocity is 30 m/s the peak pressure is 72 MPa and the impulse 13925 kPa*ms. This data refers to a much stronger blast load with Z=0.325 and a standoff distance of 3.25 m. The profile of the load is as expected from the previous simulations with the elastic foam simulation but in a more acute way. The duration of the load is nearly 1 ms and, as it can be observed, the peak comes earlier than the other case. This is normal since the impacting mass is moving faster and it hits the specimen earlier.

From Figure 51 it is obvious that as we increase the velocity the peak pressure and the impulse are getting higher, while the duration of the load is getting shorter. This effect can be used in the laboratory in the blast actuator in order to parameterize the potential of the desired blast load. If the experiment needs to simulate a weak blast load with a relative high Z value and long duration, then a small impact velocity will be selected. If the blast actuator needs to produce a strong explosive load with smaller Z value and smaller duration then a higher impact velocity will be used.

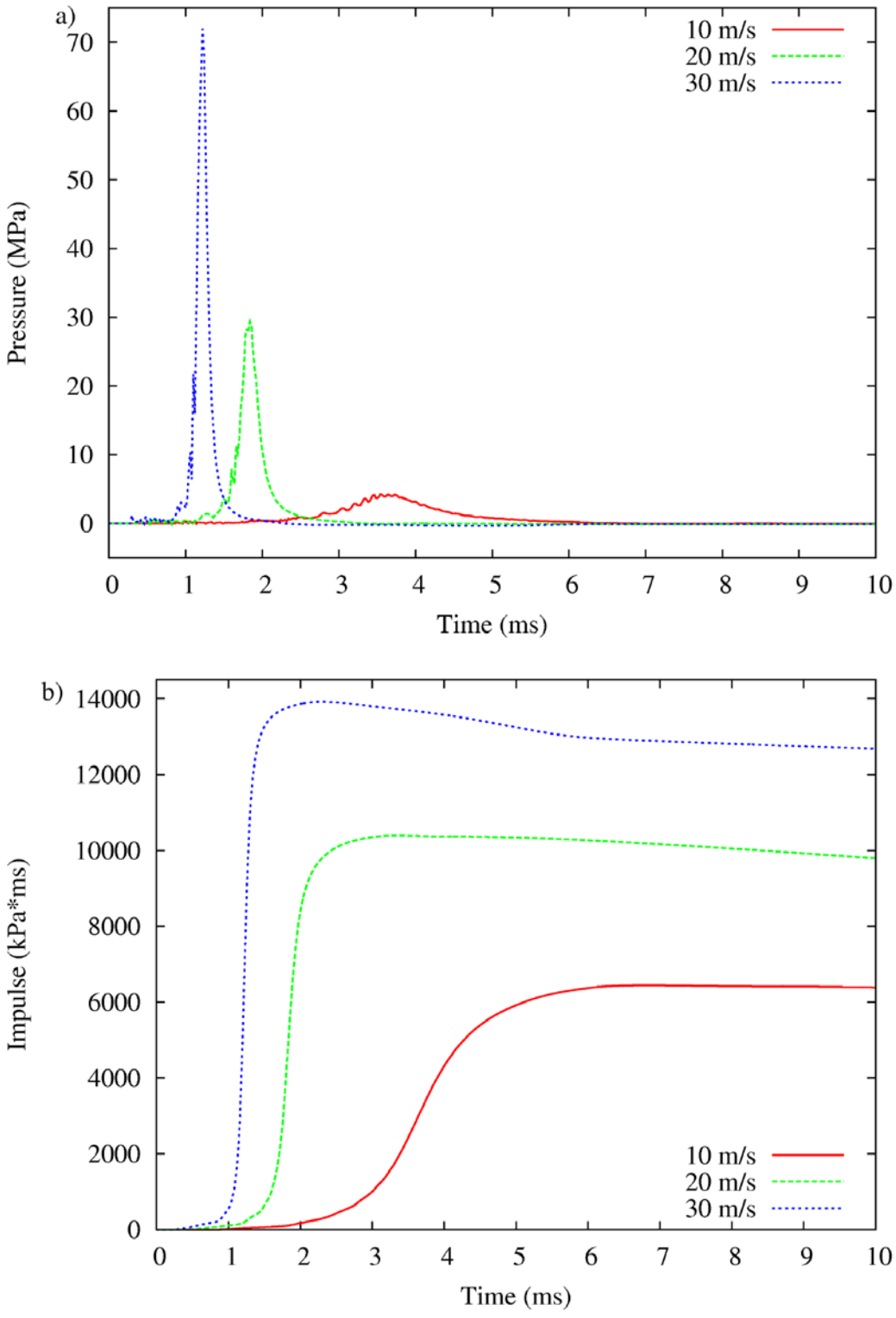

Figure 51: Comparison of pressure and Impulse profile for different impact velocities

Table 17: Blast data for different impact velocities

Velocity [m/s]	Peak pressure [MPa]	Impulse [kPa*ms]	Z [m/kg$^{1/3}$]	Standoff [m]	Peak acceleration [g]
10	4.18	6445	1.063	10.63	1082
20	29.37	10373	0.506	5.06	7481
30	72	13925	0.325	3.25	18281

Figure 52 presents the mean acceleration of the aluminium impacting mass for the several impact velocities. The shape of the curves is similar to the corresponding pressure time histories and the peak acceleration is an indicative parameter for the simulation.

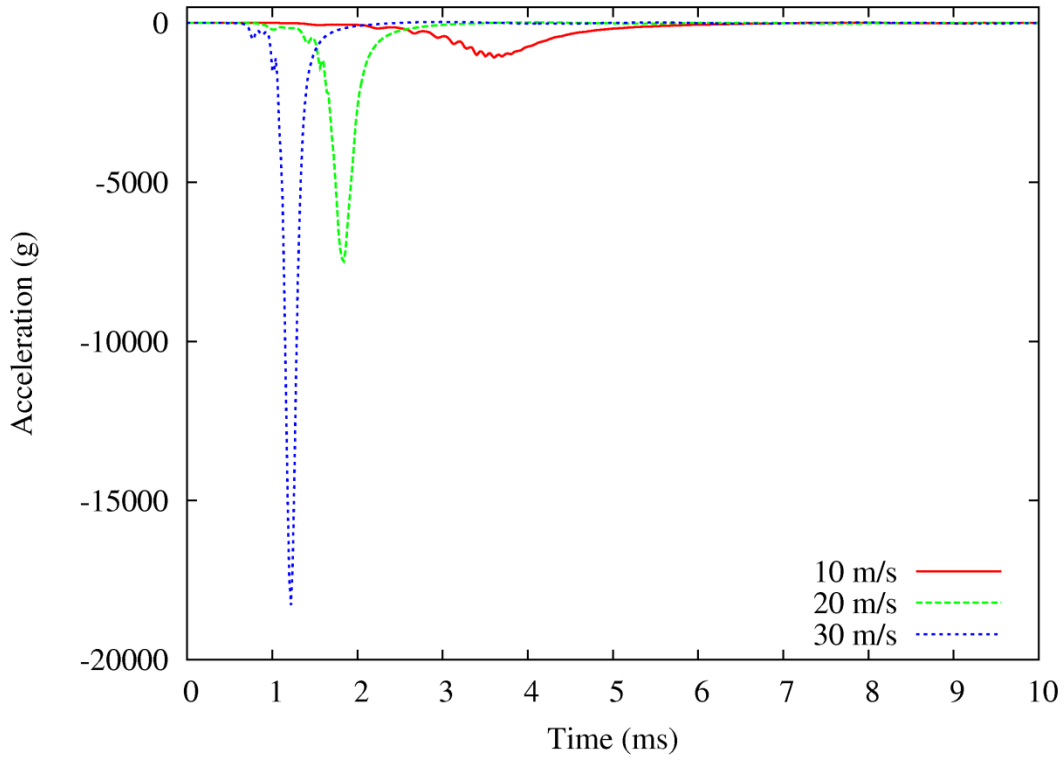

Figure 52: Mean acceleration for the aluminium mass

Figure 53 presents the final state for the three simulations with different impact velocity. As expected, in the case where the impact velocity is 10 m/s the damage is small enough since this contact load

corresponds to a weak explosive load. In the case of the 30 m/s, which is the highest tested velocity the damage is more severe than the previous cases.

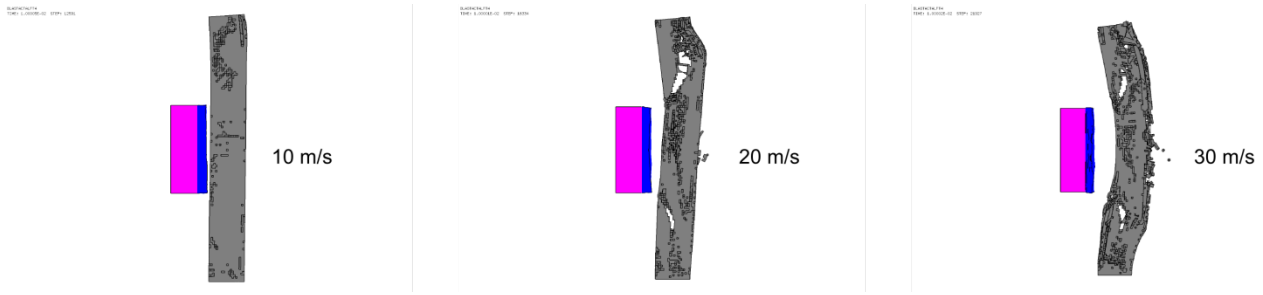

Figure 53: Final state of the simulation for different impact velocities

3.4 Thickness influence

Another important parameter that is under investigation for its influence in the produced load from the blast actuator is the thickness of the hyperelastic interlayer. For this study the elastic foam interlayer is used and the tested thicknesses are one bigger (100 mm) and one smaller (20 mm) than the already simulated one (50 mm). The calculated results are the pressure and the impulse time histories and are depicted in Figure 54.

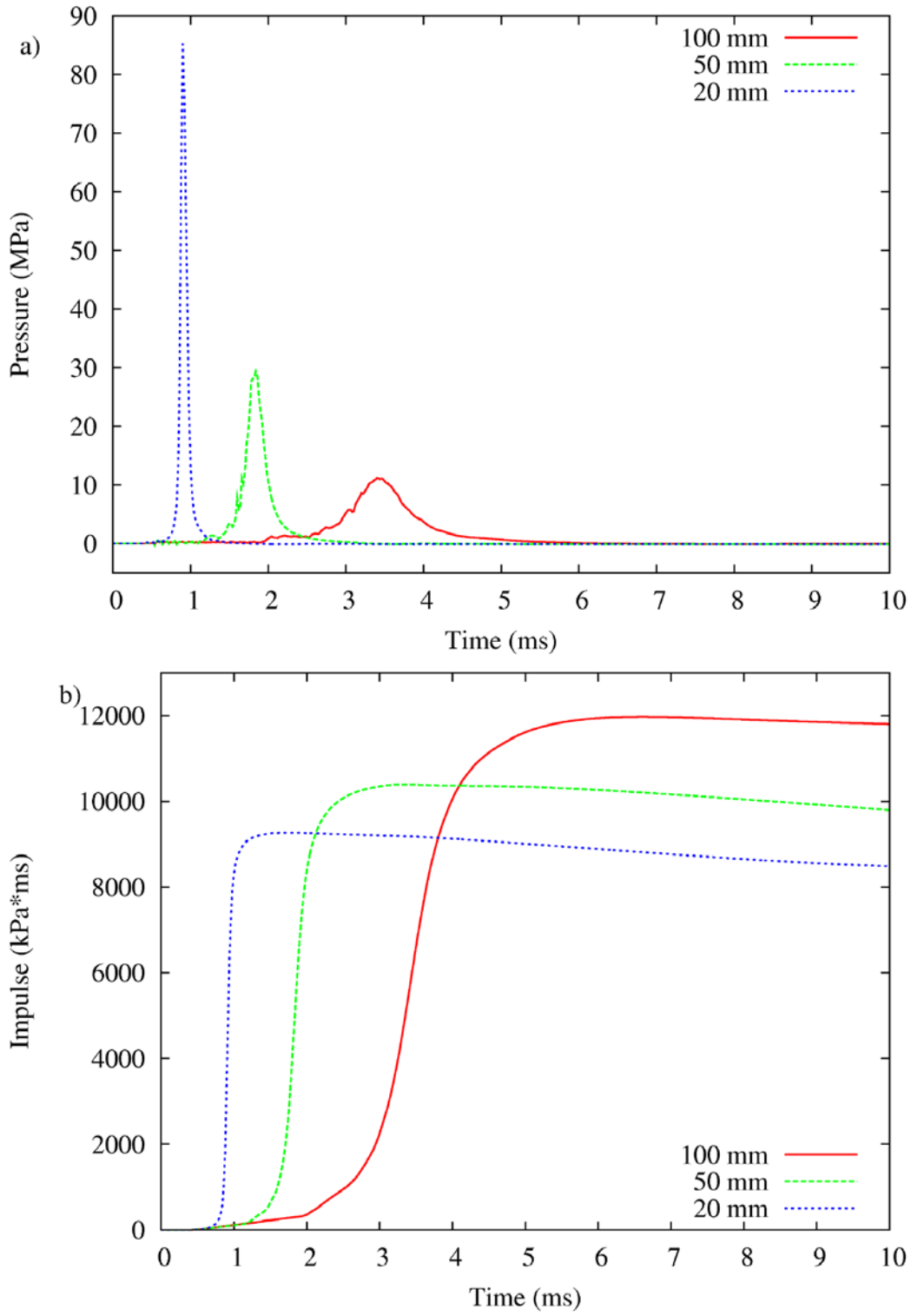

Figure 54: Comparison of pressure and Impulse profile for different hyperelastic layer thickness

The model with the interlayer of 100 mm produces an impact load with a peak pressure of 11.86 MPa and total impulse of 11970 kPa*ms and this refers to a scaled distance of 0.733. The shape of the pressure curve is smooth enough since the interlayer is bigger than the other cases and the period that the elastic foam is compressed is larger. This results to a much longer duration of the load, which is around 5 ms. The long duration of the impacting load leads to a high total impulse, higher than the total impulse of the model where the interlayer size is 50 mm.

In the model where the elastic foam interlayer thickness is 20 mm the peak pressure is 85.25 MPa and the total impulse is 9270 kPa*ms, which corresponds to a much stronger explosion with Z=0.296. The duration of the load is less than 1 ms and the inclination of the curve is much steeper. It is remarkable that in the case of the 20 mm thickness although the peak pressure is higher than that of the other two bigger thicknesses, the total impulse is smaller. This is not the case in the velocity influence where the higher velocity gives both parameters (peak pressure and total impulse) higher. This characteristic gives the opportunity to the user of the blast actuator to produce a load with high peak pressure without increasing proportionally the total impulse of the load.

Table 18: Blast data for different thickness of the hyperelastic layer

thickness [mm]	Peak pressure [MPa]	Impulse [kPa*ms]	Z [m/kg$^{1/3}$]	Standoff [m]	Peak acceleration [g]
100	11.86	11970	0.733	7.33	2751
50	29.37	10373	0.506	5.06	7481
20	85.25	9270	0.296	2.96	20305

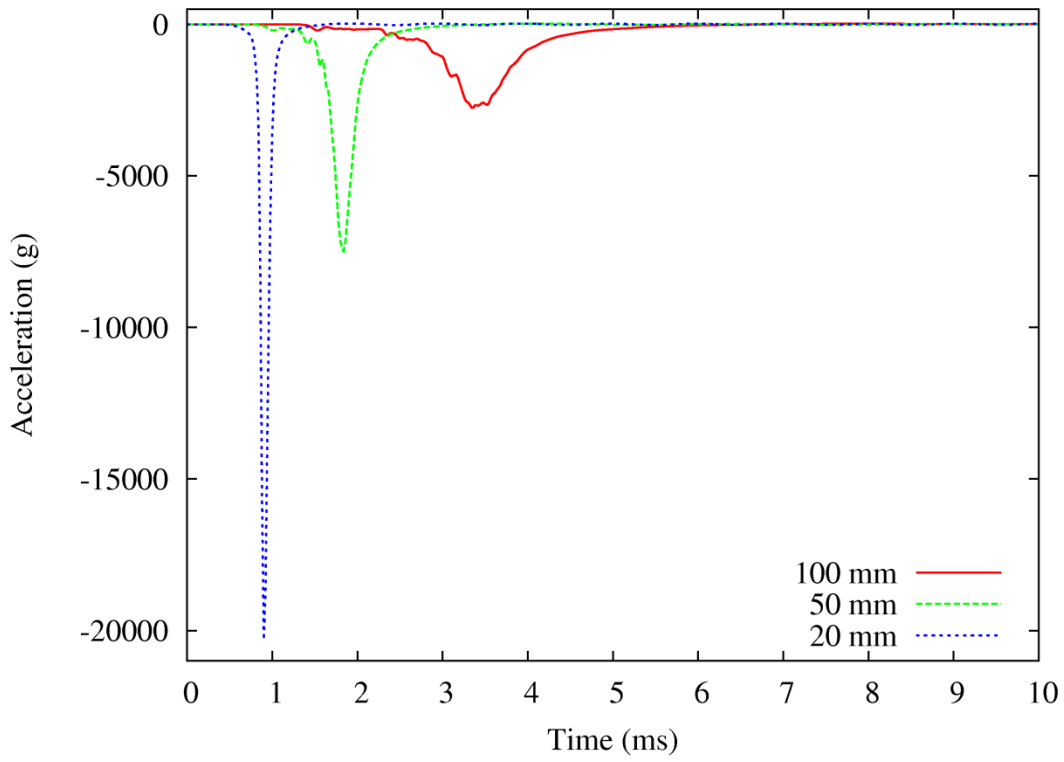

Figure 55: Mean acceleration for the aluminium mass

Figure 56 depicts the sideway view of the final state of the calculation of the finite element model for the different sizes of the thickness of the elastic foam interlayer. It is obvious from the final damage of each model that the thinner the layer is the stronger impact load is produced.

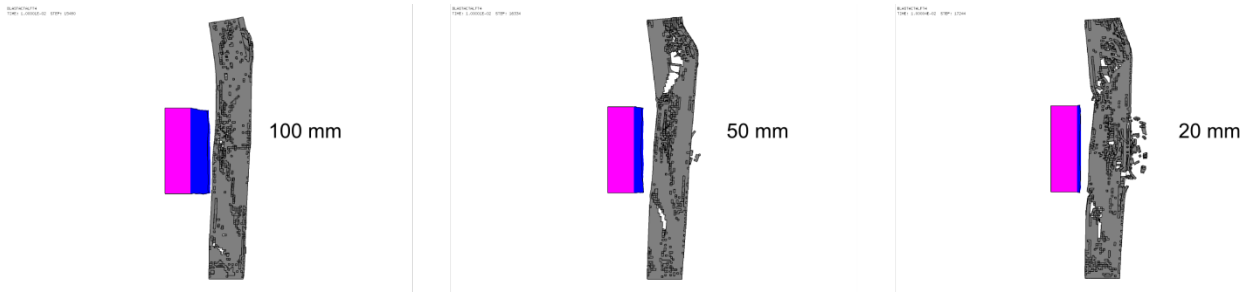

Figure 56: Final state of the simulation for different hyperelastic layer thickness

3.5 Aluminium cylinder preleminary tests

In order to test the capability of the fast actuators some preliminary tests were done. In these tests a plate with a mass of 40 kg was used as an impactor that impacts a cylindrical tube. The tube is made from aluminium (dimensions shown in Figure 57) that was treated before in an oven in order to reduce its yield strength. The yield strength was estimated to about 100 MPa. In order to get regular buckling an imperfection is introduced in 30 mm distance from the top.

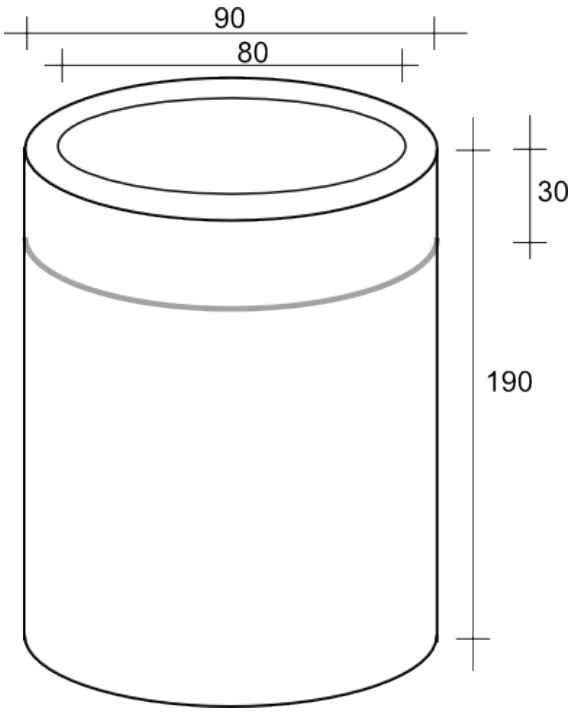

Figure 57: Dimensions of the cylindrical tube [mm]

The velocity of the impactor was 10 m/s. After the experiment a small bending on top and on the bottom can be observed.

Even though the material parameters of the tube are not known in detail, some preliminary calculations are possible in EUROPLEXUS. The EUROPLEXUS validation test “vl_cea_auto_contact” is used as a template. Thick shells of type SHB8 were used. These are shell elements that were defined by using cubes. The mesh is shown in Figure 58. The mesh is loaded from the top by using a special link feature in EUROPLEXUS that allows to impact a mass with an initial velocity of 10 m/s. The mass is built as an indefinite plate.

It can be seen that the element size is increased at the bottom. This was done in the validation test in order to introduce the buckling only on the top part of the tube. A change of the geometry should not be done here.

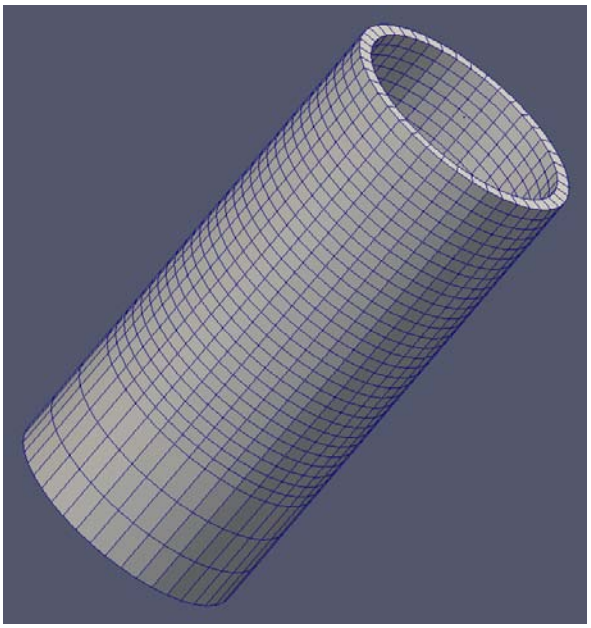

Figure 58: Finite element mesh of the cylindrical tube

The material law of the aluminium is not known and several possibilities are tried out. The first calculation with the material parameters of the validation test (Figure 59) shows no buckling. Only a displacement in the direction of the impact can be observed.

By using an ideal plastic curve with a yield strength of 100 MPa the buckling is very strong (Figure 60). This was not observed in the experiment.

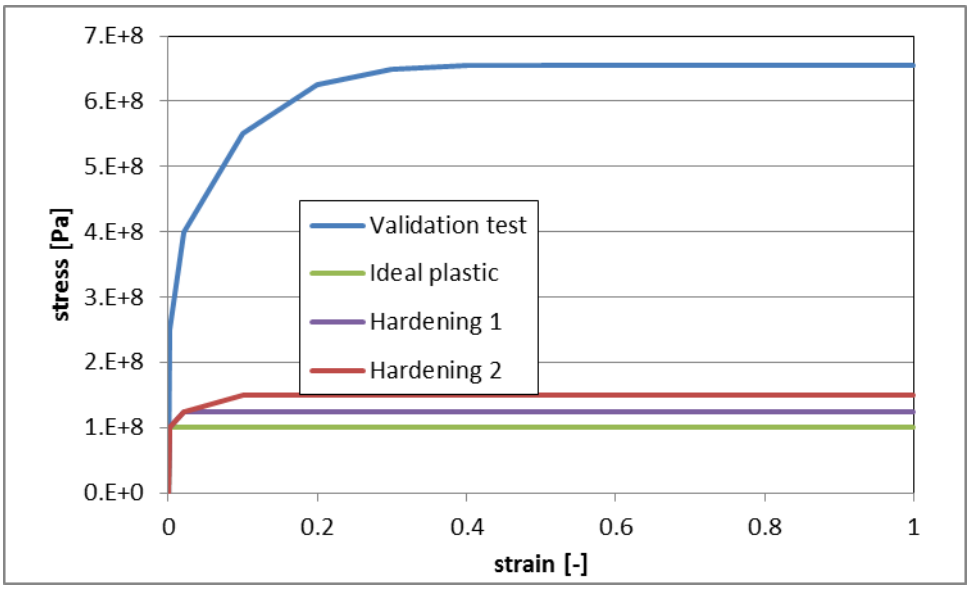

Figure 59: Material parameters tested

Figure 60: Buckling by using an ideal plastic law (yield strength 100 MPa)

To get similar results as in the experiment an imperfection was also introduced at a distance of 30 mm from the top. A reduction of the thickness at that point would be more complicated than an external load. Therefore, a very small external load is used as imperfection. The load is applied in one direction.

Hardening was introduced to reach more realistic behaviour of the tube under impact loading. The two types of hardening curves are shown in Figure 59. The simulation shows that only one folding is

introduced in case of the lower hardening curve. The result in Figure 61 (left) shows a qualitative reasonable result for that hardening. No buckling can be observed in case of a higher hardening curve Figure 61 (right).

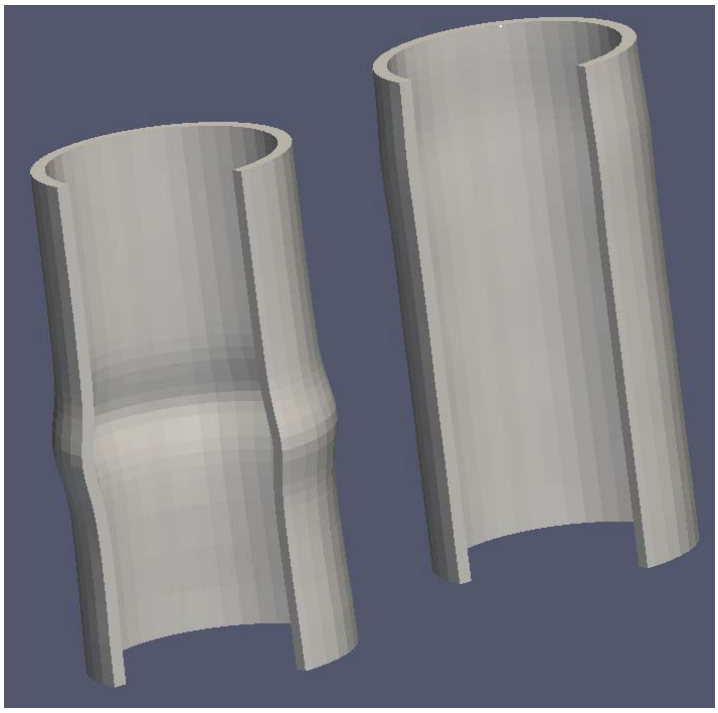

Figure 61: Buckling by using a plastic law with hardening (left: hardening 1, right: hardening 2)

The influence of the impact velocity is shown in Figure 62.

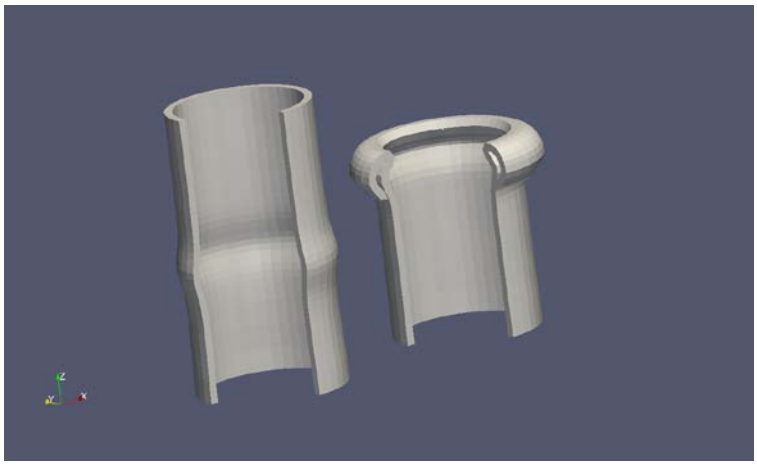

Figure 62: Influence of the impact velocity on the buckling (models with hardening 1): 10 m/s, 20 m/s

Figure 1 depicts the final state of the cylindrical specimen after several tests in the laboratory. The figure refers to the configuration of the specimen after many different preparation tests in the laboratory, so it makes no sense to be compared with the above numerical results.

Figure 63: The cylindrical specimen after several tests in the laboratory.

3.6 Real column specimen

In the previous sections the reinforced concrete column that was used as a specimen was relatively short (1.5 m) and only one impacting mass was used to produce the blast load. This approach was fair for the derivation of some important conclusions for the several parameters that affect the load produced. In a real explosion the column will be higher and the whole surface of the column will be exposed to blast wave. So it is appropriate to make a calculation with a more realistic specimen and with more blast actuators that will cover all the surface of the column that receives the explosive load.

The modelling now is very similar to the one of 2.2 with some modified sizes and with three impacting masses instead of one. The configuration of the reinforced concrete column is presented in Table 19. Also the size of each impacting mass is a little different in order to fit to the surface of the new specimen. The data concerning the size of the impacting mass are presented in Table 20.

Table 19: Configuration of the real reinforced concrete column spacemen

Width [m]	Depth [m]	Height [m]	Longitudinal reinforcement [mm]	Cover depth [mm]
0.25	0.25	3	4Ø10	30

Table 20: Configuration of the impacting mass for the real column test

Width [m]	Depth [m]	Height [m]	Aluminium mass [kg]
0.25	0.15 (0.1 aluminium and 0.05 of hyperelastic layer)	0.8	54

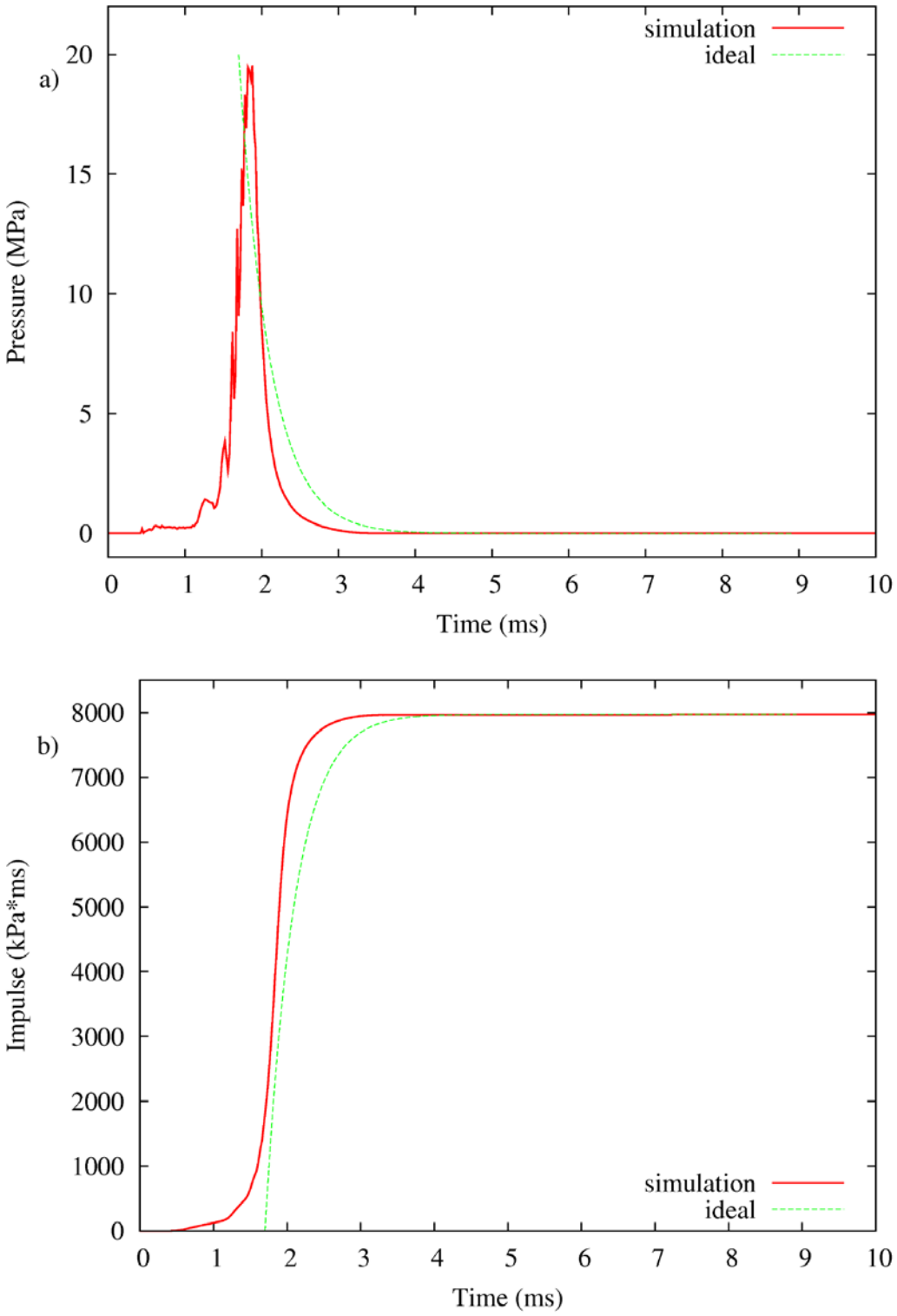

Figure 64: Pressure and Impulse profile for the real column simulation with 3 actuators

Table 21: Blast data for aluminium foam type C material

Peak pressure [MPa]	Impulse [kPa*ms]	Z [m/kg$^{1/3}$]	Standoff [m]	Charge mass [kg]
19.53	7967	0.6025	6.025	1000

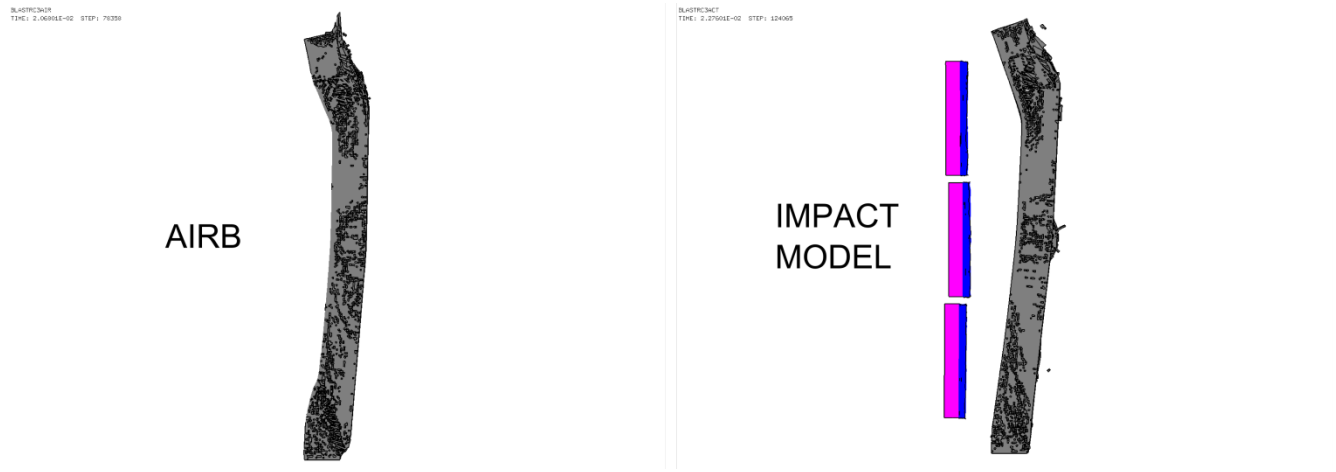

Figure 65: Comparison of AIRB and impact model

Table 22: Information about the mesh data for the impact and the AIRB model for the real column structure

Model	Element size [m]	Number of cubic elements	Number of bar elements	Total number of nodes
Impact	0.01	277500	1200	305768
AIRB	0.01	187500	1200	204680

4 Conclusion

The object of this work is to support the development of the blast actuator apparatus. The blast actuator simulator will be able to reproduce on a structure a load similar to the one derived from an explosion in a more safe and controllable way. In order to achieve that it is necessary to perform several numerical simulations to predict some important parameters before setting the final experimental device.

In the current study a finite element model was defined and tested with numerous variations. First the investigation for the material that can be used for the interlayer between the impactor and the specimen reveals that the elastic foam material a gives the better approach to the desired load. In total three different materials were tested: a rubber like material, the aluminium foam and an elastic foam. The later was the one that reproduced in the better possible way the pressure and the impulse time histories of an ideal blast load.

After having selected the material for the contact interlayer, the velocity of the impacting mass was checked for its influence to the final outcome. Three different impact velocities were tested and it has been pointed out that as the velocity increases the peak pressure and the impulse of the load are getting higher. The increase of the velocity produces load with shorter time duration, which correspond to smaller scaled distanced (strong) explosive events.

The thickness of the contact interlayer between the impacting mass and the specimen was also studied. The configuration was tested for three different thicknesses and it was concluded that the decrease of the thickness results to a pressure time history with higher peak pressure without that affecting much the total impulse of the impact load.

The produced impact load was compared with equivalent ideal blast loads. The main data that characterize an explosive event are the peak pressure and the total impulse of the load. Different values of the above data result to different blast loads, which correspond to different amounts of explosive charge or different distances from the target. The parameters that were checked give the user of the blast actuator the possibility to modify the velocity of the impacting mass or the thickness of the interlayer material or both in order to achieve the desired pressure load.

Finally, a large finite element simulation for a real structure was performed. The results from the impact model were compared with those obtained from a simulation, where the input excitation was an equivalent ideal blast load. The loading conditions in both calculations were very close and the final deformation of the specimen showed that there was a good accordance between the two models.

5 References

[1] M. Peroni, G. Solomos, G. Magonette, B. Viaccoz, P. Pegon. Blast Simulator Setup Requirements. JRC Technical Reports, EUR 26018 EN, JRC79971 , 2013.

[2] EUROPLEXUS User's Manual. 2013.

[3] CASTEM 2000, Guide d'utilisation. s.l. : CEA, France, 1990.

[4] T. Belytschko, M.O. Neal. Contact-Impact by the Pinball Algorithm with Penalty and Lagrangian Methods. pp. 547-572, s.l. : Int. J. Num. Meth. Engng, 1991, Vol. 31.

[5] F. Casadei. A General Impact-Contact Algorithm Based on Hierarchic Pinballs for the EUROPLEXUS Software System. s.l. : Technical Note N. I.03.176, December 2003.

[6] M. Larcher. Numerische Simulation des Betonverhaltens unter Stoßwellen mit Hilfe des Elementfreien Galerkin-Verfahrens. s.l. : Schriftenreihe des Instituts für Massivbau und Baustofftechnologie; Dissertation, Universität Karlsruhe, 2007.

[7] M. Larcher, G. Valsamos, G. Solomos. Numerical material modelling for the blast actuator. Joint Research Centre, JRC86348, 2013.

[8] A. Cheruet and N. Kill. Implantation d'un matériau hyperélastique dans europlexus. Technical Report SL/03/SAMTECH238/DRD, SAMTECH, Belgium, 2003.

[9] R.W. Ogden. Large deformation isotropic elasticity - on the correlation of theory and experiment for incompressible rubbrubber solids. Proceedings of the Royal Society of London A Mathematical and Physical Science, 326(1567):565–584, 1972.

[10] A. Reyes, O.S. Hopperstad, T. Berstad, A.G. Hanssen, and M. Langseth. Constitutive modeling of aluminum foam including fracture and statistical variation of density. European Journal of Mechanics - A/Solids, 22(6):815 – 835, 2003.

[11] Paul A. Du Bois. A simplified approach to the simulation of rubber-like materials under dynamic loading. 4th European LS-DYNA Users Conference, 2003.

[12] H.L. BRODE. Numerical Solutions of Spherical Blast Waves. pp. 766-775, Journal of Applied Physics, 1955, Vol. 26(6).

[13] Kingery, Charles , Bulmash, Gerald. Airblast Parameters from TNT Spherical Air Burst. Aberdeen Proving Ground, Maryland : Defense Technical Information Center, Ballistic Research Laboratory, 1984.

[14] G.F. Kinney, K.J. Graham. Explosive Shocks in Air. Berlin, 1985.

[15] M. Larcher. Pressure-Time Functions for the Description of Air Blast Waves. JRC Technical Note PUBSY, N. JRC46829, 2008.

[16] M. Larcher. Simulation of the Effects of an Air Blast Wave. JRC Technical Note PUBSY, N. JRC41337, 2007.
[17] Baker, E. Wilfrid. Explosions in the Air. University of Texas Pr., Austin, 1973.

6 Appendix

6.1 First approach

BlastAct5.dgibi

```
TITRE 'BlastAct5' ;
OPTI ECHO 1;
OPTION DIME 3 ELEM CUB8 ;
option trac PS FTRA 'BlastAct5_mesh.ps' ;
OPTI SAUV FORM 'BlastAct5.msh';
CamD = 10;
oel = CamD CamD CamD;
oelz = 0 0 CamD;
oely = 0 CamD 0;
oelx = CamD 0 0;
*
tol = 1.E-7;
*Elle = 0.025;
Elle = 0.01;
dimxS = 0.15;
dimxC = 0.2;
dimyS = 0.2;
dimxE = 0.05;
*dimxEa = 0.025;
*dimxEb = 0.025;
dimxEa = 0.03;
dimxEb = 0.02;
dimyC = 0.2;
*dimzS = 0.5;
dimzS = 0.5;
dimzC = 1.5;
dimxCn = 0.016;
dimdB = 0.01;
diamB = 0.01;
dimzAct = 0.5;

P0 = 0 0 0;

*Points for Steel
Ps1 = P0 PLUS (0 (0 - (dimyS/2.0)) (0 -
(dimzS/2.0)));
Ps2 = Ps1 PLUS (0 dimyS 0);
*Curve for steel
nsy = ENTI ((dimyS + tol) / (ElLe));
Cs1 = Ps1 d nsy Ps2;
*Surface steel
nsz = ENTI ((dimzS + tol) / (ElLe));
Ss1 = Cs1 tran nsz (0 0 dimzS);
*Volume steel
nsx = ENTI ((dimxS + tol) / (ElLe));
Vs1 = Ss1 volu tran nsx (dimxS 0 0);

TRAC oel CACH QUAL (Ps1 ET Ps2 ET P0 ET Cs1 ET
Ss1 ET Vs1);
Vs1 = Vs1 coul rose;

*Vs2 = Vs1 PLUS (0 0 dimzAct);
*Vs2 = Vs2 coul rose;
*Vs3 = Vs1 PLUS (0 0 (0 - dimzAct));
*Vs3 = Vs3 coul rose;

*Surface elastoplastic
Se1a = Ss1 PLUS (dimxS 0 0);
*Volume elastoplastic
nexa = ENTI ((dimxEa + tol) / (ElLe));
Ve1a = Se1a volu tran nexa (dimxEa 0 0);
Ve1a = Ve1a coul jaun;
Se1b = Se1a PLUS (dimxEa 0 0);
*Volume elastoplastic
nexb = ENTI ((dimxEb + tol) / (ElLe));
*nexb = 1;
Ve1b = Se1b volu tran nexb (dimxEb 0 0);
Ve1b = Ve1b coul bleu;
elim tol (Ve1a ET Ve1b);
Ve1 = Ve1a ET Ve1b;
OUBL Ve1a;
OUBL Ve1b;

Ve1 = Ve1 coul bleu;

*2 more Actuators
*Ve2a = Ve1a PLUS (0 0 dimzAct);
*Ve2a = Ve2a coul jaun;
*Ve2b = Ve1b PLUS (0 0 dimzAct);
*Ve2b = Ve2b coul bleu;
*elim tol (Vs2 ET Ve2a ET Ve2b);
*
*Ve3a = Ve1a PLUS (0 0 (0 - dimzAct));
*Ve3a = Ve3a coul jaun;
*Ve3b = Ve1b PLUS (0 0 (0 - dimzAct));
*Ve3b = Ve3b coul bleu;
*elim tol (Vs3 ET Ve1a ET Ve3b);


*Points for Column
dkad = dimxS+dimxE+dimxCn;
Pc1 = P0 PLUS ( dkad (0 - (dimyC/2.0)) (0 -
(dimzC/2.0)));
Pc2 = Pc1 PLUS (0 dimyC 0);
*Curve for Column
ncy = ENTI ((dimyC + tol) / (ElLe));
Cc1 = Pc1 d ncy Pc2;
*Surface Column
ncz = ENTI ((dimzC + tol) / (ElLe));
Sc1 = Cc1 tran ncz (0 0 dimzC);
*Volume Column
ncx = ENTI ((dimxC + tol) / (ElLe));
Vc1 = Sc1 volu tran ncx (dimxC 0 0);
Vc1 = Vc1 coul cyan;
dkad = dimdB+(diamB/2.0);
Pb1 = Pc1 PLUS ( dkad dkad 0);
Pb2 = Pb1  PLUS (0 0 dimzC);
Cb1 = Pb1 d ncz Pb2;
dkad = dimyC - (2*(diamB+(dimdB/2.0)));
list dimyC;
list diamB;
list dimdB;
list dkad;
Cb2 = Cb1 PLUS (0 (dkad) 0);
dkad = dimxC - (2*(diamB+(dimdB/2.0)));
Cb3 = Cb2 PLUS ((dkad) 0 0);
dkad = dimyC - (2*(diamB+(dimdB/2.0)));
Cb4 = Cb3 PLUS (0 (0 -(dkad)) 0);
bars = Cb1 ET Cb2 Et Cb3 ET Cb4;

TRAC oel CACH QUAL (Vs1 ET Ve1 ET Vc1);
*Vmesh = Vc1 ET Ve1a ET Ve1b ET Vs1;
Vmesh = Vc1 ET Ve1 ET Vs1;
*Vmesh = Vc1 ET Ve1a ET Ve1b ET Vs1 ET Vs2 ET
Vs3;
*Vmesh = Vmesh ET Ve2a ET Ve2b ET Ve3a ET Ve3b;
mesh = Vmesh et bars;
elim tol mesh;
LIST (NBEL mesh);
LIST (NBEL Vs1);
LIST (NBEL Ve1);
LIST (NBEL Vc1);
LIST (NBEL mesh);
***
TRAC oel CACH QUAL mesh;
TASS mesh 'NOOP';
SAUV FORM mesh;
fin;
*
```

BlastActALFT4.epx

```
BLASTACTALFT4
ECHO
CONV WIN
CAST 'BlastAct5.msh' mesh
```

```
TRID LAGR EROS 0.0
DIME
*  DEBR 30720
*  DEBR 60000
TERM
GEOM cube Vmesh BR3D bars TERM
COMP EPAI 3.1416E-4 LECT bars TERM
*     DEBR
*      ROF 1.0                              ! let
particles move in vacuum
*     FILL PLEV 0                          ! select
the level
*          RO 2400 DRAG 1.0 TRAJ OBJE LECT Vc1
TERM
     GROU 8 'cele1' LECT Vc1 TERM
                  COND NEAR POIN 0.216 0.0 0.0
            'cele2' LECT Vc1 TERM
                  COND NEAR POIN 0.416 0.0 0.0
            'fele' LECT Ve1 TERM
                  COND   NEAR   POIN   0.2   0.0
0.0001
            'rele' LECT Ve1 TERM
                  COND   NEAR   POIN   0.18   0.0
0.0001
            'sele1' LECT Vs1 TERM
                  COND   NEAR   POIN   0.15   0.0
0.0001
            'sele2' LECT Vs1 TERM
                  COND   NEAR   POIN   0.0   0.0
0.0001
            'Ccon' LECT Vc1 TERM
                  COND XB LT 0.242
                  COND ZB LT 0.321
                  COND ZB GT -0.321
            'Econ' LECT Ve1 Ve1 Vs1 TERM
                  COND XB GT 0.124
      NGRO 13   'DOWN' LECT mesh TERM COND Z LT
-0.749999
             'UP'  LECT  mesh  TERM  COND  Z  GT
0.749999
            'C1' LECT Vc1 TERM COND SPHE
                  XC 0.216 YC 0.0 ZC 0.0 R
0.005
            'C2' LECT Vc1 TERM COND SPHE
                  XC 0.416 YC 0.0 ZC 0.0 R
0.005
            'F1' LECT Ve1 TERM COND SPHE
                  XC  0.2  YC  0.0  ZC  0.0  R
0.005
            'R1' LECT Ve1 TERM COND SPHE
                  XC 0.18 YC 0.0 ZC 0.0 R
0.005
            'S1' LECT Vs1 TERM COND SPHE
                  XC 0.15 YC 0.0 ZC 0.0 R
0.005
            'S2' LECT Vs1 TERM COND SPHE
                  XC  0.0  YC  0.0  ZC  0.0  R
0.005
            'Csur'  LECT Vc1 TERM COND BOX
                     X0  0.215  Y0  -0.1  Z0  -
0.35
                     DX 0.1 DY 0.2 DZ 0.7
            'LS11'  LECT Vs1 TERM COND LINE X1
0.0 Y1 -0.1  Z1 -0.25
                        X2  0.15  Y2  -0.1  Z2  -
0.25 tol 1e-5
            'LS12'  LECT Vs1 TERM COND LINE X1
0.0 Y1 0.1  Z1 -0.25
                        X2  0.15  Y2  0.1  Z2  -
0.25 tol 1e-5
            'LS13'  LECT Vs1 TERM COND LINE X1
0.0 Y1 -0.1  Z1 0.25
                        X2  0.15  Y2  -0.1  Z2
0.25 tol 1e-5
            'LS14'  LECT Vs1 TERM COND LINE X1
0.0 Y1 0.1  Z1 0.25
                        X2  0.15  Y2  0.1  Z2
0.25 tol 1e-5
MATE
  VMIS ISOT
       RO 7800     YOUN 200E9    NU 0.3    ELAS
450.E6
            FAIL 2 LIMI 0.18
            TRAC 2  450.E6    0.00225
                   510.E6    0.18
          LECT bars term
  VMIS PARF   !ALU
       RO 2700     YOUN 70E9    NU 0.35    ELAS
120E6
*            TRAC 2  120.E6    1.7E-3
*                    120.E6    1.0
          LECT Vs1 term
*          LECT Vs1 Vs2 Vs3 term
*  VM23 RO 617.0 YOUN 2.2E6 NU 0.499
*       ELAS 1.32E6 FAIL PEPS LIMI 0.6
*       TRAC 1 1.5E6 0.65
*       LECT Ve1a TERM
*
*  HYPE
*  TYPE         1
*  RO  0.617000000000000E+03
*  CO1   10000  CO2   501187
*  BULK  3.450000000000000E+08
*          LECT Ve1a term
*
* VM23 RO 43.0 YOUN 0.3E6 NU 0.1 !FOAM
*       ELAS 0.09E6 FAIL PEPS LIMI 0.3
*       TRAC 1 0.1E6 0.35
*       LECT Ve1 TERM
***  FOAM RO_F 43.3
***           YOUN 0.34E6
***           NU   0.05
***           SIGP 17.E3
***           RO_0 866.66
***           ALFA 1.809
***           GAMM 150000
***           ALF2 2e6
***           BETA 2.9
***      LECT Ve1 TERM
    HYPE  TYPE         4
     RO  134.0
     CO1  -0.0049
     CO2  11.0
     CO3  11.3
     CO5  0.5119E+06
     CO6  0.436E+04
     CO7  0.1E+05
     BULK 0.744E+06
    LECT Ve1 TERM
* FOAM RO_F 170
*          YOUN 377.E6
*          NU   0.2
*          SIGP 1.15E6
*          RO_0 2700
*          ALFA 2.12
*          GAMM 1.87E6
*          ALF2 93.5E6
*          BETA 5.79
*     LECT Ve1a Ve1 TERM


 DPDC RO 2400 YOUN 3.4E+10 NU 0.21
      FC 42.E+6 DAGG 0.9525E-2  VERS 7
      LECT Vc1 TERM
LINK COUP BLOQ 123 LECT DOWN TERM
          BLOQ 12 LECT UP TERM
          BLOQ 23 LS11 LS12 LS13 LS14 TERM
*          BLOQ 23 LS21 LS22 LS23 LS24 TERM
*          BLOQ 23 LS31 LS32 LS33 LS34 TERM
  Armat   beton lecture Vc1 TERM
          ferr lecture  bars term
     PINB BODY LECT Econ TERM
          BODY LECT Ccon TERM
*     PINB BODY LECT Ve1a Ve1b TERM
*      PINB BODY LECT Ve1a Ve1b Ve2a Ve2b Ve3a
Ve3b TERM
*          BODY LECT Vc1 TERM
INIT VITE 1  20.0 LECT Vs1 Ve1 TERM
*INIT VITE 1  20.0 LECT Vs1 Ve1a Ve1b Vs2 Vs3
Ve2a Ve2b Ve3a Ve3b TERM
```

```
*CHAR CONS GRAV 0.0 0.0 -9.81
*                LECT _DEBR TERM ! gravity acts
only on debris particles
REGI 'CFor' FLIR RESU IRES POIN LECT Csur TERM
     'ALU' RMAS VOLU LECT Vs1 TERM
     'RUB' RMAS VOLU LECT Ve1 TERM
     'FOA' RMAS VOLU LECT Ve1 TERM
     'BET' RMAS VOLU LECT Vc1 TERM
     'REI' RMAS VOLU LECT bars TERM

ECRI DEPL TFRE 5.E-5
           POINT LECT C1 C2 S1 S2 TERM
           ELEM  LECT CELE1 TERM
     FICH SPLI ALIC TFRE 2.E-5
*     Fichier Format  PVTK  TFREQ  5.e-5
*            GROU 4 OBJET  Vc1 TERM
*               OBJET  Ve1  TERM
*               OBJET  bars  TERM
*               OBJET  Vs1  TERM
*           vari  depl ecrou vite cont FLIA
OPTI NOTE
     CSTA 0.5
     LOG 1
!    REND SAFE
CALC TINI 0 TEND 10.E-3 TFAI 1e-9
*CALC TINI 0 TEND 10.E-3 TFAI 1e-7


SUIT
ECHO
RESU SPLI ALIC GARD PSCR
SORT GRAP
*  COLO bleu roug rose vert turq jaun
AXTE 1.0 'Time [s]'

COUR 1 'F_ConX' CONT COMP 1 ELEM LECT FELE TERM
COUR 2 'F_ConX' CONT COMP 1 ELEM LECT RELE TERM
COUR 3 'F_EPST' EPST COMP 1 ELEM LECT FELE TERM
COUR 4 'F_EPST' EPST COMP 1 ELEM LECT RELE TERM
TRAC 1 2 AXES 1.0 'Stress X' YZER
TRAC 3 4 AXES 1.0 'StrainX X' YZER


COUR 101 'c_Pres' ECRO COMP 1 ELEM LECT CELE1
TERM
COUR 102 'r_Pres' ECRO COMP 1 ELEM LECT RELE
TERM
COUR 103 's_Pres' ECRO COMP 1 ELEM LECT SELE1
TERM
TRAC 101 102 103 AXES 1.0 'Pres. [M]' YZER
  COLO bleu roug rose
LIST 101 102 103 AXES 1.0 'H PRes' YZER
*TRAC 102 AXES 1.0 'Pres. [M]' YZER
*
COUR 201 'c_Pres' ECRO COMP 2 ELEM LECT CELE1
TERM
COUR 202 'r_Pres' ECRO COMP 2 ELEM LECT RELE
TERM
COUR 203 's_Pres' ECRO COMP 2 ELEM LECT SELE1
TERM
TRAC 201 202 203 AXES 1.0 'Pres. [M]' YZER
TRAC 201 202 203 AXES 1.0 'Pres. [M]' YZER
  COLO bleu roug rose
LIST 201 202 203 AXES 1.0 'VM PRes' YZER
*TRAC 202 AXES 1.0 'Pres. [M]' YZER
*
COUR 301 'c_Strain' ECRO COMP 3 ELEM LECT CELE1
TERM
COUR 302 'r_Strain' ECRO COMP 4 ELEM LECT RELE
TERM
COUR 303 'f_Strain' ECRO COMP 4 ELEM LECT FELE
TERM
COUR 304 's_Strain' ECRO COMP 3 ELEM LECT SELE1
TERM
TRAC 301 302 303 304 AXES 1.0 'Strain' YZER
  COLO bleu roug rose vert
LIST 301 302 303 304 AXES 1.0 'Strains' YZER
TRAC 303 AXES 1.0 'Strain' YZER
*
COUR 401 'c_Force1' FLIA COMP 1 POIN LECT C1
TERM
COUR 402 'c_Force2' FLIA COMP 1 POIN LECT F1
TERM
TRAC 401 402 AXES 1.0 'ConForce' YZER
  COLO bleu roug
LIST 401 402 AXES 1.0 'Forces' YZER
*
COUR 404 'TotalF' FLIR COMP 1 REGI 1
COUR 405 'PresP' MULC 404 10.0
COUR 406 'Impulse' INT 405

TRAC 404 AXES 1.0 'TotConFor' YZER
*
COUR 414 'Ave_TotF' AVER 404
TRAC 414 AXES 1.0 'AVE_TFOR' YZER
*
TRAC 405 AXES 1.0 'Pres' YZER
TRAC 406 AXES 1.0 'Impulse' YZER
LIST 405 AXES 1.0 'Pres-Impul' YZER
*
COUR 407 'TotalF' RESU COMP 1 REGI 1
COUR 408 'TotalF' RESU COMP 2 REGI 1
COUR 409 'TotalF' RESU COMP 3 REGI 1
COUR 410 'TotalF' IRES COMP 1 REGI 1
COUR 411 'TotalF' IRES COMP 2 REGI 1
COUR 412 'TotalF' IRES COMP 3 REGI 1

TRAC 407 408 409 AXES 1.0 'RESU' YZER
TRAC 410 411 412 AXES 1.0 'IRES' YZER

*
COUR 501 'c_Dx1' DEPL COMP 1 POIN LECT C1 TERM
COUR 502 'c_Dx2' DEPL COMP 1 POIN LECT C2 TERM
COUR 503 'f_Dx1' DEPL COMP 1 POIN LECT F1 TERM
COUR 504 'r_Dx1' DEPL COMP 1 POIN LECT R1 TERM
COUR 505 's_Dx1' DEPL COMP 1 POIN LECT S1 TERM
COUR 506 's_Dx2' DEPL COMP 1 POIN LECT S2 TERM
TRAC 501 502 503 504 505 506 AXES 1.0 'DispolX'
YZER
   COLO bleu roug rose vert turq jaun
TRAC 501 502 AXES 1.0 'DispolX' YZER
   COLO bleu roug
TRAC 501 503 AXES 1.0 'DispolX' YZER
   COLO bleu roug
TRAC 501 504 AXES 1.0 'DispolX' YZER
   COLO bleu roug
TRAC 501 505 AXES 1.0 'DispolX' YZER
   COLO bleu roug
LIST 501 502 503 504 505 506 AXES 1.0 'DispX'
YZER

COUR 531 'Max_C1' MAX 501
COUR 532 'Max_C2' MAX 502
TRAC 531 532 AXES 1.0 'MaxDxC' YZER
*
COUR 511 'c_Dz1' DEPL COMP 3 POIN LECT C1 TERM
COUR 512 'c_Dz2' DEPL COMP 3 POIN LECT C2 TERM
COUR 513 'f_Dz1' DEPL COMP 3 POIN LECT F1 TERM
COUR 514 'r_Dz1' DEPL COMP 3 POIN LECT R1 TERM
COUR 515 's_Dz1' DEPL COMP 3 POIN LECT S1 TERM
COUR 516 's_Dz2' DEPL COMP 3 POIN LECT S2 TERM
TRAC 511 512 513 514 515 516 AXES 1.0 'DispolZ'
YZER
   COLO bleu roug rose vert turq jaun
LIST 511 512 513 514 515 516 AXES 1.0 'DispZ'
YZER
TRAC 511 512 AXES 1.0 'DispolZ' YZER
   COLO bleu roug
*
COUR 611 'c_Vy1' VITE COMP 1 POIN LECT C1 TERM
COUR 612 'c_Vy2' VITE COMP 1 POIN LECT C2 TERM
COUR 613 'f_Vy1' VITE COMP 1 POIN LECT F1 TERM
COUR 614 'r_Vy1' VITE COMP 1 POIN LECT R1 TERM
COUR 615 's_Vy1' VITE COMP 1 POIN LECT S1 TERM
COUR 616 's_Vy2' VITE COMP 1 POIN LECT S2 TERM
TRAC 611 612 613 614 615 616 AXES 1.0 'VeloX'
YZER
   COLO bleu roug rose vert turq jaun
```

```
LIST 611 612 613 614 615 616 AXES 1.0 'VeloX'
YZER
TRAC 611 613 AXES 1.0 'VeloX' YZER
   COLO bleu roug
TRAC 611 614 AXES 1.0 'VeloX' YZER
   COLO bleu roug
TRAC 611 615 AXES 1.0 'VeloX' YZER
   COLO bleu roug
*
COUR 711 'c_Vy1' ACCE COMP 1 POIN LECT C1 TERM
COUR 712 'c_Vy2' ACCE COMP 1 POIN LECT C2 TERM
COUR 713 'f_Vy1' ACCE COMP 1 POIN LECT F1 TERM
COUR 714 'r_Vy1' ACCE COMP 1 POIN LECT R1 TERM
COUR 715 's_Vy1' ACCE COMP 1 POIN LECT S1 TERM
COUR 716 's_Vy2' ACCE COMP 1 POIN LECT S2 TERM
TRAC 711 712 713 714 715 716 AXES 1.0 'ACCEX'
YZER
   COLO bleu roug rose vert turq jaun
LIST 711 712 713 714 715 716 AXES 1.0 'ACCEX'
YZER
TRAC 711 713 AXES 1.0 'ACCEX' YZER
   COLO bleu roug
TRAC 711 714 AXES 1.0 'ACCEX' YZER
   COLO bleu roug
TRAC 711 715 AXES 1.0 'ACCEX' YZER
   COLO bleu roug
TRAC 711 716 AXES 1.0 'ACCEX' YZER
   COLO bleu roug
COUR 721 'Ave_C1' AVER 711
COUR 722 'Ave_C2' AVER 712
COUR 725 'Ave_S1' AVER 716
COUR 726 'Ave_S2' AVER 716
TRAC 721 722 AXES 1.0 'AVE_AxC' YZER
TRAC 725 726 AXES 1.0 'AVE_AxS' YZER
*
COUR 735 'MAX_S1' MAX 716
COUR 736 'MAX_S2' MAX 716
TRAC 735 736 AXES 1.0 'MAX_AxS' YZER
*
COUR 801 'MassAl' MASS COMP 1 REGI 2
COUR 802 'MassR' MASS COMP 1 REGI 3
COUR 803 'MassF' MASS COMP 1 REGI 4
COUR 804 'MassB' MASS COMP 1 REGI 5
COUR 805 'MassRi' MASS COMP 1 REGI 6
TRAC 801 802 803 804 805 AXES 1.0 'MASS' YZER
   COLO bleu roug rose vert turq
LIST 801 802 803 804 805 AXES 1.0 'MASS' YZER
*
COUR 901 'VOLUAl' VOLU REGI 2
COUR 902 'VOLUR' VOLU REGI 3
COUR 903 'VOLUF' VOLU REGI 4
COUR 904 'VOLUB' VOLU REGI 5
COUR 905 'VOLURi' VOLU REGI 6
TRAC 901 902 903 904 905 AXES 1.0 'VOLU' YZER
   COLO bleu roug rose vert turq
LIST 901 902 903 904 905 AXES 1.0 'VOLU' YZER
```

BlastActF.dgibi

```
TITRE 'BlastRC3act' ;
OPTI ECHO 1;
OPTION DIME 3 ELEM CUB8 ;
option trac PS FTRA 'BlastRC3act_mesh.ps' ;
OPTI SAUV FORM 'BlastRC3act.msh';
CamD = 10;
oel = CamD CamD CamD;
oelz = 0 0 CamD;
oely = 0 CamD 0;
oelx = CamD 0 0;
*
tol = 1.E-7;
*Elle = 0.025;
Elle = 0.01;
dimxS = 0.1;
dimxC = 0.25;
dimyS = 0.25;
dimxE = 0.05;
*dimxEa = 0.025;
*dimxEb = 0.025;
dimxEa = 0.03;
dimxEb = 0.02;
dimyC = 0.25;
dimzS = 0.8;
dimzC = 3.0;
dimxCn = 0.016;
dimdB = 0.03;
diamB = 0.01;
dimzAct = 0.85;

P0 = 0 0 0;

*Points for Steel
Ps1 = P0 PLUS (0 (0 - (dimyS/2.0)) (0 -
(dimzS/2.0)));
Ps2 = Ps1 PLUS (0 dimyS 0);
*Curve for steel
nsy = ENTI ((dimyS + tol) / (ElLe));
Cs1 = Ps1 d nsy Ps2;
*Surface steel
nsz = ENTI ((dimzS + tol) / (ElLe));
Ss1 = Cs1 tran nsz (0 0 dimzS);
*Volume steel
nsx = ENTI ((dimxS + tol) / (ElLe));
Vs1 = Ss1 volu tran nsx (dimxS 0 0);

TRAC oel CACH QUAL (Ps1 ET Ps2 ET P0 ET Cs1 ET
Ss1 ET Vs1);
Vs1 = Vs1 coul rose;

Vs2 = Vs1 PLUS (0 0 dimzAct);
Vs2 = Vs2 coul rose;
Vs3 = Vs1 PLUS (0 0 (0 - dimzAct));
Vs3 = Vs3 coul rose;

*Surface elastoplastic
Se1a = Ss1 PLUS (dimxS 0 0);
*Volume elastoplastic
nexa = ENTI ((dimxEa + tol) / (ElLe));
Ve1a = Se1a volu tran nexa (dimxEa 0 0);
Ve1a = Ve1a coul bleu;
Se1b = Se1a PLUS (dimxEa 0 0);
*Volume elastoplastic
nexb = ENTI ((dimxEb + tol) / (ElLe));
*nexb = 1;
Ve1b = Se1b volu tran nexb (dimxEb 0 0);
Ve1b = Ve1b coul bleu;
elim tol (Ve1a ET Ve1b);
Ve1 = Ve1a ET Ve1b;
OUBL Ve1a;
OUBL Ve1b;

elim tol (Vs1 ET Ve1);
*2 more Actuators
Ve2 = Ve1 PLUS (0 0 dimzAct);
*Ve2 = Ve2 coul jaun;
elim tol (Vs2 ET Ve2);
*
Ve3 = Ve1 PLUS (0 0 (0 - dimzAct));
*Ve3 = Ve3 coul jaun;
elim tol (Vs3 ET Ve3);


*Points for Column
dkad = dimxS+dimxE+dimxCn;
Pc1 = P0 PLUS ( dkad (0 - (dimyC/2.0)) (0 -
(dimzC/2.0)));
Pc2 = Pc1 PLUS (0 dimyC 0);
*Curve for Column
ncy = ENTI ((dimyC + tol) / (ElLe));
Cc1 = Pc1 d ncy Pc2;
*Surface Column
ncz = ENTI ((dimzC + tol) / (ElLe));
Sc1 = Cc1 tran ncz (0 0 dimzC);
*Volume Column
ncx = ENTI ((dimxC + tol) / (ElLe));
Vc1 = Sc1 volu tran ncx (dimxC 0 0);
Vc1 = Vc1 coul cyan;
dkad = dimdB+(diamB/2.0);
*dkad = dimdB;
```

```
Pb1 = Pc1 PLUS ( dkad dkad 0);
Pb2 = Pb1  PLUS (0 0 dimzC);
Cb1 = Pb1 d ncz Pb2;
dkad = dimyC - (2*(diamB+(dimdB/2.0)));
*dkad = dimyC - (2*dimdB);
list dimyC;
list diamB;
list dimdB;
list dkad;
Cb2 = Cb1 PLUS (0 (dkad) 0);
dkad = dimxC - (2*(diamB+(dimdB/2.0)));
Cb3 = Cb2 PLUS ((dkad) 0 0);
dkad = dimyC - (2*(diamB+(dimdB/2.0)));
Cb4 = Cb3 PLUS (0 (0 -(dkad)) 0);
bars = Cb1 ET Cb2 Et Cb3 ET Cb4;

TRAC oel CACH QUAL (Vs1 ET Ve1 ET Vc1);
Vmesh = Vc1 ET Ve1 ET Ve2 ET Ve3 ET Vs1 ET Vs2
ET Vs3;
*Vmesh = Vc1 ET Ve1a ET Ve1b ET Vs1 ET Vs2 ET
Vs3;
*Vmesh = Vmesh ET Ve2a ET Ve2b ET Ve3a ET Ve3b;
mesh = Vmesh et bars;
elim tol mesh;
LIST (NBEL mesh);
LIST (NBEL Vs1);
LIST (NBEL Ve1);
LIST (NBEL Ve1);
LIST (NBEL Vc1);
LIST (NBEL mesh);
***
TRAC oel CACH QUAL mesh;
TASS mesh 'NOOP';
SAUV FORM mesh;
fin;
*
```

BlastRC3act.epx

```
BLASTRC3ACT
ECHO
CONV WIN
CAST 'BlastRC3act.msh' mesh
TRID LAGR EROS 0.0
DIME
*  DEBR 30720
*  DEBR 60000
TERM
GEOM cube Vmesh BR3D bars TERM
COMP EPAI 3.1416E-4 LECT bars TERM
*     DEBR
*      ROF 1.0                              ! let
particles move in vacuum
*     FILL PLEV 0                         ! select
the level
*          RO 2400 DRAG 1.0 TRAJ OBJE LECT Vc1
TERM
     GROU 8 'cele1' LECT Vc1 TERM
                  COND NEAR POIN 0.166 0.0 0.0
            'cele2' LECT Vc1 TERM
                  COND NEAR POIN 0.416 0.0 0.0
            'fele' LECT Ve1 TERM
                  COND   NEAR   POIN   0.15   0.0
0.0001
            'rele' LECT Ve1 TERM
                  COND   NEAR   POIN   0.12   0.0
0.0001
            'sele1' LECT Vs1 TERM
                  COND   NEAR   POIN   0.1   0.0
0.0001
            'sele2' LECT Vs1 TERM
                  COND   NEAR   POIN   0.0   0.0
0.0001
            'Ccon' LECT Vc1 TERM
                  COND XB LT 0.1965
                  COND ZB LT 1.3
                  COND ZB GT -1.3
            'Econ' LECT Ve1 Ve2 Ve3 Vs1 Vs2 Vs3
TERM
                  COND XB GT 0.085
      NGRO 21  'DOWN' LECT mesh TERM COND Z LT
-1.49999
             'UP'  LECT  mesh  TERM  COND  Z  GT
1.49999
            'C1' LECT Vc1 TERM COND SPHE
                      XC 0.166 YC 0.0 ZC 0.0 R
0.005
            'C2' LECT Vc1 TERM COND SPHE
                      XC 0.416 YC 0.0 ZC 0.0 R
0.005
            'F1' LECT Ve1 TERM COND SPHE
                      XC 0.15 YC 0.0 ZC 0.0 R
0.005
            'R1' LECT Ve1 TERM COND SPHE
                      XC 0.13 YC 0.0 ZC 0.0 R
0.005
            'S1' LECT Vs1 TERM COND SPHE
                      XC 0.1 YC 0.0 ZC 0.0 R
0.005
            'S2' LECT Vs1 TERM COND SPHE
                      XC 0.0 YC 0.0 ZC 0.0 R
0.005
            'Csur'  LECT Vc1 TERM COND BOX
                        X0 0.165 Y0 -0.125 Z0 -
1.3
                        DX 0.02 DY 0.25 DZ 2.6
            'LS11'  LECT Vs1 TERM COND LINE X1
0.0 Y1 -0.125  Z1 -0.4
                        X2 0.1 Y2 -0.125 Z2 -
0.4 tol 1e-5
            'LS12'  LECT Vs1 TERM COND LINE X1
0.0 Y1 0.125  Z1 -0.4
                        X2 0.1 Y2 0.125 Z2 -
0.4 tol 1e-5
            'LS13'  LECT Vs1 TERM COND LINE X1
0.0 Y1 -0.125  Z1 0.4
                        X2  0.1  Y2  -0.125  Z2
0.4 tol 1e-5
            'LS14'  LECT Vs1 TERM COND LINE X1
0.0 Y1 0.125  Z1 0.4
                        X2  0.1  Y2  0.125  Z2
0.4 tol 1e-5
*
            'LS21'  LECT Vs2 TERM COND LINE X1
0.0 Y1 -0.125  Z1 0.45
                        X2  0.1  Y2  -0.125  Z2
0.45 tol 1e-5
            'LS22'  LECT Vs2 TERM COND LINE X1
0.0 Y1 0.125  Z1 0.45
                        X2  0.1  Y2  0.125  Z2
0.45 tol 1e-5
            'LS23'  LECT Vs2 TERM COND LINE X1
0.0 Y1 -0.125  Z1 1.25
                        X2  0.1  Y2  -0.125  Z2
1.25 tol 1e-5
            'LS24'  LECT Vs2 TERM COND LINE X1
0.0 Y1 0.125  Z1 1.25
                        X2  0.1  Y2  0.125  Z2
1.25 tol 1e-5
*
            'LS31'  LECT Vs3 TERM COND LINE X1
0.0 Y1 -0.125  Z1 -0.45
                        X2 0.1 Y2 -0.125 Z2 -
0.45 tol 1e-5
            'LS32'  LECT Vs3 TERM COND LINE X1
0.0 Y1 0.125  Z1 -0.45
                        X2 0.1 Y2 0.125 Z2 -
0.45 tol 1e-5
            'LS33'  LECT Vs3 TERM COND LINE X1
0.0 Y1 -0.125  Z1 -1.25
                        X2 0.1 Y2 -0.125 Z2 -
1.25 tol 1e-5
            'LS34'  LECT Vs3 TERM COND LINE X1
0.0 Y1 0.125  Z1 -1.25
                        X2 0.1 Y2 0.125 Z2 -
1.25 tol 1e-5
MATE
  VMIS ISOT
       RO 7800     YOUN 200E9    NU 0.3    ELAS
450.E6
```

```
            FAIL 2 LIMI 0.18
            TRAC 2  450.E6    0.00225
                    510.E6    0.18
          LECT bars term
  VMIS PARF   !ALU
       RO 2700     YOUN 70E9    NU 0.35    ELAS
120E6
          LECT Vs1 Vs2 Vs3 term
    HYPE  TYPE         4
     RO  134.0
     CO1  -0.0049
     CO2  11.0
     CO3  11.3
     CO5  0.5119E+06
     CO6  0.436E+04
     CO7  0.1E+05
     BULK 0.744E+06
    LECT Ve1 Ve2 Ve3 TERM
*
 DPDC RO 2400 YOUN 3.4E+10 NU 0.21
      FC 42.E+6 DAGG 0.9525E-2  VERS 7
      LECT Vc1 TERM
LINK COUP BLOQ 123 LECT DOWN TERM
          BLOQ 12 LECT UP TERM
          BLOQ 23 LS11 LS12 LS13 LS14 TERM
          BLOQ 23 LS21 LS22 LS23 LS24 TERM
          BLOQ 23 LS31 LS32 LS33 LS34 TERM
  Armat   beton lecture Vc1 TERM
          ferr lecture  bars term
     PINB BODY LECT Econ TERM
          BODY LECT Ccon TERM
*     PINB BODY LECT Ve1a Ve1b TERM
*      PINB BODY LECT Ve1a Ve1b Ve2a Ve2b Ve3a
Ve3b TERM
*          BODY LECT Vc1 TERM
INIT VITE 1  20.0 LECT Vs1 Vs2 Vs3 Ve1 Ve2 Ve3
TERM
*INIT VITE 1  20.0 LECT Vs1 Ve1a Ve1b Vs2 Vs3
Ve2a Ve2b Ve3a Ve3b TERM
*CHAR CONS GRAV 0.0 0.0 -9.81
*                LECT _DEBR TERM ! gravity acts
only on debris particles
REGI 'CFor' FLIR RESU IRES POIN LECT Csur TERM
     'ALU1' RMAS VOLU LECT Vs1 TERM
     'RUB' RMAS VOLU LECT Ve1 TERM
     'FOA' RMAS VOLU LECT Ve1 TERM
     'BET' RMAS VOLU LECT Vc1 TERM
     'REI' RMAS VOLU LECT bars TERM
     'ALU2' RMAS VOLU LECT Vs2 TERM
     'ALU3' RMAS VOLU LECT Vs3 TERM

ECRI DEPL TFRE 5.E-5
          POINT LECT C1 C2 S1 S2 TERM
          ELEM  LECT CELE1 TERM
     FICH SPLI ALIC TFRE 2.E-5
*     Fichier Format  PVTK  TFREQ  5.e-5
*            GROU 4 OBJET  Vc1 TERM
*               OBJET  Ve1  TERM
*               OBJET  bars  TERM
*               OBJET  Vs1  TERM
*           vari  depl ecrou vite cont FLIA
OPTI NOTE
     CSTA 0.6
     LOG 1
!    REND SAFE
CALC TINI 0 TEND 10.0E-3 TFAI 1e-9
*CALC TINI 0 TEND 10.E-3 TFAI 1e-7


SUIT
ECHO
RESU SPLI ALIC GARD PSCR
SORT GRAP
*  COLO bleu roug rose vert turq jaun
AXTE 1.0 'Time [s]'

COUR 1 'F_ConX' CONT COMP 1 ELEM LECT FELE TERM
COUR 2 'F_ConX' CONT COMP 1 ELEM LECT RELE TERM
COUR 3 'F_EPST' EPST COMP 1 ELEM LECT FELE TERM
COUR 4 'F_EPST' EPST COMP 1 ELEM LECT RELE TERM
TRAC 1 2 AXES 1.0 'Stress X' YZER
TRAC 3 4 AXES 1.0 'StrainX X' YZER


COUR 101 'c_Pres' ECRO COMP 1 ELEM LECT CELE1
TERM
COUR 102 'r_Pres' ECRO COMP 1 ELEM LECT RELE
TERM
COUR 103 's_Pres' ECRO COMP 1 ELEM LECT SELE1
TERM
TRAC 101 102 103 AXES 1.0 'Pres. [M]' YZER
  COLO bleu roug rose
LIST 101 102 103 AXES 1.0 'H PRes' YZER
*TRAC 102 AXES 1.0 'Pres. [M]' YZER
*
COUR 201 'c_Pres' ECRO COMP 2 ELEM LECT CELE1
TERM
COUR 202 'r_Pres' ECRO COMP 2 ELEM LECT RELE
TERM
COUR 203 's_Pres' ECRO COMP 2 ELEM LECT SELE1
TERM
TRAC 201 202 203 AXES 1.0 'Pres. [M]' YZER
TRAC 201 202 203 AXES 1.0 'Pres. [M]' YZER
  COLO bleu roug rose
LIST 201 202 203 AXES 1.0 'VM PRes' YZER
*TRAC 202 AXES 1.0 'Pres. [M]' YZER
*
COUR 301 'c_Strain' ECRO COMP 3 ELEM LECT CELE1
TERM
COUR 302 'r_Strain' ECRO COMP 4 ELEM LECT RELE
TERM
COUR 303 'f_Strain' ECRO COMP 4 ELEM LECT FELE
TERM
COUR 304 's_Strain' ECRO COMP 3 ELEM LECT SELE1
TERM
TRAC 301 302 303 304 AXES 1.0 'Strain' YZER
  COLO bleu roug rose vert
LIST 301 302 303 304 AXES 1.0 'Strains' YZER
TRAC 303 AXES 1.0 'Strain' YZER
*
COUR 401 'c_Force1' FLIA COMP 1 POIN LECT C1
TERM
COUR 402 'c_Force2' FLIA COMP 1 POIN LECT F1
TERM
TRAC 401 402 AXES 1.0 'ConForce' YZER
  COLO bleu roug
LIST 401 402 AXES 1.0 'Forces' YZER
*
COUR 404 'TotalF' FLIR COMP 1 REGI 1
COUR 405 'PresP' MULC 404 1.66666
COUR 406 'Impulse' INT 405

TRAC 404 AXES 1.0 'TotConFor' YZER
*
COUR 414 'Ave_TotF' AVER 404
TRAC 414 AXES 1.0 'AVE_TFOR' YZER
*
TRAC 405 AXES 1.0 'Pres' YZER
TRAC 406 AXES 1.0 'Impulse' YZER
LIST 405 AXES 1.0 'Pres-Impul' YZER
*
COUR 407 'TotalF' RESU COMP 1 REGI 1
COUR 408 'TotalF' RESU COMP 2 REGI 1
COUR 409 'TotalF' RESU COMP 3 REGI 1
COUR 410 'TotalF' IRES COMP 1 REGI 1
COUR 411 'TotalF' IRES COMP 2 REGI 1
COUR 412 'TotalF' IRES COMP 3 REGI 1

TRAC 407 408 409 AXES 1.0 'RESU' YZER
TRAC 410 411 412 AXES 1.0 'IRES' YZER

*
COUR 501 'c_Dx1' DEPL COMP 1 POIN LECT C1 TERM
COUR 502 'c_Dx2' DEPL COMP 1 POIN LECT C2 TERM
COUR 503 'f_Dx1' DEPL COMP 1 POIN LECT F1 TERM
COUR 504 'r_Dx1' DEPL COMP 1 POIN LECT R1 TERM
COUR 505 's_Dx1' DEPL COMP 1 POIN LECT S1 TERM
COUR 506 's_Dx2' DEPL COMP 1 POIN LECT S2 TERM
TRAC 501 502 503 504 505 506 AXES 1.0 'DispolX'
YZER
```

```
   COLO bleu roug rose vert turq jaun
TRAC 501 502 AXES 1.0 'DispolX' YZER
   COLO bleu roug
TRAC 501 503 AXES 1.0 'DispolX' YZER
   COLO bleu roug
TRAC 501 504 AXES 1.0 'DispolX' YZER
   COLO bleu roug
TRAC 501 505 AXES 1.0 'DispolX' YZER
   COLO bleu roug
LIST 501 502 503 504 505 506 AXES 1.0 'DispX'
YZER

COUR 531 'Max_C1' MAX 501
COUR 532 'Max_C2' MAX 502
TRAC 531 532 AXES 1.0 'MaxDxC' YZER
*
COUR 511 'c_Dz1' DEPL COMP 3 POIN LECT C1 TERM
COUR 512 'c_Dz2' DEPL COMP 3 POIN LECT C2 TERM
COUR 513 'f_Dz1' DEPL COMP 3 POIN LECT F1 TERM
COUR 514 'r_Dz1' DEPL COMP 3 POIN LECT R1 TERM
COUR 515 's_Dz1' DEPL COMP 3 POIN LECT S1 TERM
COUR 516 's_Dz2' DEPL COMP 3 POIN LECT S2 TERM
TRAC 511 512 513 514 515 516 AXES 1.0 'DispolZ'
YZER
   COLO bleu roug rose vert turq jaun
LIST 511 512 513 514 515 516 AXES 1.0 'DispZ'
YZER
TRAC 511 512 AXES 1.0 'DispolZ' YZER
   COLO bleu roug
*
COUR 611 'c_Vy1' VITE COMP 1 POIN LECT C1 TERM
COUR 612 'c_Vy2' VITE COMP 1 POIN LECT C2 TERM
COUR 613 'f_Vy1' VITE COMP 1 POIN LECT F1 TERM
COUR 614 'r_Vy1' VITE COMP 1 POIN LECT R1 TERM
COUR 615 's_Vy1' VITE COMP 1 POIN LECT S1 TERM
COUR 616 's_Vy2' VITE COMP 1 POIN LECT S2 TERM
TRAC 611 612 613 614 615 616 AXES 1.0 'VeloX'
YZER
   COLO bleu roug rose vert turq jaun
LIST 611 612 613 614 615 616 AXES 1.0 'VeloX'
YZER
TRAC 611 613 AXES 1.0 'VeloX' YZER
   COLO bleu roug
TRAC 611 614 AXES 1.0 'VeloX' YZER
   COLO bleu roug
TRAC 611 615 AXES 1.0 'VeloX' YZER
   COLO bleu roug
*
COUR 711 'c_Vy1' ACCE COMP 1 POIN LECT C1 TERM
COUR 712 'c_Vy2' ACCE COMP 1 POIN LECT C2 TERM
COUR 713 'f_Vy1' ACCE COMP 1 POIN LECT F1 TERM
COUR 714 'r_Vy1' ACCE COMP 1 POIN LECT R1 TERM
COUR 715 's_Vy1' ACCE COMP 1 POIN LECT S1 TERM
COUR 716 's_Vy2' ACCE COMP 1 POIN LECT S2 TERM
TRAC 711 712 713 714 715 716 AXES 1.0 'ACCEX'
YZER
   COLO bleu roug rose vert turq jaun
LIST 711 712 713 714 715 716 AXES 1.0 'ACCEX'
YZER
TRAC 711 713 AXES 1.0 'ACCEX' YZER
   COLO bleu roug
TRAC 711 714 AXES 1.0 'ACCEX' YZER
   COLO bleu roug
TRAC 711 715 AXES 1.0 'ACCEX' YZER
   COLO bleu roug
TRAC 711 716 AXES 1.0 'ACCEX' YZER
   COLO bleu roug
COUR 721 'Ave_C1' AVER 711
COUR 722 'Ave_C2' AVER 712
COUR 725 'Ave_S1' AVER 716
COUR 726 'Ave_S2' AVER 716
TRAC 721 722 AXES 1.0 'AVE_AxC' YZER
TRAC 725 726 AXES 1.0 'AVE_AxS' YZER
*
COUR 735 'MAX_S1' MAX 716
COUR 736 'MAX_S2' MAX 716
TRAC 735 736 AXES 1.0 'MAX_AxS' YZER
*
COUR 801 'MassAl' MASS COMP 1 REGI 2
COUR 802 'MassR' MASS COMP 1 REGI 3
COUR 803 'MassF' MASS COMP 1 REGI 4
COUR 804 'MassB' MASS COMP 1 REGI 5
COUR 805 'MassRi' MASS COMP 1 REGI 6
TRAC 801 802 803 804 805 AXES 1.0 'MASS' YZER
   COLO bleu roug rose vert turq
LIST 801 802 803 804 805 AXES 1.0 'MASS' YZER
*
COUR 901 'VOLUAl' VOLU REGI 2
COUR 902 'VOLUR' VOLU REGI 3
COUR 903 'VOLUF' VOLU REGI 4
COUR 904 'VOLUB' VOLU REGI 5
COUR 905 'VOLURi' VOLU REGI 6
TRAC 901 902 903 904 905 AXES 1.0 'VOLU' YZER
   COLO bleu roug rose vert turq
LIST 901 902 903 904 905 AXES 1.0 'VOLU' YZER
FIN
```

BlastAirF.dgibi

```
TITRE 'BlastRC3air' ;
OPTI ECHO 1;
OPTION DIME 3 ELEM CUB8 ;
option trac PS FTRA 'BlastRC3air_mesh.ps' ;
OPTI SAUV FORM 'BlastRC3air.msh';
CamD = 10;
oel = CamD CamD CamD;
oelz = 0 0 CamD;
oely = 0 CamD 0;
oelx = CamD 0 0;
*
tol = 1.E-7;
*Elle = 0.025;
Elle = 0.01;
dimxS = 0.1;
dimxC = 0.25;
dimyS = 0.25;
dimxE = 0.05;
*dimxEa = 0.025;
*dimxEb = 0.025;
dimxEa = 0.03;
dimxEb = 0.02;
dimyC = 0.25;
dimzS = 0.8;
dimzC = 3.0;
dimxCn = 0.016;
dimdB = 0.03;
diamB = 0.01;
dimzAct = 0.85;

P0 = 0 0 0;

*Points for Steel
Ps1 = P0 PLUS (0 (0 - (dimyS/2.0)) (0 -
(dimzS/2.0)));
Ps2 = Ps1 PLUS (0 dimyS 0);
*Curve for steel
nsy = ENTI ((dimyS + tol) / (ElLe));
Cs1 = Ps1 d nsy Ps2;
*Surface steel
nsz = ENTI ((dimzS + tol) / (ElLe));
Ss1 = Cs1 tran nsz (0 0 dimzS);

Sb1 = Ss1 PLUS ( (dimxS+dimxE+dimxCn) 0 0);
Sb2 = Sb1 PLUS ( 0 0 (0 + dimzAct));
Sb3 = Sb1 PLUS ( 0 0 (0 - dimzAct));
Sbl = Sb1 ET Sb2 ET Sb3;
*
*Points for Column
dkad = dimxS+dimxE+dimxCn;
Pc1 = P0 PLUS ( dkad (0 - (dimyC/2.0)) (0 -
(dimzC/2.0)));
Pc2 = Pc1 PLUS (0 dimyC 0);
*Curve for Column
ncy = ENTI ((dimyC + tol) / (ElLe));
Cc1 = Pc1 d ncy Pc2;
*Surface Column
ncz = ENTI ((dimzC + tol) / (ElLe));
Sc1 = Cc1 tran ncz (0 0 dimzC);
*Volume Column
ncx = ENTI ((dimxC + tol) / (ElLe));
```

```
Vc1 = Sc1 volu tran ncx (dimxC 0 0);
Vc1 = Vc1 coul cyan;
dkad = dimdB+(diamB/2.0);
*dkad = dimdB;
Pb1 = Pc1 PLUS ( dkad dkad 0);
Pb2 = Pb1  PLUS (0 0 dimzC);
Cb1 = Pb1 d ncz Pb2;
dkad = dimyC - (2*(diamB+(dimdB/2.0)));
*dkad = dimyC - (2*dimdB);
list dimyC;
list diamB;
list dimdB;
list dkad;
Cb2 = Cb1 PLUS (0 (dkad) 0);
dkad = dimxC - (2*(diamB+(dimdB/2.0)));
Cb3 = Cb2 PLUS ((dkad) 0 0);
dkad = dimyC - (2*(diamB+(dimdB/2.0)));
Cb4 = Cb3 PLUS (0 (0 -(dkad)) 0);
bars = Cb1 ET Cb2 Et Cb3 ET Cb4;

TRAC oel CACH QUAL (Vc1);
Vmesh = Vc1;
mesh = Vmesh ET Sbl ET bars;
elim tol mesh;
LIST (NBEL mesh);
LIST (NBEL Vc1);
LIST (NBEL mesh);
***
TRAC oel CACH QUAL mesh;
TASS mesh 'NOOP';
SAUV FORM mesh;
fin;
*
```

BlastRC3air.epx

```
BLASTRC3AIR
ECHO
CONV WIN
CAST 'BlastRC3air.msh' mesh
TRID LAGR EROS 0.0
DIME
*  DEBR 30720
*  DEBR 60000
TERM
GEOM cube Vmesh BR3D bars CL3Q Sbl TERM
COMP EPAI 3.1416E-4 LECT bars TERM
     GROU 2 'cele1' LECT Vc1 TERM
                    COND NEAR POIN 0.166 0.0 0.0
            'cele2' LECT Vc1 TERM
                    COND NEAR POIN 0.416 0.0 0.0
      NGRO 4  'DOWN' LECT mesh TERM COND Z LT -
1.49999
              'UP'  LECT  mesh  TERM  COND  Z  GT
1.49999
             'C1' LECT Vc1 TERM COND SPHE
                       XC 0.166 YC 0.0 ZC 0.0 R
0.005
             'C2' LECT Vc1 TERM COND SPHE
                       XC 0.416 YC 0.0 ZC 0.0 R
0.005
MATE
  VMIS ISOT
       RO 7800     YOUN 200E9    NU 0.3    ELAS
450.E6
             FAIL 2 LIMI 0.18
             TRAC 2  450.E6    0.00225
                     510.E6    0.18
           LECT bars term
*
 DPDC RO 2400 YOUN 3.4E+10 NU 0.21
      FC 42.E+6 DAGG 0.9525E-2  VERS 7
      LECT Vc1 TERM
     IMPE AIRB CONF 6 PMAX 20.0e6 TD 4.11e-3 B
9.189
          LECT Sbl TERM
LINK COUP BLOQ 123 LECT DOWN TERM
          BLOQ 12 LECT UP TERM
  Armat   beton lecture Vc1 TERM
          ferr lecture  bars term

REGI 'BET' RMAS VOLU LECT Vc1 TERM
     'REI' RMAS VOLU LECT bars TERM

ECRI DEPL TFRE 5.E-5
           POINT LECT C1 C2 TERM
           ELEM  LECT CELE1 TERM
     FICH SPLI ALIC TFRE 2.E-5
*     Fichier Format  PVTK  TFREQ  5.e-5
*            GROU 4 OBJET  Vc1 TERM
*               OBJET  Ve1  TERM
*               OBJET  bars  TERM
*               OBJET  Vs1  TERM
*           vari  depl ecrou vite cont FLIA
OPTI NOTE
     CSTA 0.6
     LOG 1
!    REND SAFE
CALC TINI 0 TEND 10.0E-3 TFAI 1e-9
*CALC TINI 0 TEND 10.E-3 TFAI 1e-7
SUIT
BLASTACT5D
ECHO
RESU SPLI ALIC GARD PSCR
SORT GRAP
AXTE 1.0 'Time [s]'
COUR 101 'c_Pres' ECRO COMP 1 ELEM LECT CELE1
TERM
TRAC 101 AXES 1.0 'Pres. [M]' YZER
*
COUR 201 'c_Pres' ECRO COMP 2 ELEM LECT CELE1
TERM
TRAC 201 AXES 1.0 'Pres. [M]' YZER
*
COUR 301 'c_Strain' ECRO COMP 3 ELEM LECT CELE1
TERM
TRAC 301 AXES 1.0 'Strain' YZER
*
**
*COUR 404 'PresBlast' ECRO COMP 1 ELEM LECT
4100 TERM
*LIST 404 AXES 1.0 'Pres' YZER
*TRAC 404 AXES 1.0 'Pres. [M]' YZER
**
COUR 404 'p_Pres1' ECRO COMP 1 ELEM LECT 190000
TERM
LIST 404 AXES 1.0 'Pres' YZER
TRAC 404 AXES 1.0 'Pres. [M]' YZER
COUR 405 'Impulse' INT 404
TRAC 405 AXES 1.0 'Impulse' YZER
*
COUR 501 'c_Dx1' DEPL COMP 1 POIN LECT C1 TERM
COUR 502 'c_Dx2' DEPL COMP 1 POIN LECT C2 TERM
TRAC 501 502 AXES 1.0 'DispolX' YZER
COUR 531 'Max_C1' MAX 501
COUR 532 'Max_C2' MAX 502
TRAC 531 532 AXES 1.0 'MaxDxC' YZER
*
COUR 511 'c_Dz1' DEPL COMP 3 POIN LECT C1 TERM
COUR 512 'c_Dz2' DEPL COMP 3 POIN LECT C2 TERM
TRAC 511 512 AXES 1.0 'DispolZ' YZER
*
COUR 611 'c_Vy1' VITE COMP 1 POIN LECT C1 TERM
COUR 612 'c_Vy2' VITE COMP 1 POIN LECT C2 TERM
TRAC 611 612 AXES 1.0 'VeloX' YZER
*
COUR 711 'c_Vy1' ACCE COMP 1 POIN LECT C1 TERM
COUR 712 'c_Vy2' ACCE COMP 1 POIN LECT C2 TERM
TRAC 711 712 AXES 1.0 'ACCEX' YZER
COUR 721 'Ave_C1' AVER 711
COUR 722 'Ave_C2' AVER 712
TRAC 721 722 AXES 1.0 'AVE_AxC' YZER
*
COUR 804 'MassB' MASS COMP 1 REGI 1
COUR 805 'MassRi' MASS COMP 1 REGI 2
TRAC 804 805 AXES 1.0 'MASS' YZER
*
COUR 904 'VOLUB' VOLU REGI 1
COUR 905 'VOLURi' VOLU REGI 2
TRAC 904 905 AXES 1.0 'VOLU' YZER
FIN
```

European Commission
Joint Research Centre – Institute for the Protection and Security of the Citizen

Title: Numerical Simulations n Support of the Blast Actuator development

Author(s): Georgios Valsamos, Martin Larcher, George Solomos, Armelle Anthoine

Luxembourg: Publications Office of the European Union

2013 – 72 pp. – 21.0 x 29.7 cm

EUR – Scientific and Technical Research series – ISSN 1831-9424

ISBN 978-92-79-35069-6 (PDF)
ISBN 978-92-79-35070-2 (print)

ISSN 1018-5593 (print)
ISSN 1831-9424 (online)

doi: 10.2788/53372

Abstract

Nowadays there is a need to develop special techniques to protect the critical infrastructures from exposing events. The use of real explosive material on the experiments is very expensive and a lot of security measures should be taken. Especially in the case that the test should be repeated many times in order to obtain accurate results is almost impossible to perform the real explosive experiments. That for came up the idea of a blast simulator that can reproduce an explosive charge in a most economic and controllable way. The setup of such an apparatus is a very difficult task where many details should be studied. The most appropriate way to study the several parameters that influence the performance of the blast actuator is to use numerical simulation techniques. This report performs numerous numerical investigations and gives answers to many questions concerning the performance of the impacting mass of the blast actuator on the specimen. The numerical results have been generated with the fast explicit transient dynamic finite element code EUROPLEXUS.

LB-NA-26430-EN-N

JRC Mission

As the Commission's in-house science service, the Joint Research Centre's mission is to provide EU policies with independent, evidence-based scientific and technical support throughout the whole policy cycle.

Working in close cooperation with policy Directorates-General, the JRC addresses key societal challenges while stimulating innovation through developing new methods, tools and standards, and sharing its know-how with the Member States, the scientific community and international partners.

Serving society
Stimulating innovation
Supporting legislation

Publications Office

ISBN 978-92-79-35069-6